Defense Threat Reduction Agency
8725 John J. Kingman Road, MS 6201
Fort Belvoir, VA 22060-6201

DTRA-TR-03-2

TECHNICAL REPORT

Regional Seismic Threshold Monitoring

Approved for public release; distribution is unlimited.

March 2006

DTRA01-00-C-0107

Dr. Tormod Kvaerna

Prepared by:
NORSAR
P.O. Box 51
N-2027 Kjeller
Norway

DARE Tracking
73735

DESTRUCTION NOTICE

FOR CLASSIFIED documents, follow the procedures in DoD 5550.22-M, National Industrial Security Program Operating Manual, Chapter 5, Section 7 (NISPOM) or DoD 5200.1-R, Information Security Program Regulation, Chapter 1X.

FOR UNCLASSIFIED limited documents, destroyed by any method that will prevent disclosure of contents or reconstruction of the document.

Retention of this document by DoD contractors is authorized in accordance with DoD 5220.22-M, Industrial Security Manual.

PLEASE NOTIFY THE DEFENSE THREAT REDUCTION AGENCY, ATTN: BDMI, 8725 JOHN J. KINGMAN ROAD, MS-6201, FT BELVOIR, VA 22060-6201, IF YOUR ADDRESS IS INCORRECT, IF YOU WISH IT DELETED FROM THE DISTRIBUTION LIST, OR IF THE ADDRESSEE IS NO LONGER EMPLOYED BY YOUR ORGANIZATION.

DISTRIBUTION LIST UPDATE

This mailer is provided to enable DTRA to maintain current distribution lists for reports. (We would appreciate you providing the requested information.)

- ❑ Add the individual listed to your distribution list.
- ❑ Delete the cited organization/individual.
- ❑ Change of address.

Note:
Please return the mailing label from the document so that any additions, changes, corrections or deletions can be made easily. For distribution cancellation or more information call DTRA/BDLMI (703) 767-4725.

NAME: _____

ORGANIZATION: _____

OLD ADDRESS	NEW ADDRESS
_____	_____
_____	_____
_____	_____

TELEPHONE NUMBER: ( ) _____

DTRA PUBLICATION NUMBER/TITLE	CHANGES/DELETIONS/ADDITONS, etc. *(Attach Sheet if more Space is Required)*
_____	_____
_____	_____
_____	_____

DTRA or other GOVERNMENT CONTRACT NUMBER: _____

CERTIFICATION of NEED-TO-KNOW BY GOVERNMENT SPONSOR (if other than DTRA):

SPONSORING ORGANIZATION: _____

CONTRACTING OFFICER or REPRESENTATIVE: _____

SIGNATURE: _____

DEFENSE THREAT REDUCTION AGENCY
ATTN: BDLMI
8725 John J Kingman Road, MS 6201
Fort Belvoir, VA 22060-6201

DEFENSE THREAT REDUCTION AGENCY
ATTN: BDLMI
8725 John J Kingman Road, MS 6201
Fort Belvoir, VA 22060-6201

REPORT DOCUMENTATION PAGE

Form Approved
OMB No. 0704-0188

1. REPORT DATE *(DD-MM-YYY)*	2. REPORT TYPE	3. DATES COVERED *(From - To)*
31 December 2002	Technical Report	

4. TITLE AND SUBTITL
Regional Seismic Threshold Monitoring

5a. CONTRACT NUMBER
DTRA 01-00-C-0107

5b. GRANT NUMBER

5c. PROGRAM ELEMENT NUMBER
463D

6. AUTHOR(S)
Tormod Kvaerna

5d. PROJECT NUMBER
CD

5e. TASK NUMBER
CD

5f. WORK UNIT NUMBER
PRDA0

7. PERFORMING ORGANIZATION NAME(S) AND ADDRESS(ES)

Stiftelsen NORSAR
Post Box 53
NO-2027 Kjeller, NOrway

8. PERFORMING ORGANIZATION REPORT NUMBER

794

9. SPONSORING / MONITORING AGENCY NAME(S) AND ADDRESS(ES)
Defense Threat Reduction Agency
8725 John J. Kingman Rd., MS 6201
Fort Belvoir, VA 22060-6201

10. SPONSOR/MONITOR'S ACRONYM(S)
DTRA

11. SPONSOR/MONITOR'S REPORT NOS.
TR-03-2

12. DISTRIBUTION / AVAILABILITY STATEMENT
Approved for public release; distribution is unlimited.

13. SUPPLEMENTARY NOTES

14. ABSTRACT
A database comprising 45 seismic events, selected to provide the best possible ray path coverage of the Barents Sea and adjacent areas, has been compiled and reanalyzed. This has resulted in a mapping of the propagation efficiency of the different regional phases, new regional attenuation relations for Pn, Sn, Pg and Lg, together with a preferred average velocity model to be used for predicting the travel times of regional phases. We have applied these attenuation relations to develop and assess a regional threshold monitoring scheme for selected subregions of the European Arctic. Specifically, we have demonstrated how a number of small underwater explosions in the area following the Kursk accident in the Barents Sea have been detected using the threshold monitoring technique.

This first case study on regional threshold monitoring concerns the Novaya Zemlya region, and illustrates the performance of the method using different combinations of monitoring stations. The second case study focuses on the Kola Peninsula. This study gives us an impression of the potential TM performance in a case where a local network is available. For the most active mining areas in this region, the magnitude thresholds during "normal" noise conditions vary between 0.7 and 1.0 magnitude units.

15. SUBJECT TERMS
Seismology Test sites
Threshold Monitoring

a. REPORT	b. ABSTRACT	c. THIS PAGE	17. LIMITATION OF ABSTRACT	18. NUMBER OF PAGES	19a. NAME OF RESPONSIBLE PERSON
Unclassified	Unclassified	Unclassified	SAR	82	19b. TELEPHONE NUMBER *(include area code)*

CONVERSION TABLE

Conversion Factors for U.S. Customary to metric (SI) units of measurement.

MULTIPLY →	BY →	TO GET
TO GET ←	BY ←	DIVIDE

angstrom	1.000 000 x E -10	meters (m)
atmosphere (normal)	1.013 25 x E +2	kilo pascal (kPa)
bar	1.000 000 x E +2	kilo pascal (kPa)
barn	1.000 000 x E -28	meter^2 (m^2)
British thermal unit (thermochemical)	1.054 350 x E +3	joule (J)
calorie (thermochemical)	4.184 000	joule (J)
cal (thermochemical/cm^2)	4.184 000 x E -2	mega joule/m^2 (MJ/m^2)
curie	3.700 000 x E +1	*giga bacquerel (GBq)
degree (angle)	1.745 329 x E -2	radian (rad)
degree Fahrenheit	$t_k = (t°f + 459.67)/1.8$	degree kelvin (K)
electron volt	1.602 19 x E -19	joule (J)
erg	1.000 000 x E -7	joule (J)
erg/second	1.000 000 x E -7	watt (W)
foot	3.048 000 x E -1	meter (m)
foot-pound-force	1.355 818	joule (J)
gallon (U.S. liquid)	3.785 412 x E -3	meter^3 (m^3)
inch	2.540 000 x E -2	meter (m)
jerk	1.000 000 x E +9	joule (J)
joule/kilogram (J/kg) radiation dose absorbed	1.000 000	Gray (Gy)
kilotons	4.183	terajoules
kip (1000 lbf)	4.448 222 x E +3	newton (N)
kip/inch^2 (ksi)	6.894 757 x E +3	kilo pascal (kPa)
ktap	1.000 000 x E +2	newton-second/m^2 ($N-s/m^2$)
micron	1.000 000 x E -6	meter (m)
mil	2.540 000 x E -5	meter (m)
mile (international)	1.609 344 x E +3	meter (m)
ounce	2.834 952 x E -2	kilogram (kg)
pound-force (lbs avoirdupois)	4.448 222	newton (N)
pound-force inch	1.129 848 x E -1	newton-meter (N-m)
pound-force/inch	1.751 268 x E +2	newton/meter (N/m)
pound-force/foot^2	4.788 026 x E -2	kilo pascal (kPa)
pound-force/inch^2 (psi)	6.894 757	kilo pascal (kPa)
pound-mass (lbm avoirdupois)	4.535 924 x E -1	kilogram (kg)
pound-mass-foot^2 (moment of inertia)	4.214 011 x E -2	kilogram-meter^2 ($kg-m^2$)
pound-mass/foot^3	1.601 846 x E +1	kilogram-meter^3 (kg/m^3)
rad (radiation dose absorbed)	1.000 000 x E -2	**Gray (Gy)
roentgen	2.579 760 x E -4	coulomb/kilogram (C/kg)
shake	1.000 000 x E -8	second (s)
slug	1.459 390 x E +1	kilogram (kg)
torr (mm Hg, 0^0 C)	1.333 22 x E -1	kilo pascal (kPa)

*The bacquerel (Bq) is the SI unit of radioactivity; 1 Bq = 1 event/s.
**The Gray (GY) is the SI unit of absorbed radiation.

Summary

This Final Scientific Report covers work conducted under a project to develop and test a new, advanced method for applying regional seismic array technology to the field of nuclear test ban monitoring. The report addresses the development and testing of this method for optimized, regional seismic monitoring, using a sparse network of regional arrays and three-component stations. Emphasis of the research is placed on algorithms that can be efficiently applied in a real-time monitoring environment, which are using primarily automated processing, and which can be readily implemented in an operational monitoring system.

The report comprises seven main technical topics, addressed in separate report sections. **Section 1** is an introductory chapter. **Section 2** is a case study demonstrating the capability of the method for experimental application to a region in the Barents Sea. We have chosen for this application the region surrounding the accident of the Russian submarine Kursk in August 2000. We demonstrate how a number of small underwater explosions in the area following the accident have been detected using the threshold monitoring technique.

Section 3 is a description of the reviewed NORSAR bulletin used as an input data base for some of our studies, and a preliminary study of Pn amplitude attenuation relationships in the Barents Sea and adjacent regions. The development of such relationships is mandatory in order to optimize the magnitude correction constants that are used in the regional threshold monitoring algorithm. The study shows that the Pn attenuation model developed by previous investigators (Jenkins et al., 1998) provide quite consistent Pn station magnitudes for events in this region.

Section 4 concerns the development of a regional database for the Barents Sea, with carefully analyzed seismic phases. This analysis is different from that in the standard analyst reviewed bulletin, described in the preceding chapter, in that we have required that all discernible phases should be timed, regardless of whether or not they provide a good fit in the event location process. There readings were used for a mapping of phases observable for the different propagation paths, and for an assessment of the travel-time models applicable to this region. Finally, these readings will then be used to develop and verify attenuation models for all phases of interest in the threshold monitoring for the Barents Sea region.

Section 5 is a detailed attenuation and inversion study aimed at obtaining attenuation relations for each of the major regional phases (Pn, Pg, Sn, Lg). We show that these new attenuation relations represent an improvement relative to previously available relations, and that they provide consistent magnitude estimates based on different phase amplitudes. However, some significant blockage features in the Barents Sea and adjacent regions are noted.

Section 6 is the first of two case studies of regional seismic monitoring. This first case concerns the Novaya Zemlya region, and illustrates the performance of the regional threshold monitoring method using different combinations of monitoring stations. Using as an example a recent small seismic event about 100 km from the Novaya Zemlya test

site, we make a special study addressing the trade-off between the beam radius and the beam focusing sharpness (noting the desire to have a single beam represent the largest

possible area with no significant loss in performance). In general, we find that with a beam radius of up to 100 km, one site-specific beam is reasonably representative for the corresponding target region for an array geometry based on two distant monitoring stations. For denser monitoring networks, the beam radius should be smaller in order to fully exploit the power of the TM method.

Section 7 contains the second case study - this time focusing on the Kola Peninsula. This study gives us the opportunity to obtain an impression of the potential TM performance in a case where a local network is available. Not unexpectedly, the monitoring thresholds turn out to be much lower than for the case of Novaya Zemlya, and this is illustrated by examples of known mining events.

Section 8 describes the software architecture of the Threshold Monitoring system, including a brief program description and a description of the basic operational procedures.

Section 9 contains conclusions and recommendations resulting from this project.

1. Introduction

1.1 Objective

The main objective of this research is to develop and test a new, advanced method for applying regional seismic array technology to the field of nuclear test ban monitoring. To that end, we address the development and testing of a method for optimized seismic monitoring of an extended geographical region, using a sparse network of regional arrays and three-component stations. Our earlier work on optimized site-specific threshold monitoring serves as a basis for the development of this new method. Emphasis of the research is on algorithms that can be efficiently applied in a real-time monitoring environment, which are using primarily automated processing, and which can be readily implemented in an operational CTBT monitoring system.

1.2 Report Overview

This final report covers work conducted under a project to develop and test a method for *optimized regional seismic threshold monitoring*, with experimental application to the Barents/Kara Sea region, including Novaya Zemlya. Data from a sparse network of regional arrays and three-component stations is used. The work builds on the *optimized site-specific threshold monitoring* technique developed under a previous contract. The continuous seismic threshold monitoring method (TM), which was developed at NORSAR over the past few years, provides a continuous assessment of the size of events that may have occurred in a given geographical area. The main purpose of this technique is to highlight instances when a given threshold magnitude is exceeded, thereby helping the analyst focus on those events truly of interest in a monitoring situation.

The overall aim of the project is to obtain an *optimized, automatic* capability to monitor seismic events originating in an extended geographical region. We investigate incorporating region-specific calibration information like travel time, slowness and magnitude anomalies, and optimal bandpass filters for assessment of magnitude thresholds. The output from the optimized regional threshold monitoring is integrated with results from "traditional" data analysis of detected signals, and we are developing an "automatic explanation facility" to assist the analyst in evaluating the results.

This report comprises seven technical parts (Sections 2 through 8). Section 2 is a case study demonstrating the capability of the method for experimental application to a region of relatively small geographical extent in the Barents Sea. We have chosen for this application the region surrounding the accident of the Russian submarine Kursk in August 2000. In this section, we also develop an automatic explanation facility for peaks on the threshold trace. Section 3 is a preliminary study of Pn amplitude attenuation relationships in the Barents Sea and adjacent regions. Section 4 describes the development of a regional database for the Barents Sea, for use in developing attenuation relationships for secondary phases. Section 5 describes the results from this attenuation study for the major regional phases (Pn, Pg, Sn, Lg). Sections 6 and 7 are case studies describing application of the regional threshold monitoring method to regions of relatively large geographical extent:

Novaya Zemlya and the Kola Peninsula, respectively. These studies also address the trade-off between beam coverage and the sharpness of the peaks. Section 8 describes the software architecture of the Threshold Monitoring system, including a brief program description, installation instructions and basic operation procedures. Overall conclusions and recommendations are provided in Section 9.

2 Threshold monitoring of the area near the Kursk submarine accident

2.1 Recording of the accident

On 12 August 2000, signals from two presumed underwater explosions in the Barents Sea were recorded by Norwegian seismic stations. The first of these, at 07.28.27 GMT, was relatively small, measuring 1.5 on the Richter scale. The second explosion, 2 minutes and 15 seconds later, was much more powerful, with a Richter magnitude of 3.5. These explosions were associated with the accident of the Russian submarine "Kursk", although the exact sequence of events leading to this disaster is still unknown.

The area in the Barents Sea where the Kursk accident occurred has no known history of significant earthquake activity. Beginning in September 2000, a number of small seismic events were detected in this area (Ringdal et al., 2000). According to an official Russian announcement in November, these signals were generated by underwater explosions near the Kursk accident area, carried out by the Russian Navy.

This explosion sequence, with numerous explosions ranging in magnitude from very small (about 1.0 on the Richter scale) to fairly large (about magnitude 3.0) provides a unique opportunity to investigate the performance of the threshold monitoring technique to a relatively small geographical target area (some tens of kilometers across). We have implemented an experimental threshold monitoring procedure to monitor the Kursk accident area in the Barents Sea, and present some of the results in this report

We first note that the timing patterns of the explosions show some single explosions and some compressed sequences with explosion intervals of 1-2 minutes. The waveforms have similar characteristics, although they are not identical. These explosions, although their magnitudes were only about 2.0 on the Richter scale, were well recorded by the ARCES array (distance 500 km), but the FINES, SPITS and NORES arrays also detected several of the events. In addition, the Apatity array station in the Kola Peninsula (not an IMS station) provided useful recordings.

2.2 Automatic processing

In developing the parameters for optimized monitoring of the Kursk accident area, we have built on previous efforts to develop a fully automated tool for site-specific monitoring of a given target site. We have included additional functionality to facilitate the review of the computed threshold traces, and examples of this new functionality are shown below.

As outlined in reports under previous contracts, we have already available a robust method for detecting peaks on the threshold traces. The next step is to identify the peaks that are caused by events located outside the actual target area. We will in the following describe the procedure developed for monitoring of the Kursk accident area using data from the SPITS, ARCES, FINES, Apatity and NORES arrays.

2.3 Automatic explanation facility

The automatic explanation facility for threshold peaks builds on an integration of traditional detector and event information with the results of continuous Threshold Monitoring.

The first step in the automatic analysis of threshold traces is to identify significant threshold peaks. Our approach has been to develop a peak detection method based on estimates of the noise variance and the long term trend of the threshold trace. From experiments with various data sets, we have developed a method which comprises the following steps:

- Calculate the long-term-median (LTM) of the threshold trace with a typical window length of 60 minutes and a sampling interval of 5 minutes.
- Calculate the overall standard deviation (SIGMA) of the threshold trace around the long-term-median after removing the upper 5% of the data values. The removal of the upper 5% of the data values is done to reduce the influence of the threshold peaks on the estimate of the standard deviation.
- Define the peak detection limit as LTM + n * SIGMA, where n is the number of standard deviations above the LTM. Optionally, the peak detection limit can be set by the user, and in this study the limit is set to approximately 0.4 m_b units above the LTM.

Figure 2.1 shows a panel with threshold traces for 20 November 2000 (day 325) with the peak detection limits superimposed. Notice that several peaks are identified on the network threshold trace which we have to investigate in more detail.

In order to relate the peaks of the network threshold trace to information obtained by traditional signal processing at each array, we have to determine the time intervals associated with each network threshold peak as well as the expected azimuths and velocities from the site to be monitored (**Table 2.1**). The following procedure has been established:

- Detect peaks on the threshold traces calculated for each individual phase.
- For each phase considered, find the peak detection intervals overlapping the peak detection intervals of the network threshold trace, and use the union as the time interval of interest.
- The X-axes of the threshold traces show hypothetical origin times at the Kursk accident area. When searching the detection lists for signals associated with the threshold peaks, we need to shift the detection times in accordance with the expected phase travel time from the Kursk accident area to the actual array.
- We define for each phase a critical azimuth and slowness range for events in the vicinity of the Kursk accident area. Detected signals with azimuth and slowness estimates falling outside the critical ranges are assumed to be caused by events located outside the Kursk area.
- For all panels, green peaks indicate that none of the associated detections were considered critical. Yellow peaks indicate that there were no associated detections whatsoever (see the FINES-P panel in **Figure 2.1** between 7:00 and 9:00). All peaks are flagged on the X-axis for easy identification.

- Each individual phase is given a weight (0 or 1) based on the sensitivity of the array and the usefulness of the phase. The P-phases from Apatity, ARCES, and FINES are given a weight of 1; all other phases have a weight of 0. Critical detections and their associated peaks will be either orange (phase weight 0) or red (phase weight 1).
- Critical peaks on the network trace are assigned a weight which is the sum of the phase weights of the corresponding individual phase peaks. These network peak weights are shown on the top of the panel. Critical peaks with a total weight of at least 2 are red (see **Figure 2.1**, 7:00-9:00); otherwise they are orange (see **Figure 2.1** at about 3:00 and just after midnight). The orange network peak at about 18:20 has an associated critical Lg phase at ARCES. The individual threshold traces for ARCES Lg, Apatity Lg, FINES Lg, and NORES Lg are not shown in **Figure 2.1**, but these phases are all included in the calculation of the network thresholds.
- The causes of the red threshold peaks have to be investigated in more detail, e.g. by comparing to existing event bulletins or by offline analysis of the raw seismic data.

2.4 Comments on the Kursk TM case study (day 325/2000)

The plot in **Figure 2.1** shows seven consecutive red color peaks on the network (top) trace. These peaks all correspond to real explosions from the Kursk accident area, as has been verified by interactive waveform analysis. The explosions occur between 7 and 9 GMT, and are almost equidistant in time (15 minute intervals). The software tool has the functionality to provide a higher resolution of the plot, if so desired by the analyst. **Figure 2.2** shows a plot of the one-hour interval 07.00-08.00 for the same day, and it is possible to analyze the peaks in somewhat more detail.

Another new feature is the option to focus on one particular phase, and compare the results with the network trace. **Figure 2.3** shows an example, focusing on the ARCES Pg phase for the day 325/2000. Together with **Figure 2.4**, which is a blow-up of **Figure 2.3** covering the time interval 07.00-08.00, these figures show (from top to bottom);

- The network Threshold Monitoring trace
- The TM trace using the ARCES Pg phase only
- The SNR (in dB) for the ARCES Pg detections
- The ray parameter (s/deg) for the ARCES Pg phase, with the critical interval for the Kursk accident area marked in yellow
- The calculated azimuth for the ARCES Pg phase, with the critical interval for the Kursk accident area marked in yellow
- The slowness difference (absolute value) compared to the expected ray parameter for Pg.

We note from **Figure 2.3** that one red peak in the ARCES plot (at around 03 GMT) is only orange on the network trace. A closer investigation reveals that this peak corresponds to a small mining explosion near the Norway-Russia Border (The Zapolyarnyi/Nikel mine). The azimuth of this mining site from ARCES is almost exactly the same as for the Kursk accident area, but the slowness resolution is not sufficient to distinguish this phase from the Kursk phases using ARCES alone.

It is important to note that the availability of additional array data in this case provide some important contributions to the threshold monitoring results:

- They reduce the size of this "false" peak on the network trace
- They ensure that the peak is not marked in red on the network trace, because the azimuths from the other arrays do not correspond to events at the Kursk accident area.

The development of the automatic explanation facility for analysis of the threshold monitoring results as illustrated in this section can easily be extended to cover larger regions. The key here is the trade-off between beam coverage and the sharpness of the peak. This point is further discussed in Section 6.

Table 2.1: Definition of critical azimuth and slowness ranges for phases from events near the Kursk accident area

Array	Phase	Expected Azimuth (degrees)	Lower Azimuth (degrees)	Higher Azimuth (degrees)	Expected Slowness (sec/deg)	Lower Slowness (sec/deg)	Higher Slowness (sec/deg)
APA	Pg	50.65	25.0	65.0	13.97	10.1	22.2
APA	Lg	46.57	20.0	60.0	25.78	18.5	37.1
ARCES	Pg	88.1	75.0	100.0	13.7	10.6	15.9
ARCES	Lg	88.4	70.0	100.0	26.2	22.2	37.1
FINES	P	23.15	10.0	40.0	13.28	10.11	18.53
FINES	Lg	21.75	5.00	35.0	28.88	22.24	44.48
SPITS	P	142.70	135.0	155.0	15.27	11.12	24.71
NORES	P	33.38	20.0	45.0	12.47	9.27	15.88
NORES	Lg	29.75	20.0	45.0	32.42	22.24	55.60

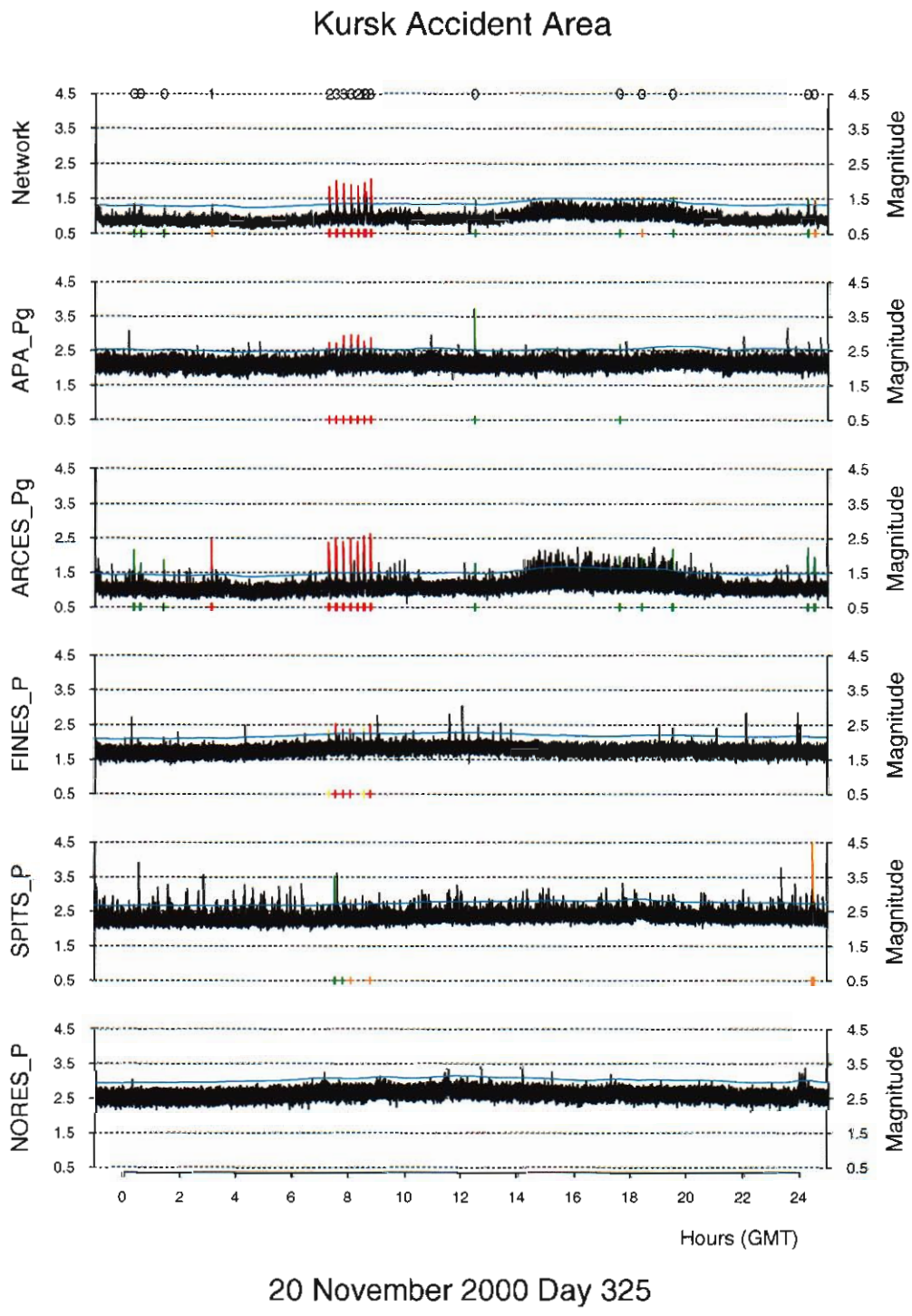

Figure 2.1. *Site-specific Threshold Monitoring of the Kursk accident area for 20 November 2000 (day 325). The plot shows the 5 individual station thresholds (P-phases), with the combined threshold trace on top. Peaks which are likely to be caused by events near the Kursk accident area are shown in red.*

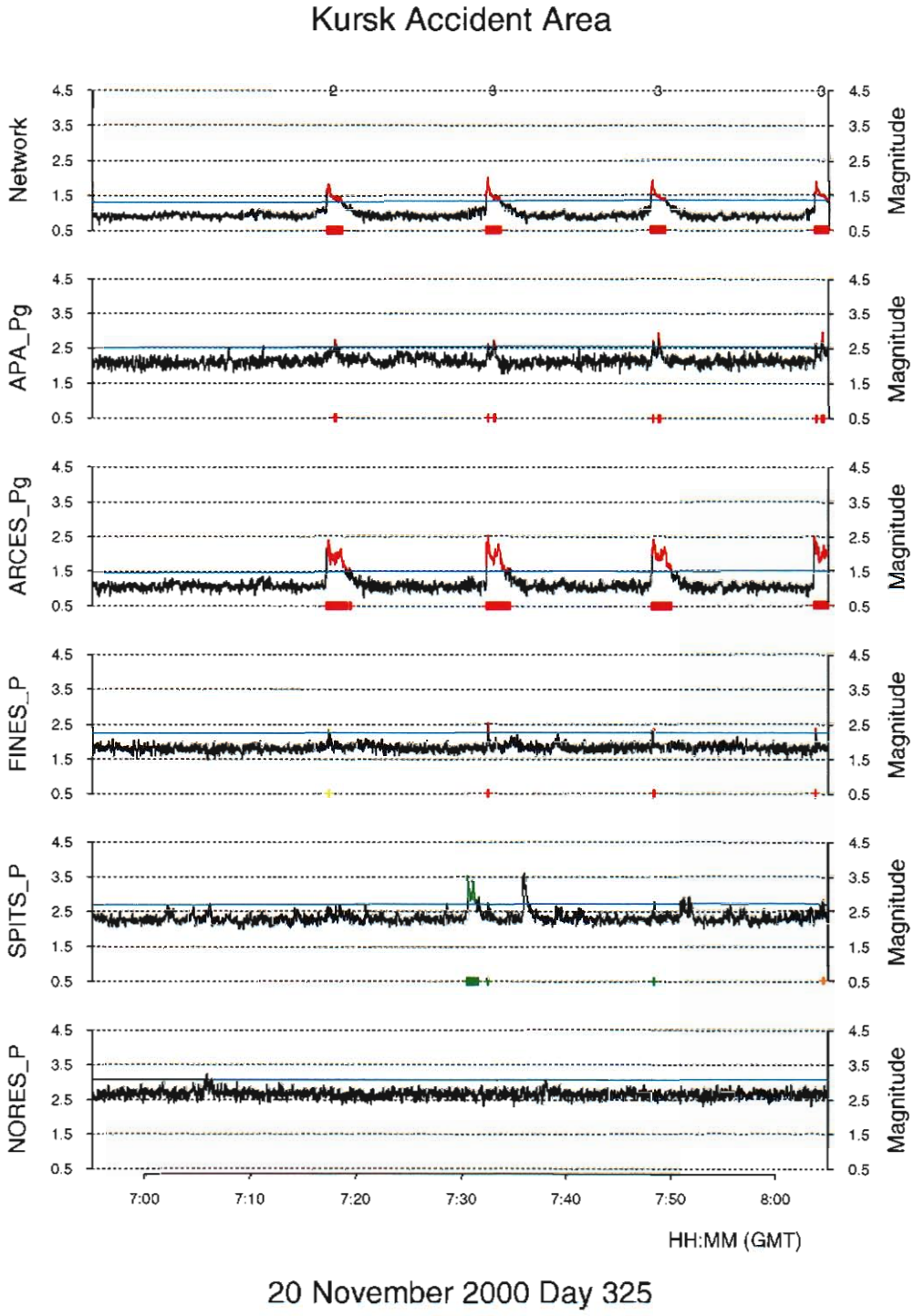

Figure 2.2. *Same as* ***Figure 2.1****, but covering only the one-hour interval 07.00-08.00 on day 325/2000. Note that the detailed plot for ARCES shows two peaks for each event. This corresponds to the P and S phases, and these two peaks are merged into one for each event on the network trace.*

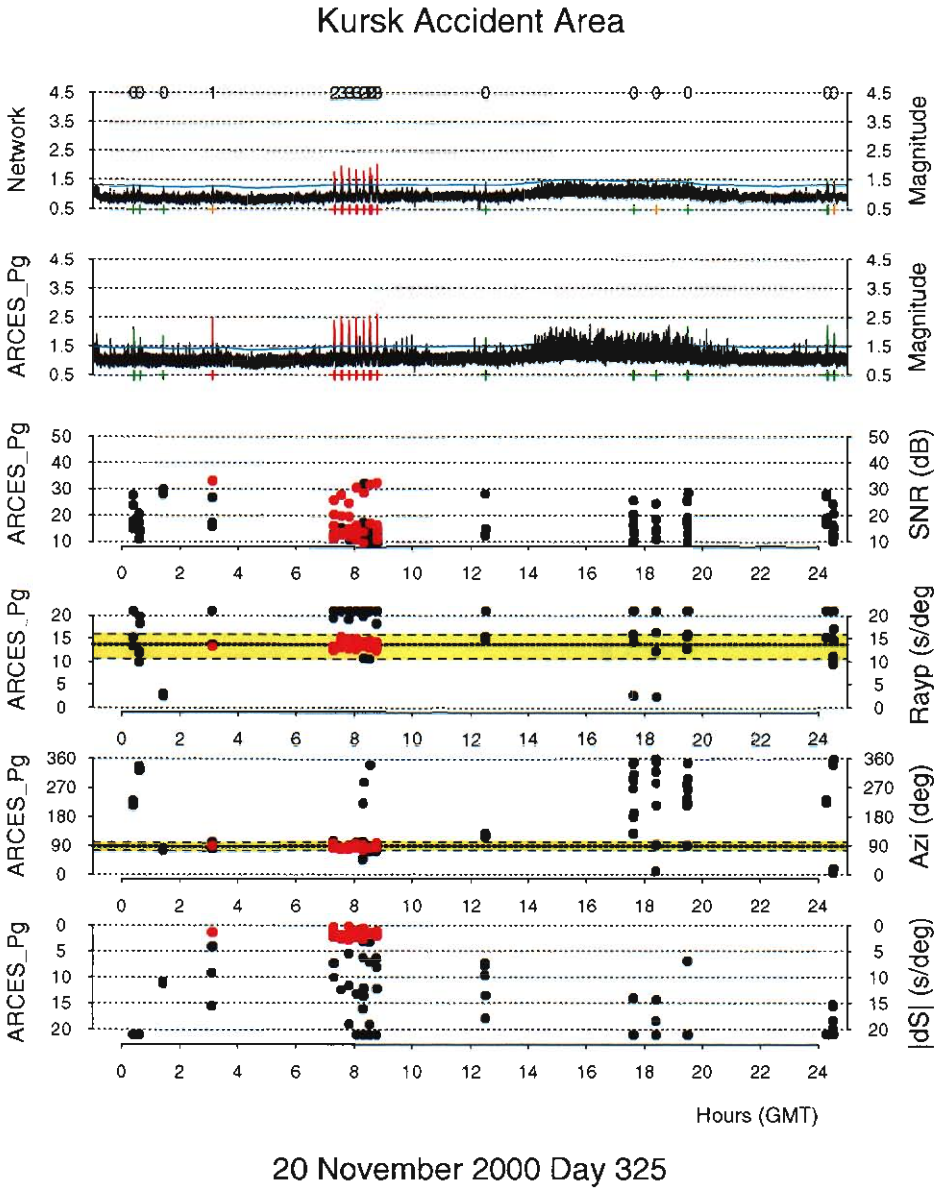

Figure 2.3. *Site-specific Threshold Monitoring of the Kursk accident area for 20 November 2000 (day 325) with information from the signal detector at ARCES. The two upper panels show the threshold traces for the network and for the ARCES Pg-phase. Peaks which are likely to be caused by events near the Kursk accident area are shown in red. Information about the signal detections associated with the network threshold peaks is displayed in the four lower panels. The critical ranges of slowness (ray parameter) and azimuth are indicated in yellow in panels 4 and 5, and the bold dashed lines indicate the expected values of Pg-phases from the Kursk accident area.*
The panel at the bottom indicates the differences in horizontal slowness estimates between the detected signals and the expected value for P-phases from the Kursk accident area (in s/deg). Signals satisfying both the azimuth and slowness criteria are shown in red.

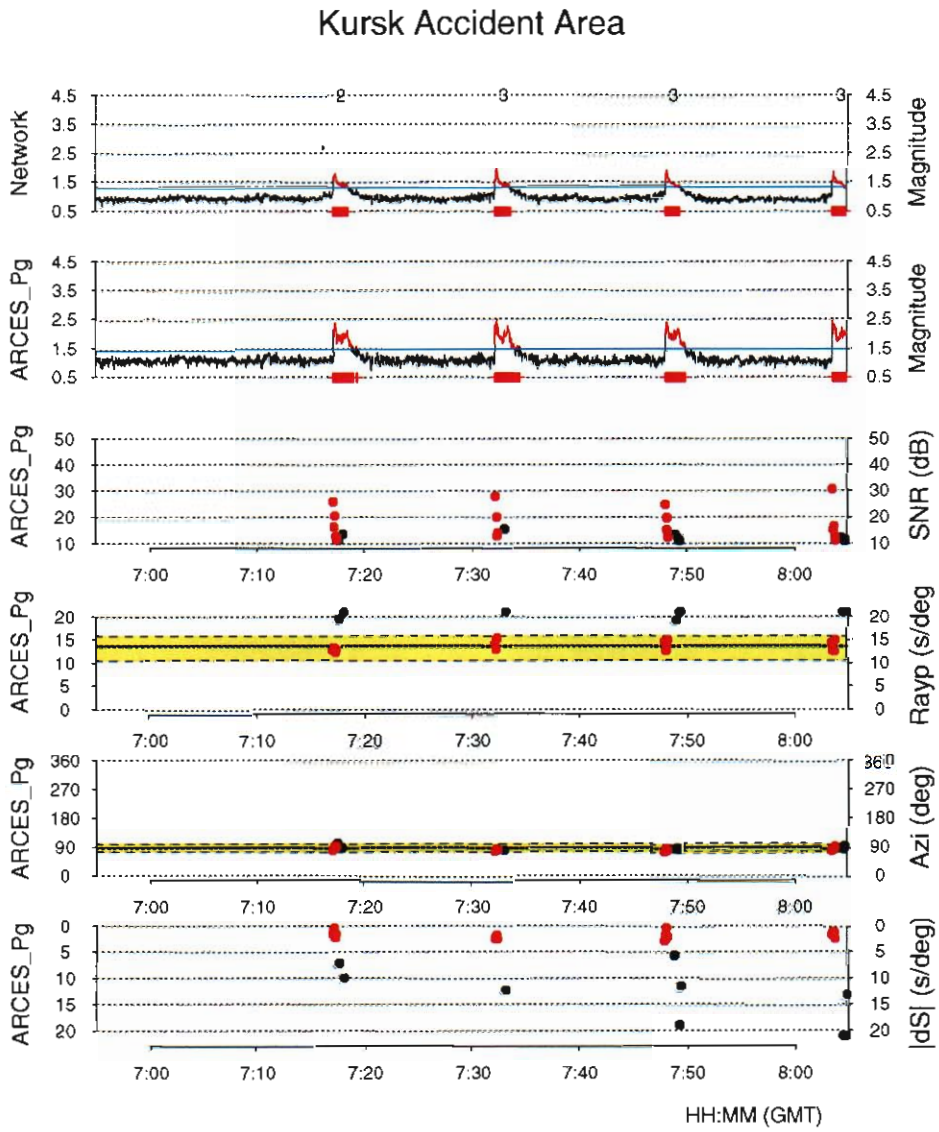

Figure 2.4. *Same as* ***Figure 2.3****, but covering only the one-hour interval 07.00-08.00 on day 325/2000. The red dots on the four lower panels correspond to Pg detections from events at the Kursk accident area, whereas the other (black) detections on these plots actually correspond to S-phases from the same events. Their azimuths are consistent with the Kursk accident area, while their slownesses are outside the critical area.*

3. Regional seismic bulletin and initial Pn attenuation study

3.1 Introduction

Access to applicable amplitude attenuation curves for the different regional phases is key to developing the method of regional seismic threshold monitoring. The study by Jenkins et al. (1998) provides useful results on this subject for regional phases in Fennoscandia as well as in other stable tectonic regions. In order to utilize their results, we have to validate our time-domain measurements used for threshold monitoring, and we would also like to evaluate the applicability of their attenuation models for distances below 200 km and for events located in the Novaya Zemlya and Barents Sea regions.

For this purpose we have from 10 November 2000 stored all data from the available regional arrays (NORES, ARCES, HFS, FINES, Apatity, and SPITS) on disk for subsequent rapid access. Using the phase readings of NORSAR's analyst reviewed regional seismic bulletin as a starting point, we have carried out time-domain measurements of the regional phases and compared these to the predictions of the regional phase attenuation models of Jenkins et al. (1998).

3.2 NORSAR's analyst reviewed regional seismic bulletin

Figure 3.1 shows the locations of events in NORSAR's analyst reviewed regional seismic bulletin for November 2000. Using data from the regional arrays NORES, ARCES, HFS, FINES, Apatity, and SPITS, an average of about 90 events are analyzed every month. However, due to numerous explosions in the Kursk accident area, a total number of 167 events were analyzed during November 2000. The starting point for the analyst review are the locations and magnitudes provided by NORSAR's fully automatic bulletin generated by the Generalized Beamforming method (Kværna et al., 1999). The analyst is focusing on regional events with magnitude greater that 1.5, but also other events of interest in the European Arctic are included in the reviewed bulletin.

In order to utilize the analyzed reviewed bulletin for research purposes we have created a Web application with maps showing the event locations, the event bulletins with phase readings, and plots showing the waveforms at the different recording stations. We will in the following show some plots illustrating the structure of this Web application (see **Figures 3.1-3.4**):

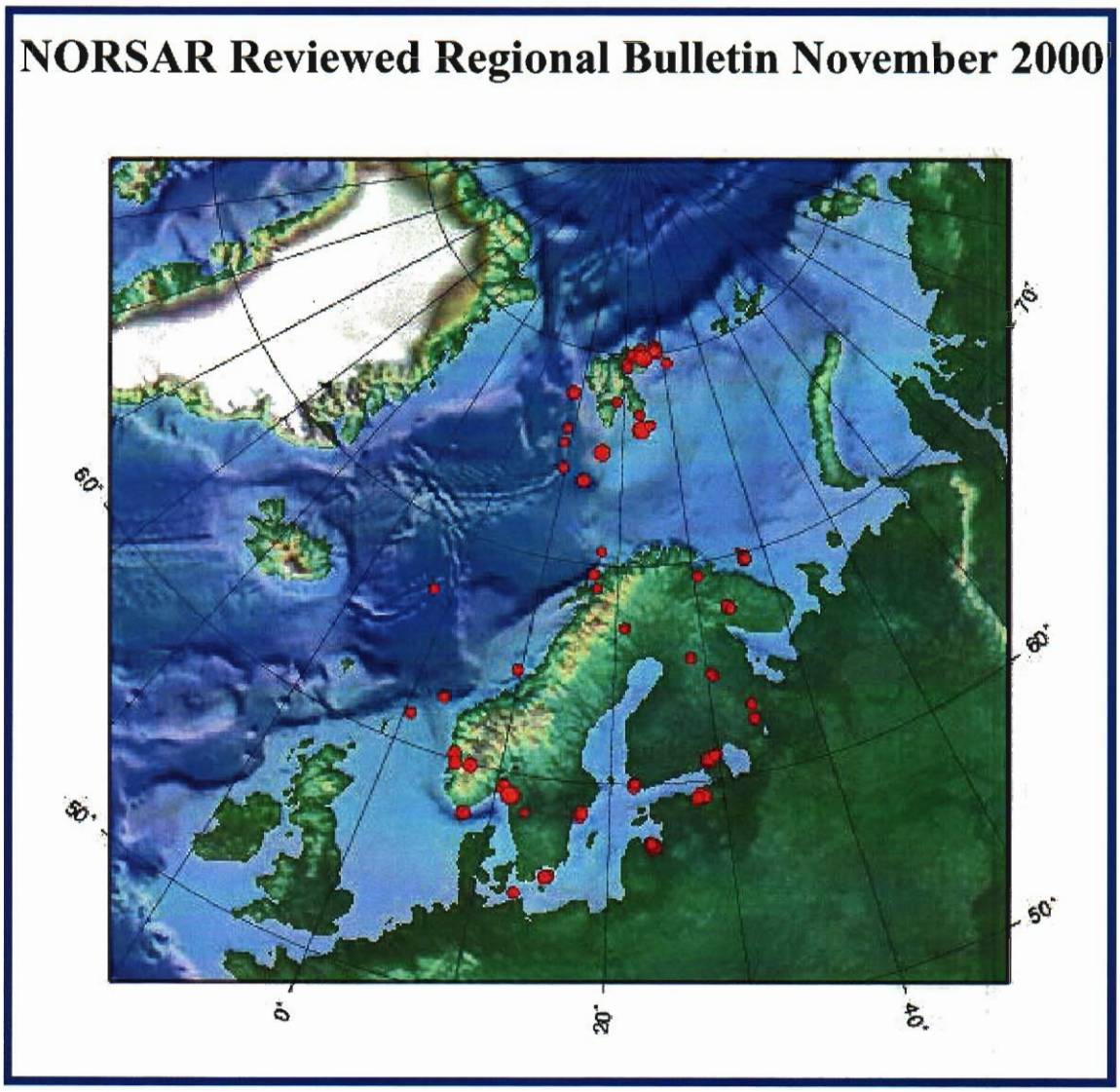

Figure 3.1: *After selecting a given month from a Web calendar, the corresponding map of events in NORSAR's Reviewed Regional Bulletin is displayed, in this case for November 2000. The size of the event symbols are proportional to the event magnitude. By clicking on the map we can zoom in on the following regions: South Norway, North Norway/Kola, Svalbard/Norwegian Sea, Finland/Baltic.*

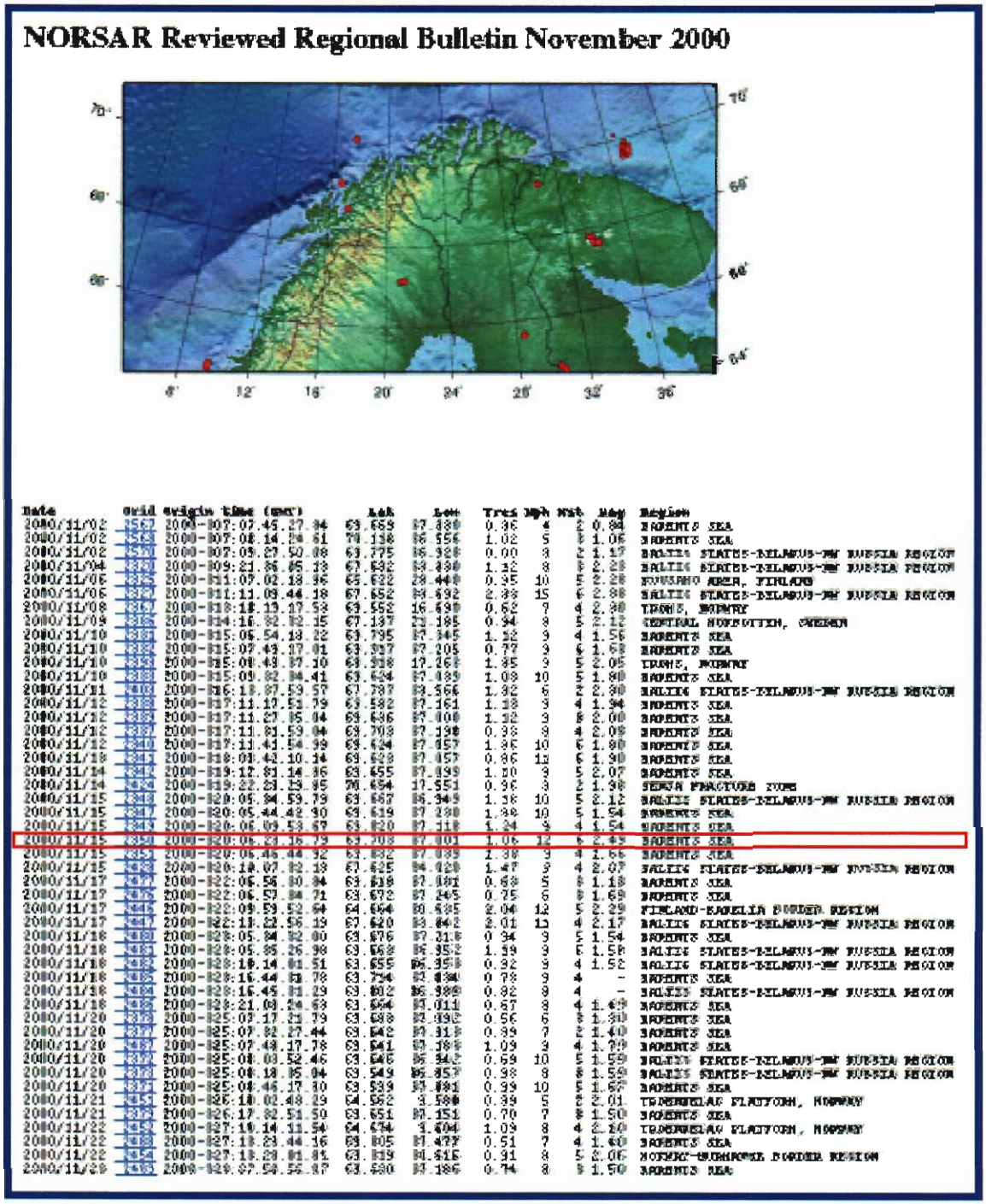

Date	Orid	origin time (GMT)	Lat	Lon	Trst	Nph	Nst	Mag	Region
2000/11/02	4567	2000-307:07.46.27.94	69.669	37.439	0.36	4	2	0.84	BARENTS SEA
2000/11/02	4568	2000-307:08.14.28.61	70.138	36.556	1.02	5	3	1.06	BARENTS SEA
2000/11/02	4569	2000-307:05.27.50.08	63.775	36.928	0.00	3	2	1.17	BALTIC STATES-BELARUS-NW RUSSIA REGION
2000/11/04	4570	2000-309:21.36.05.13	67.542	34.430	1.32	8	3	2.28	BALTIC STATES-BELARUS-NW RUSSIA REGION
2000/11/05	4571	2000-311:07.02.18.96	65.622	29.448	0.35	10	5	2.28	KUUSAMO AREA, FINLAND
2000/11/06	4572	2000-311:11.09.44.18	67.652	34.692	2.38	15	6	2.88	BALTIC STATES-BELARUS-NW RUSSIA REGION
2000/11/08	4573	2000-313:18.13.17.53	69.552	16.490	0.62	7	4	2.30	TROMS, NORWAY
2000/11/09	4574	2000-314:16.32.12.15	67.137	21.185	0.94	8	5	2.12	CENTRAL NORDSVEN, SWEDEN
2000/11/10	4575	2000-315:06.54.18.22	69.795	37.345	1.22	9	4	1.56	BARENTS SEA
2000/11/10	4576	2000-315:07.43.17.01	69.917	37.205	0.72	9	6	1.68	BARENTS SEA
2000/11/10	4577	2000-315:08.43.37.10	69.918	17.168	1.85	9	5	2.05	TROMS, NORWAY
2000/11/10	4578	2000-315:09.32.34.41	69.484	37.439	1.09	10	5	1.80	BARENTS SEA
2000/11/11	4579	2000-316:18.37.59.57	67.787	34.566	1.32	6	2	2.30	BALTIC STATES-BELARUS-NW RUSSIA REGION
2000/11/12	4580	2000-317:11.17.51.79	69.582	37.161	1.22	9	4	1.94	BARENTS SEA
2000/11/12	4581	2000-317:11.27.35.04	69.636	37.400	1.22	9	5	2.00	BARENTS SEA
2000/11/12	4582	2000-317:11.31.59.04	69.703	37.198	0.98	9	4	2.09	BARENTS SEA
2000/11/12	4583	2000-317:11.41.54.99	69.624	37.357	1.36	10	6	1.80	BARENTS SEA
2000/11/13	4584	2000-318:01.42.10.14	69.623	37.457	0.86	12	6	1.90	BARENTS SEA
2000/11/14	4585	2000-319:12.31.14.86	63.655	37.899	1.20	9	5	2.07	BARENTS SEA
2000/11/14	4586	2000-319:22.23.29.85	70.654	17.551	0.96	3	2	1.98	SENJA FRACTURE ZONE
2000/11/15	4587	2000-320:05.04.59.79	63.667	36.349	1.36	10	5	2.12	BALTIC STATES-BELARUS-NW RUSSIA REGION
2000/11/15	4588	2000-320:05.44.42.90	69.619	37.230	1.38	10	5	1.54	BARENTS SEA
2000/11/15	4589	2000-320:06.09.53.67	63.820	37.318	1.24	9	4	1.54	BARENTS SEA
2000/11/15	4590	2000-320:06.23.16.79	69.708	37.801	1.06	12	6	2.45	BARENTS SEA
2000/11/15	4591	2000-320:06.46.44.92	63.832	37.885	1.38	9	4	1.66	BARENTS SEA
2000/11/15	4592	2000-320:10.07.32.19	67.425	34.020	1.47	9	4	2.07	BALTIC STATES-BELARUS-NW RUSSIA REGION
2000/11/17	4593	2000-322:06.56.30.84	69.618	37.181	0.69	5	3	1.18	BARENTS SEA
2000/11/17	4594	2000-322:06.57.34.71	63.672	37.245	0.75	6	3	1.69	BARENTS SEA
2000/11/17	4595	2000-322:09.59.52.64	64.664	30.535	2.04	12	5	2.29	FINLAND-KARELIA BORDER REGION
2000/11/17	4596	2000-322:11.22.56.19	67.620	33.842	2.01	13	4	2.17	BALTIC STATES-BELARUS-NW RUSSIA REGION
2000/11/18	4597	2000-323:05.34.32.00	63.676	37.218	0.94	9	5	1.54	BARENTS SEA
2000/11/18	4598	2000-323:05.35.26.98	63.662	36.952	1.19	9	5	1.58	BALTIC STATES-BELARUS-NW RUSSIA REGION
2000/11/18	4599	2000-323:10.14.01.51	63.655	36.359	0.92	9	4	1.52	BALTIC STATES-BELARUS-NW RUSSIA REGION
2000/11/18	4600	2000-323:16.44.53.78	63.724	37.430	0.78	9	4	-	BARENTS SEA
2000/11/18	4601	2000-323:16.45.01.29	63.802	36.989	0.82	9	4	-	BALTIC STATES-BELARUS-NW RUSSIA REGION
2000/11/18	4602	2000-323:21.08.24.69	63.664	37.011	0.67	8	4	1.49	BARENTS SEA
2000/11/20	4603	2000-325:07.17.21.79	63.688	37.992	0.56	6	3	1.30	BARENTS SEA
2000/11/20	4604	2000-325:07.32.27.44	69.642	37.318	0.89	7	2	1.40	BARENTS SEA
2000/11/20	4605	2000-325:07.48.17.78	63.641	37.186	1.09	8	4	1.29	BARENTS SEA
2000/11/20	4606	2000-325:08.03.52.46	63.648	36.342	0.69	10	5	1.59	BALTIC STATES-BELARUS-NW RUSSIA REGION
2000/11/20	4607	2000-325:08.18.05.04	63.549	36.857	0.98	8	5	1.59	BALTIC STATES-BELARUS-NW RUSSIA REGION
2000/11/20	4608	2000-325:08.46.17.30	63.539	37.891	0.99	10	5	1.67	BARENTS SEA
2000/11/21	4609	2000-326:10.02.48.29	64.562	3.588	0.39	5	2	2.01	TRONDHEIMS FJORDEN, NORWAY
2000/11/21	4610	2000-326:17.32.51.50	63.651	37.151	0.70	7	3	1.50	BARENTS SEA
2000/11/22	4611	2000-327:10.14.11.54	64.574	3.604	1.09	8	4	2.10	TRONDHEIMS FJORDEN, NORWAY
2000/11/22	4612	2000-327:10.23.44.16	63.805	37.477	0.51	7	4	1.40	BARENTS SEA
2000/11/22	4613	2000-327:10.28.01.81	63.819	36.816	0.91	8	5	2.06	NORWAY-RUSSIAN BORDER REGION
2000/11/23	4614	2000-328:07.50.55.87	63.680	37.186	0.74	8	3	1.50	BARENTS SEA

Figure 3.2: *After clicking on the Kola region of* ***Figure 3.1****, this window is shown. Below the map with event symbols follows a summary list with the basic event information (Origin Id, Origin Time, Location, Magnitude and Region). More information on each event can be found by mouse clicking on the Origin Id (Orid).*

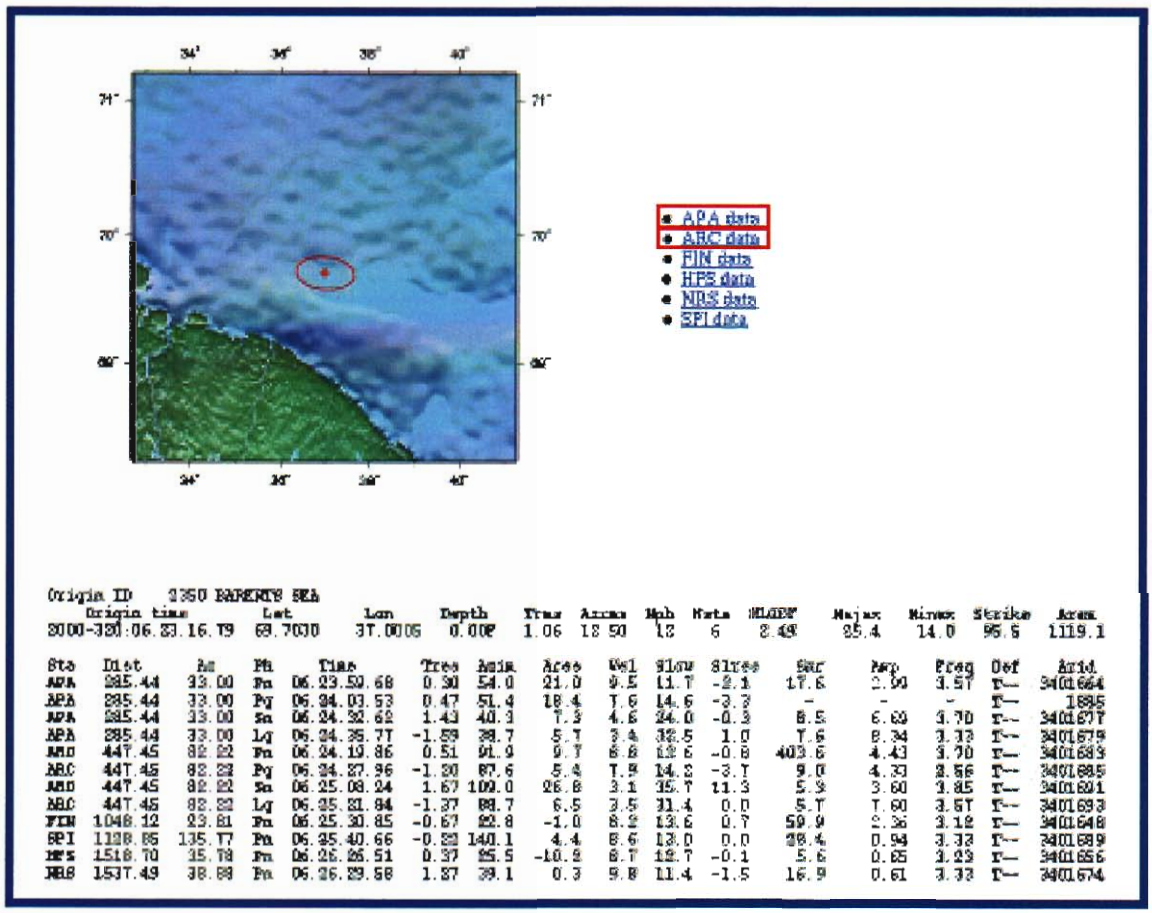

Figure 3.3: *After clicking on Orid 2350 of* ***Figure 3.2****, this window is displayed. This is an event (explosion) in the Kursk accident area. Below the high resolution map showing the event location and the associated error ellipse, follows the detailed bulletin information for this event including the phase readings. For each station used in the event location a station field is displayed to the right of the map. By clicking on a station field, the station waveforms for the given event will be shown.*

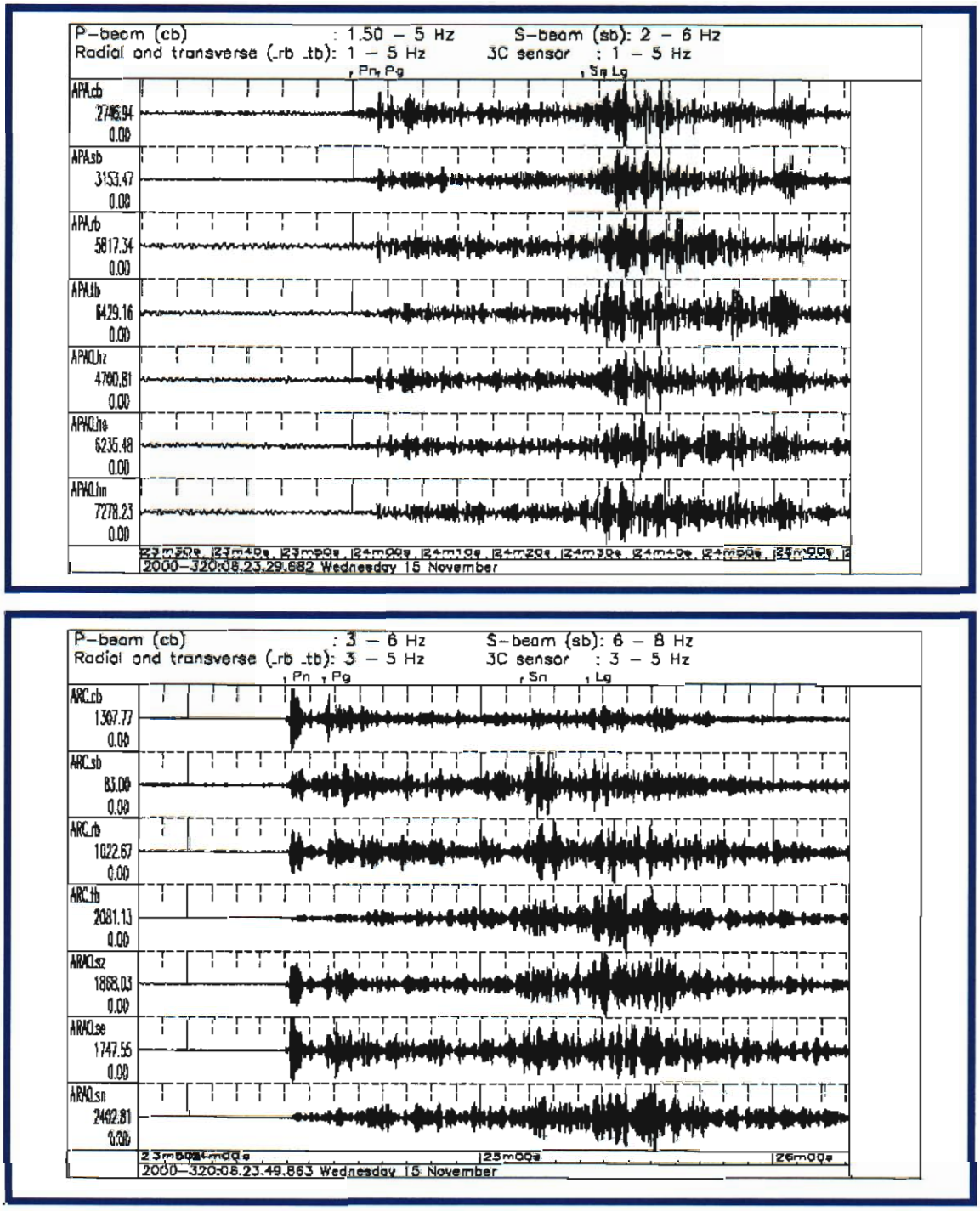

Figure 3.4: *Apatity and ARCES waveforms for Orid 2350. The small markers on top of the plots show the analyst reviewed phase readings. The traces correspond to various array beams and single channels, and have been filtered in a bandpass filter designed to enhance various phases. The top trace is a P-type beam focusing on the first arrivals. The second trace is an S-type beam, and traces nos. 3 and 4 are the radial and transverse components, all focusing on the S-phases. The three lower traces show the data of the three-component sensor located centrally within the arrays.*

3.3 Pn station magnitudes

In the time period 10 November 2000 to 28 February 2001 NORSAR's regional bulletin contains a total of 376 events. Since 10 November 2000 all data have been stored permanently on disk and can thereby be directly accessed by any analysis program. We have therefore developed an application which analyzes phase amplitudes reported in the regional bulletin. The main purpose of this research has been to validate the time-domain measurements to be used for regional threshold monitoring and to evaluate the regional phase attenuation models of Jenkins et al. (1998).

So far we have focused our attention to the Pn phase, but we also plan to include analysis of the other regional phases (Pg, Sn, Lg).

The Pn amplitude was measured on a beam steered with the azimuth and apparent velocity estimated from f-k analysis. The amplitude was measured in four different frequency bands using the short-term-average (STA) within a 5 second window starting at the onset of the arriving phase. The frequency bands used were 2-4 Hz, 3-6 Hz, 4-8 Hz, and 8-16 Hz.

The time-domain STA amplitudes of each filter band were made comparable with the spectral amplitudes used by Jenkins et al. (1998) using the following relation:

$$\overline{A} \approx \frac{STA \cdot resp_{f_c}}{f_c}$$

where f_c is the center frequency of the passband and $resp_{f_c}$ is the displacement response at this center frequency. The amplitudes were then corrected for frequency dependent attenuation using the distance dependent term

$$acorr = \left(\frac{\Delta}{200}\right)^{-(af_c+b)}$$

where Δ is the distance in km, f_c is the center frequency and a and b are the Pn attenuation coefficients derived by Jenkins et al. (1998) for stable continental regions ($a = 0.08$, $b = 1.44$).

Station magnitudes were then calculated using the relation

$$stamag = log_{10}(\overline{A} \cdot acorr)$$

Notice that the absolute scale of these station magnitudes is arbitrary, but that they are internally consistent for measurements within each separate frequency band. The problem of addressing the absolute scale of the station magnitudes will be discussed at a later stage.

3.4 Statistics on Pn station magnitudes

For each of the four frequency bands both the Pn amplitude and the corresponding signal-to-noise ratio (SNR) were measured. The frequency band 3 to 6 Hz provides the overall best SNR for the Pn phases analyzed in this study, and we will in the following present statistics on the station magnitudes for this frequency band considering phases with SNR > 3.

Out of the total number of 376 events, 75 were associated with explosions detonated in the vicinity of the site of the submarine Kursk accident. **Figures 3.5** and **3.6** show pairwise comparisons of Pn station magnitudes, using ARCES as the reference station. We have split the events into two groups.

- Events not in the Kursk accident area
- Events in the Kursk accident area, believed to have a location scatter of a few tens of kilometers

ARCES-the Apatity array

The two upper panels of **Figure 3.5** show the comparison between ARCES and the Apatity array. The 36 events not in the Kursk accident area are quite randomly distributed on mainland Fennoscandia and in the western part of the Barents Sea, as exemplified in **Figure 3.1**. The Pn magnitudes at the Apatity array have a negative bias of -0.135 as compared to ARCES, and the magnitude difference has a scatter of 0.263.

For the 57 events in the Kursk accident area satisfying the SNR criterion, the Apatity array has a comparable negative bias (-0.137) seen in relation to ARCES, and the magnitude difference has a slightly smaller scatter of 0.196.

ARCES-SPITS

The two middle panels of **Figure 3.5** show the comparison between ARCES and SPITS. The 50 events not in the Kursk accident area are almost all located in the western part of the Barents Sea and on the mid-Atlantic ridge. The Pn magnitudes at SPITS have a consistent positive bias of 0.228 as compared to ARCES, and the magnitude difference has a scatter of 0.328.

For the 23 events in the Kursk accident area the positive bias is only 0.09 with a scatter of 0.143.

Six events in the Khibiny Massif area are the only events from mainland Fennoscandia providing Pn observations at SPITS. For these six events SPITS has a negative bias of -0.333 as compared to ARCES, and the magnitude difference has a scatter of 0.122.

ARCES-FINES

The two lower panels of **Figure 3.5** show the comparison between ARCES and FINES. The 121 events not in the Kursk accident area are quite randomly distributed on mainland Fennoscandia and a few events are located on the mid-Atlantic ridge. The Pn magnitudes at FINES have a negative bias of -0.119 as compared to ARCES, and the magnitude difference has a scatter of 0.264.

For the 48 events in the Kursk accident area, FINES has a very large positive bias as compared to ARCES (0.473), and the scatter is only 0.168.

For the five common events located in the Khibiny Massif, the pattern is quite reversed. FINES has a negative bias of -0.638 as compared to ARCES, and the scatter is 0.132.

ARCES-NORES

The two upper panels of **Figure 3.6** show the comparison between ARCES and NORES. The 106 events not in the Kursk accident area are quite randomly distributed on mainland Fennoscandia and a few events are located on the mid-Atlantic ridge. The Pn magnitudes at NORES have a small negative bias of -0.025 as compared to ARCES, and the magnitude difference has a scatter of 0.277.

For the 14 common events in the Kursk accident area, NORES has a consistent positive bias as compared to ARCES (0.219) with a scatter of 0.129.

For the five common events located in the Khibiny Massif, the pattern is again quite different. NORES has a negative bias of -0.401 as compared to ARCES, and the scatter is 0.119.

ARCES-HFS

The two middle panels of **Figure 3.6** show the comparison between ARCES and HFS. The 80 events not in the Kursk accident area are quite randomly distributed on mainland Fennoscandia and a few events are located on the mid-Atlantic ridge. The Pn magnitudes at HFS has a positive bias of 0.198 as compared to ARCES, and the magnitude difference has a scatter of 0.264.

For the common events in the Kursk accident area, HFS has a positive bias of 0.501 as compared to ARCES, with a scatter of 0.213, but the number of events (5) is very low.

NORES-HFS

NORES and HFS are located only 135 km apart, and we would like to investigate any systematic biases in Pn station magnitudes between these stations. The two lower panels of **Figure 3.6** show the comparison between NORES and HFS, and we see that HFS has a consistent positive bias of 0.221, with a standard deviation of 0.211, for the 98 events outside the Kursk area. The number of events (3) within the Kursk area is too low to draw any conclusions.

We have earlier experienced that HFS also consistently provides larger M_L estimates than NORES, based on Lg amplitudes. With these observations at hand we would like to further investigate this, e.g., by comparing the background noise levels and by independent measurements of the system response at HFS. The NORES system response has been verified through several independent measurements.

3.5 Summary

The pairwise comparisons of the station magnitudes confirm that the Pn regional phase attenuation model of Jenkins et al. (1998) is a valid approximation for Fennoscandia and adjacent areas. Excluding events in the Kursk accident area, the pairwise scatter with ARCES is almost similar (0.26-0.28) for all arrays on mainland Fennoscandia (Apatity, FINES, NORES, and HFS). For SPITS the scatter is somewhat larger (0.328), but the majority of these events are located in the western part of the Barents Sea and on the mid-Atlantic ridge, which may have a more tectonic style of Pn attenuation characteristics.

We conclude that it is possible to develop a Pn-based regional magnitude scale for Fennoscandia and adjacent waters with a pairwise "scatter" (or standard deviation) of 0.26-0.28. This excludes the tectonic areas near the Mid-Atlantic ridge, as discussed above.

If we assign equal variance to the individual array estimates (which would seem to be a reasonable assumption), the inherent single array magnitude scatter would be 0.2 magnitude units (dividing by $\sqrt{2}$) and in the Khibiny area about 0.10.

There is clearly a potential for improvement (i.e. reduced scatter) by regionalization. However, it would appear that it is necessary to limit the subregions to very small geographical areas to obtain significant improvements.

In Section 5, we will extend the analysis described in this section to include attenuation of all the major regional phases (Pn, Pg, Sn, Lg), including investigating the tradeoffs involved in detailed regionalization of attenuation relations. For this purpose, we need to develop a more carefully analyzed reference data base, i.e. with more emphasis on reading secondary phases that is done in the NORSAR analyst reviewed bulletin, and this will be the topic of the next section (Section 4).

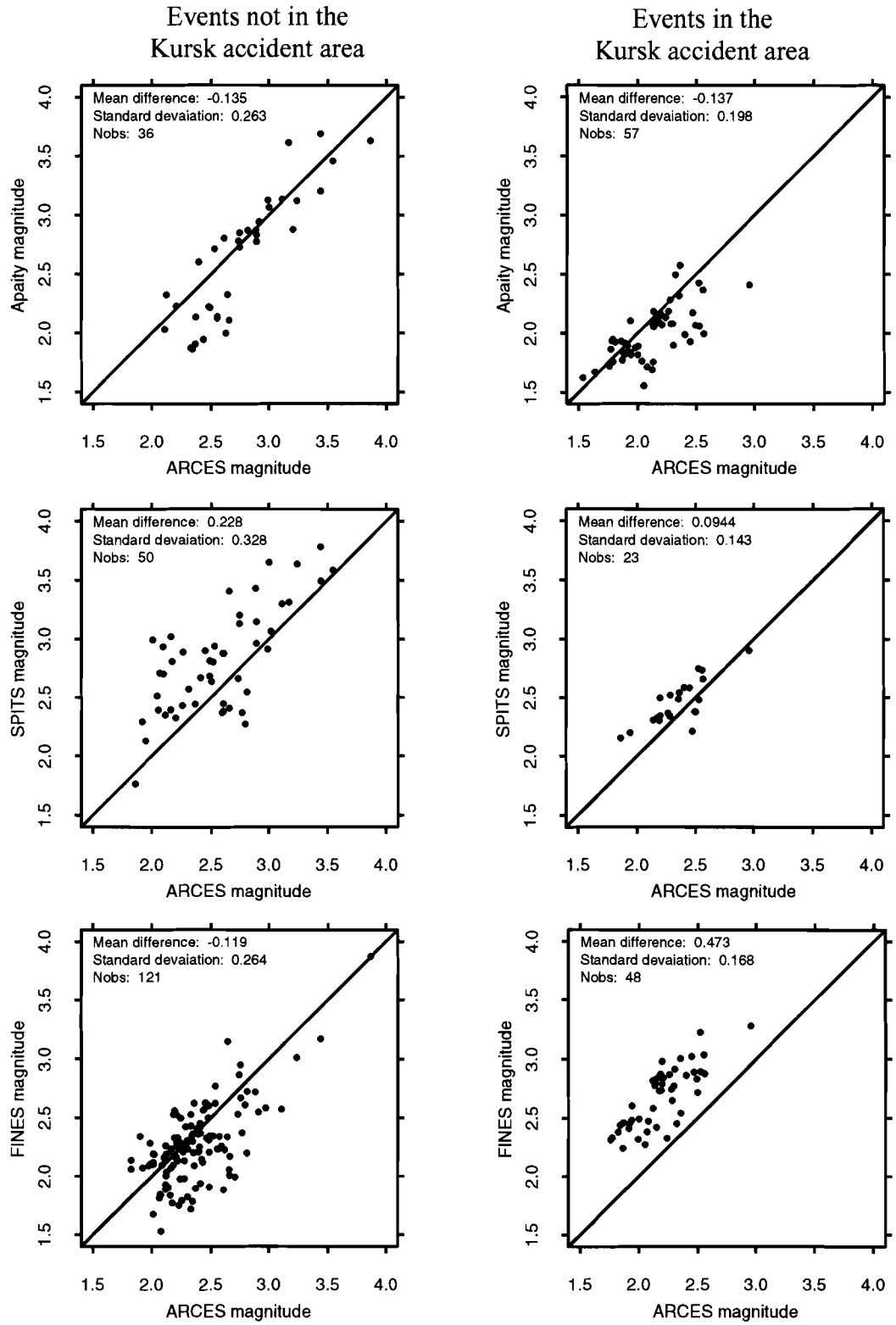

Figure 3.5: *Pairwise comparisons of STA-based Pn station magnitudes in the frequency band 3.0-6.0 Hz. Notice that the absolute level of the magnitude scale is not yet determined, such that the plots only give information on the internal consistency.*

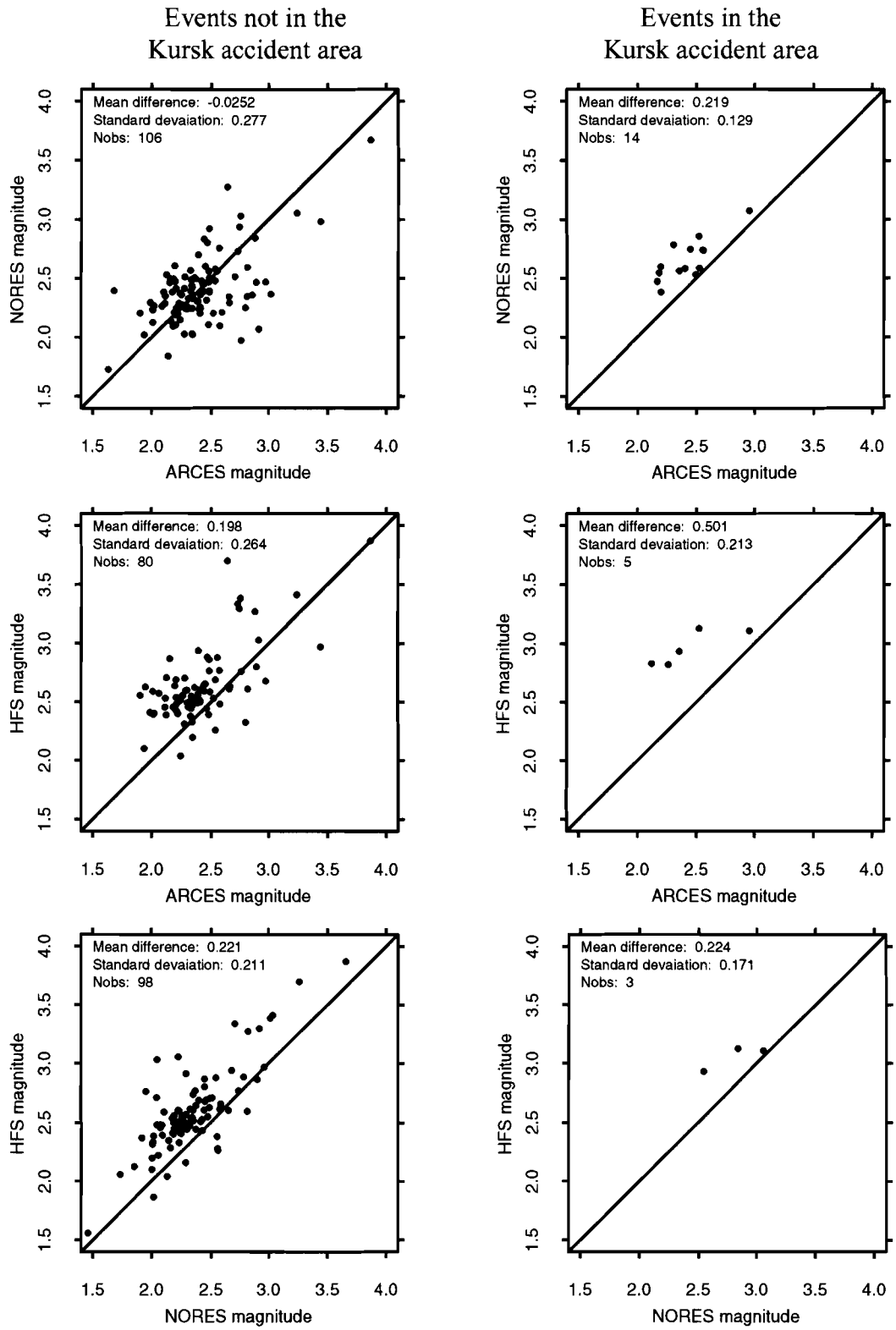

Figure 3.6: *Pairwise comparisons of STA-based Pn station magnitudes in the frequency band 3.0-6.0 Hz. Notice that the two lower plots contain a comparison between NORES and HFS.*

4. Development of a regional database

The work described in this chapter relates to the development of a regional database for the European Arctic, with emphasis on accurate and consistent reading of all discernible phases on the seismograms.

Access to applicable amplitude attenuation curves for the different regional phases is key to this project. The study by Jenkins et al. (1998) provides useful results on this subject for regional phases in Fennoscandia as well as in other stable tectonic regions.

Another important input parameter to regional seismic threshold monitoring is the uncertainty associated with the regional phase attenuation models. From pair-wise comparisons of P-amplitudes from the explosions detonated in the area near the Kursk accident, we find for the arrays on mainland Fennoscandia (ARCES, Apatity, FINES, NORES, and HFS) an inherent single-array magnitude scatter (standard deviation) of about 0.10-0.13 magnitude units (see Section 3 of this report).

The locations of these explosions show a distribution over a 30-50 km wide area, which is significantly smaller than the resolution of a regional threshold monitoring scheme for Novaya Zemlya and adjacent waters of the Kara and Barents Seas. This suggests that we would be unable to operate any regional threshold monitoring application with a uncertainty better than 0.1 magnitude units for P-phases. Preliminary data analysis (see section 3) indicates that an existing regional P-based attenuation model for Fennoscandia and adjacent areas exhibits a scatter of about 0.25 magnitude units when considering events in the entire Barents Sea region.

4.1 An event database for Novaya Zemlya and adjacent waters of the Kara and Barents Seas

As an integral part of our work to develop an optimized, automatic capability to monitor the seismicity of Novaya Zemlya and adjacent waters of the Kara and Barents Seas, a database of records from seismic events in the area has been compiled, based on information contained in bulletins published by various agencies.

The initial database comprised records from 43 events (see **Figure 4.1** and **Table 4.1**), carefully selected so as to cover the area with ray paths in the best possible way. Since the major part of the area under study is basically aseismic, the majority of the events in this database is confined to Svalbard, the western Barents Sea, northern Norway, the Kola Peninsula and Novaya Zemlya. The events are earthquakes, mining blasts, other chemical and nuclear explosions, and some are of unknown nature. Magnitudes range from 2 to 4.5, except for two nuclear explosions with magnitudes exceeding 5. Records have been compiled from the ARCES, FINES, NORES, Apatity and Spitsbergen arrays and from the Amderma 3-component station, and have been supplemented by waveforms for KBS, KEV and LVZ requested from Incorporated Research Institutions for Seismology (IRIS). **Figures 4.2-4.4** show the ray-paths to the stations SPITS, ARCES and Amderma (AMD).

All events have been reanalyzed, and revised event origins as well as consolidated phase identifications have been obtained. **Figures 4.5** and **4.6** show analyzed waveforms for two events in the database

The database is being used to determine travel times and frequency-dependent attenuation relations for the various regional phases. This effort will also provide information on the efficiency of Sn and Lg propagation in this area and its correlation with regional geological structures. The information derived from this study will be quantified in terms of parameters that will be needed in the regional seismic threshold monitoring of Novaya Zemlya and adjacent areas.

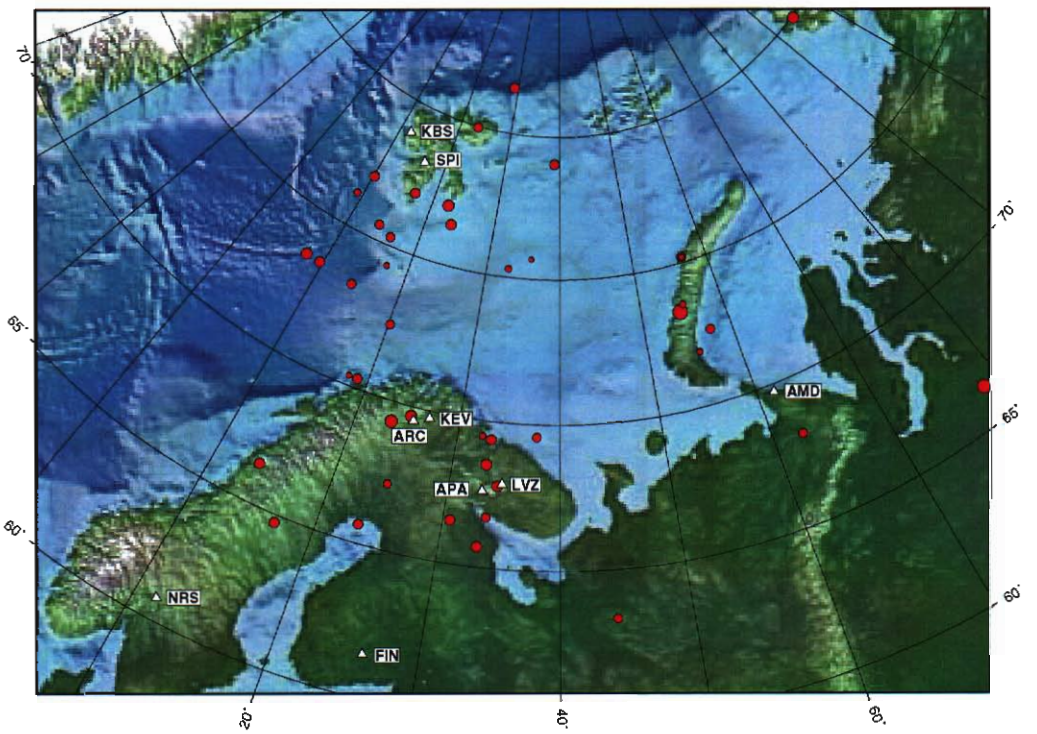

Figure 4.1. *Map with events and stations used for deriving wave propagation characteristics of the Barents Sea and adjacent areas. The event symbol sizes are proportional to the event magnitudes.*

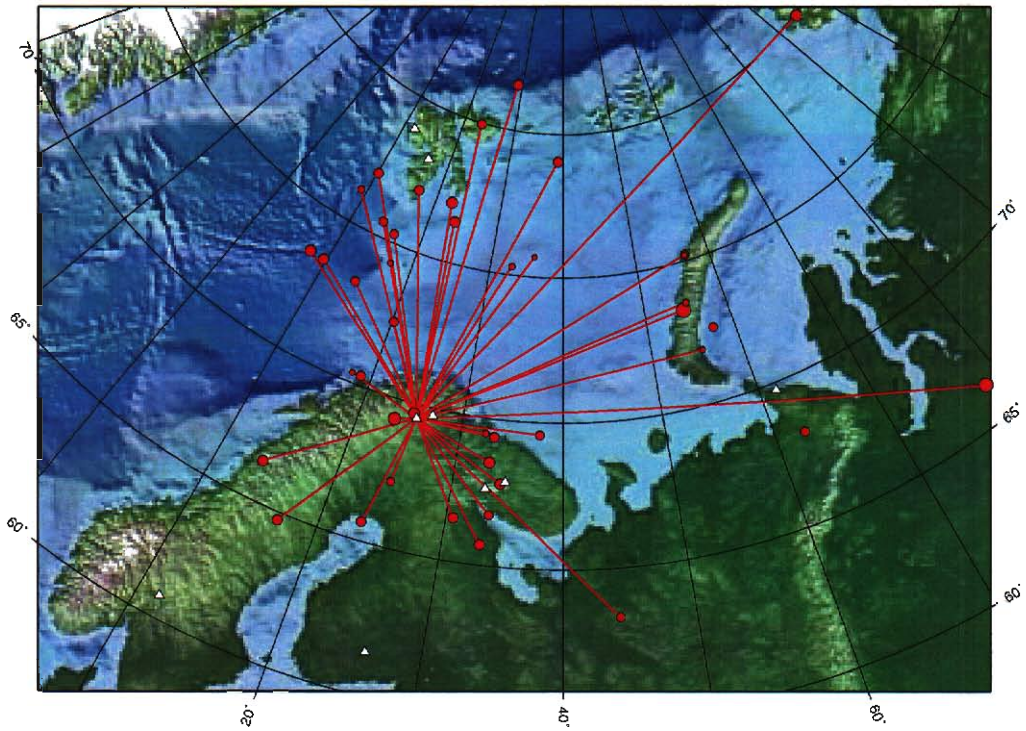

Figure 4.2. *Map showing the ray-paths of the database events recorded at the ARCES array.*

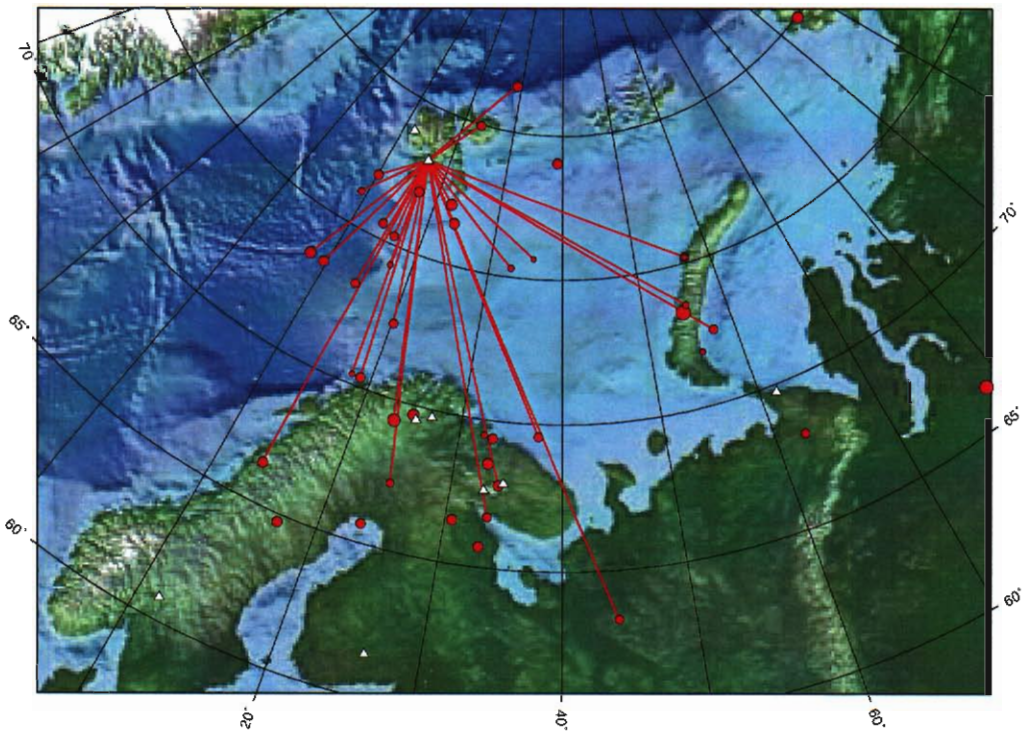

Figure 4.3. *Map showing the ray-paths of the database events recorded at the SPITS array.*

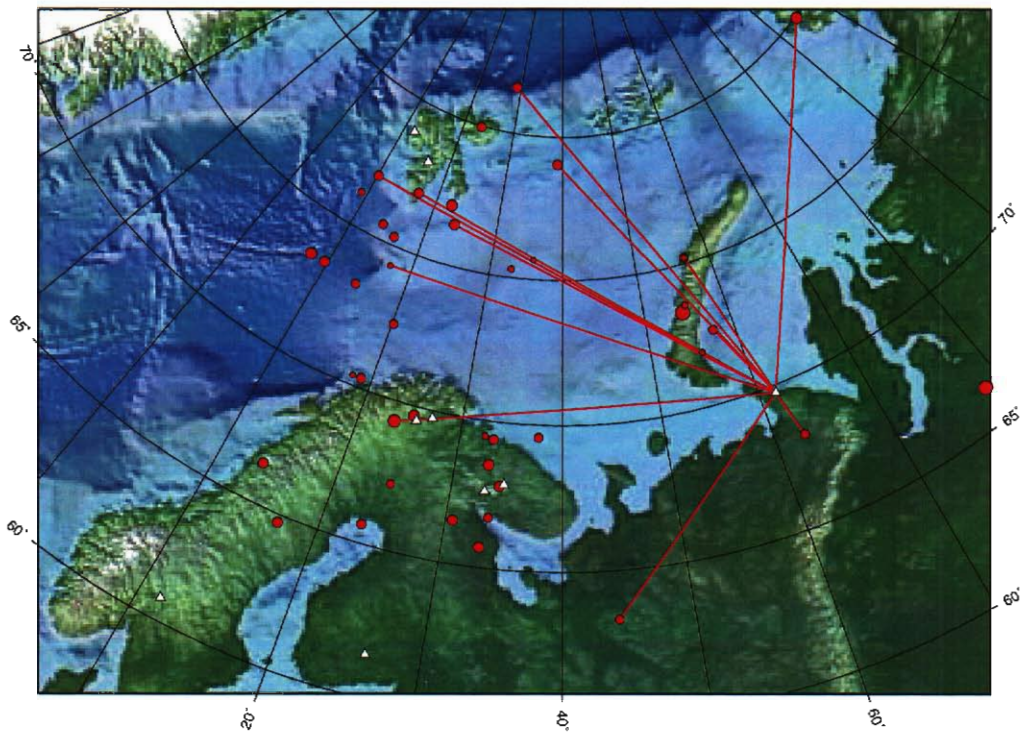

Figure 4.4. *Map showing the ray-paths of the database events recorded at the Amderma station.*

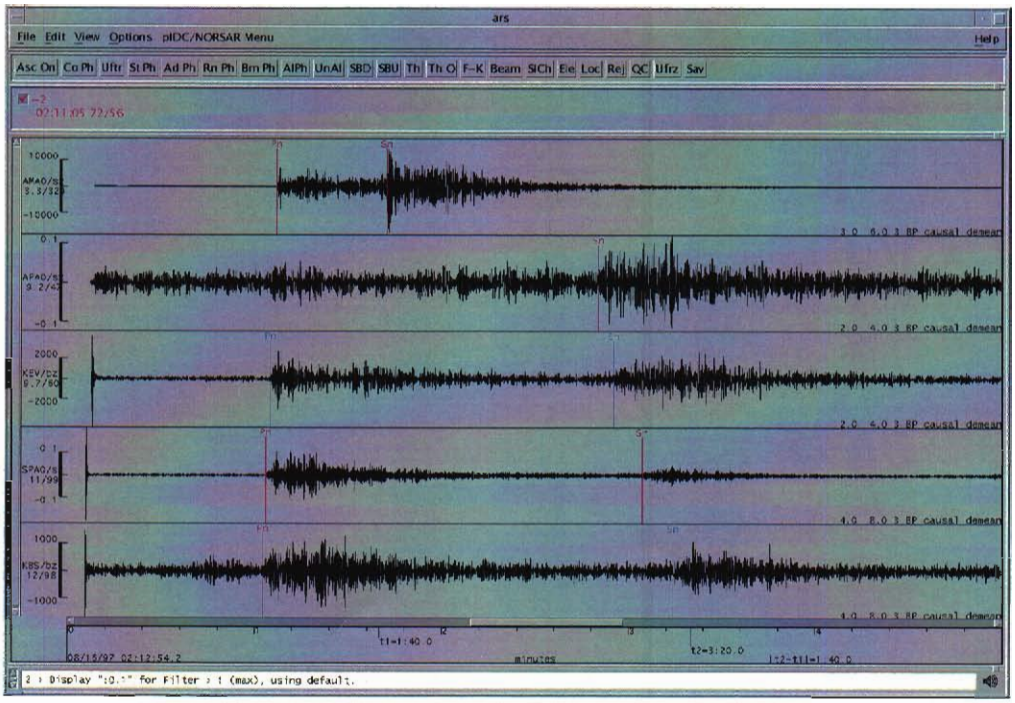

Figure 4.5. *Panels showing the results after analyst review of the 16 August 1997 event located in the Kara Sea. Notice that Sn is the dominating secondary phase, whereas the Lg phase is almost absent. The panels show vertical-component recordings at the following stations from top to bottom: 1-Amderma, 2-Apatity, 3-KEV, 4-SPITS, and 5-KBS.*

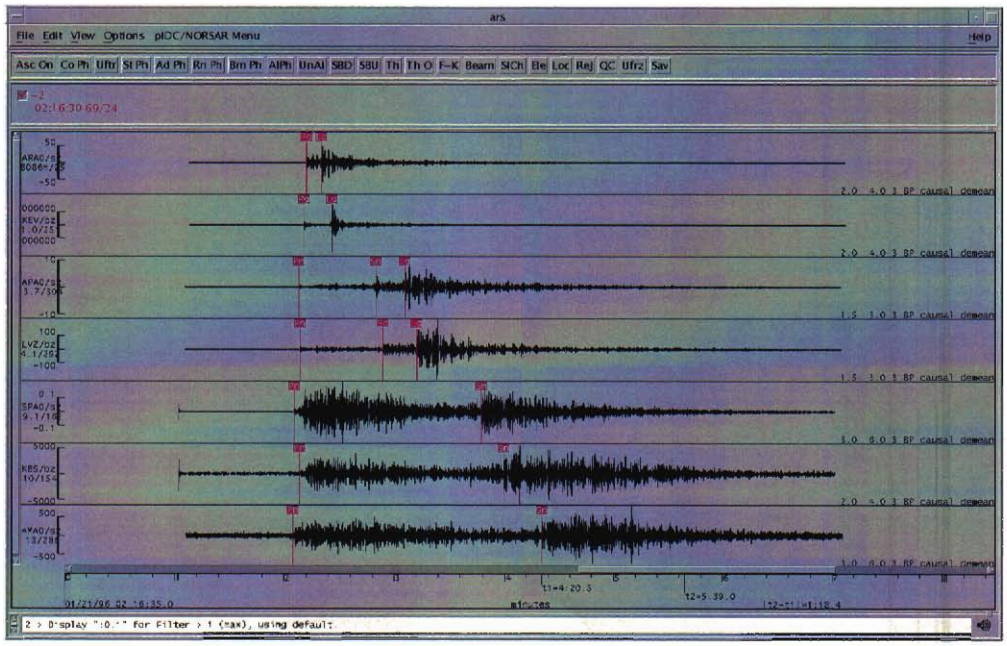

Figure 4.6. *Panels showing the results after analyst review of the 21 January 1996 event located in Finnmark, northern Norway. Again, notice the absence of Lg for paths crossing the Barents Sea. The panels show vertical component recordings at the following stations from top to bottom: 1-ARCES, 2-KEV, 3-Apatity, 4-LVZ, 5-SPITS, 6-KBS, and 7-AMD.*

Table 4.1: Origin time, location, magnitude, and recording stations of the events in the assembled database.

Date/time	Lat.	Lon.	Mag.	Stations
1988-235:16.20.00.07	66.280	78.461	5.3	ARC, NRS
1990-167:12.43.27.7	68.523	33.090	4.3	ARC, NRS
1990-297:14.57.58.3	73.360	54.670	5.6	ARC, FIN, NRS
1991-157:12.46.15.5	65.637	23.232	3.7	ARC, FIN, NRS
1991-236:10.56.29.0	65.7	33.1	4.0	ARC, FIN
1992-366:09.29.24.0	73.6	55.2	2.7	ARC, FIN, SPI
1993-005:10.19.36.4	64.740	16.894	4.0	APA, ARC, FIN, LVZ, NRS
1995-013:04.34.37.6	74.320	17.190	2.5	AMD, ARC, FIN, KBS, KEV, LVZ, NRS, SPI
1995-021:01.58.07.7	70.330	17.970	2.5	APA, ARC, FIN, LVZ, NRS, SPI
1995-054:21.50.00.0	71.856	55.685	2.5	AMD, ARC
1995-063:18.29.03.9	81.600	28.990	3.6	AMD, APA, ARC, FIN, KBS, KEV, LVZ, NRS, SPI
1995-101:20.07.26.2	79.050	39.000	3.7	AMD, ARC, FIN, KBS, KEV, LVZ, NRS
1995-102:08.18.52.7	69.390	33.260	3.8	APA, ARC, FIN, KBS, KEV, LVZ
1995-133:22.38.52.0	76.950	10.170	3.6	AMD, APA, ARC, FIN, KBS, KEV, LVZ, NRS, SPI
1995-161:18.45.32.6	75.704	35.865	2.1	ARC, KBS, SPI
1995-162:19.27.21.1	75.302	32.896	2.7	ARC, APA, FIN, KBS, LVZ, SPI
1995-164:19.22.37.9	75.200	56.700	3.5	AMD, APA, FIN, KBS, LVZ, SPI
1995-184:12.49.35.0	69.680	25.150	4.3	APA, ARC, FIN, KBS, KEV
1995-185:03.26.15.2	79.930	94.920	4.4	AMD, ARC, FIN, KBS, KEV
1995-241:22.12.14.4	77.040	22.500	4.3	APA, ARC, FIN, NRS, SPI
1995-261:03.26.05.8	66.480	30.600	4.0	APA, ARC, FIN, KEV, LVZ, NRS
1995-313:01.10.24.5	66.730	33.580	3.4	APA, ARC, FIN, KEV, LVZ, NRS, SPI
1995-329:19.41.26.0	77.050	16.980	3.6	AMD, APA, ARC, FIN, KBS, KEV, LVZ, NRS, SPI
1996-013:17.17.23.0	75.200	56.700	2.4	AMD, ARC, SPI
1996-021:02.16.24.5	69.324	23.431	4.8	AMD, APA, ARC, FIN, KBS, KEV, LVZ, NRS, SPI
1996-218:20.04.37.5	75.530	14.080	3.5	APA, ARC, FIN, KBS, KEV, LVZ, NRS, SPI
1996-272:06.08.44.6	69.480	32.410	2.7	APA, ARC, LVZ
1996-301:23.55.15.4	79.960	23.430	3.5	APA, ARC, KBS, KEV, SPI

Table 4.1: Origin time, location, magnitude, and recording stations of the events in the assembled database.

Date/time	Lat.	Lon.	Mag.	Stations
1996-361:04.41.11.2	63.350	44.310	3.4	AMD, APA, ARC, FIN, KBS, KEV, LVZ, NRS, SPI
1997-012:09.37.16.8	68.070	62.720	3.4	AMD
1997-122:07.31.16.5	72.465	20.195	3.5	APA, ARC, KBS, KEV, LVZ, SPI
1997-228:02.11.00.0	72.510	57.550	3.5	AMD, APA, FIN, KBS, KEV, NRS, SPI
1997-279:12.33.29.4	76.429	23.689	4.1	AMD, APA, ARC, FIN, NRS, SPI
1997-279:21.17.26.4	73.417	9.622	4.0	ARC, NRS, KBS, KEV, LVZ, SPI
1997-279:21.29.17.8	73.435	7.714	4.2	ARC, KBS, NRS, SPI
1999-229:04.44.38.27	67.821	34.258	3.9	APA. AMD. ARC. FIN, KBS, KEV, NRS. SPI
1999-290:12.07.15.99	70.332	18.921	3.7	APA, FIN, KBS, KEV, LVZ, NRS, SPI
2000-225:07.30.41.76	69.573	37.643	3.5	AMD, APA, ARC, FIN, KBS, KEV, LVZ, NRS, SPI
2000-316:02.01.05.1	75.289	16.199	3.5	APA, ARC, FIN, KBS, LVZ, SPI
2000-341:00.34.43.2	76.160	9.136	2.9	APA, ARC, FIN, KBS, LVZ, SPI
2000-360:03.50.28.8	73.254	14.186	3.4	APA, ARC, FIN, KBS, KEV, LVZ, NRS, SPI
2001-090:11.30.54.29	66.354	13.783	4.0	APA, ARC, FIN, KBS, KEV, LVZ, NRS, SPI
2001-122:15.59.45.0	67.23	24.68	3.1	APA, ARC, FIN, KBS, LVZ, NRS, SPI

4.2 Phase mapping

A map showing events with Pn, Sn, Pg and Lg phase readings for the ARC station is shown in **Figure 4.7**. For each event, only the regional phases that could be 'clearly' observed were picked and used in the subsequent event location. The figure shows that Pg and Lg phases are generally only observed for events within the Baltic shield area. This observation is very important, and confirms and amplifies previous studies indicating the blockage of the Lg phase for paths crossing the Barents Sea. The absence of visible Pg and Lg phases for these paths is presumably due to the presence of large sedimentary structures in the central Barents Sea. We also note from the figure that Pn and Sn are generally visible at distances above 2-3 degrees. We have therefore initially concentrated our efforts on the Pn and Sn phases, as they offer the broadest and most consistent range of distance coverage. However, similar relations can readily be calculated for Pg and Lg using the methods developed during the work with the Pn and Sn phase data, should it be deemed necessary at a later date.

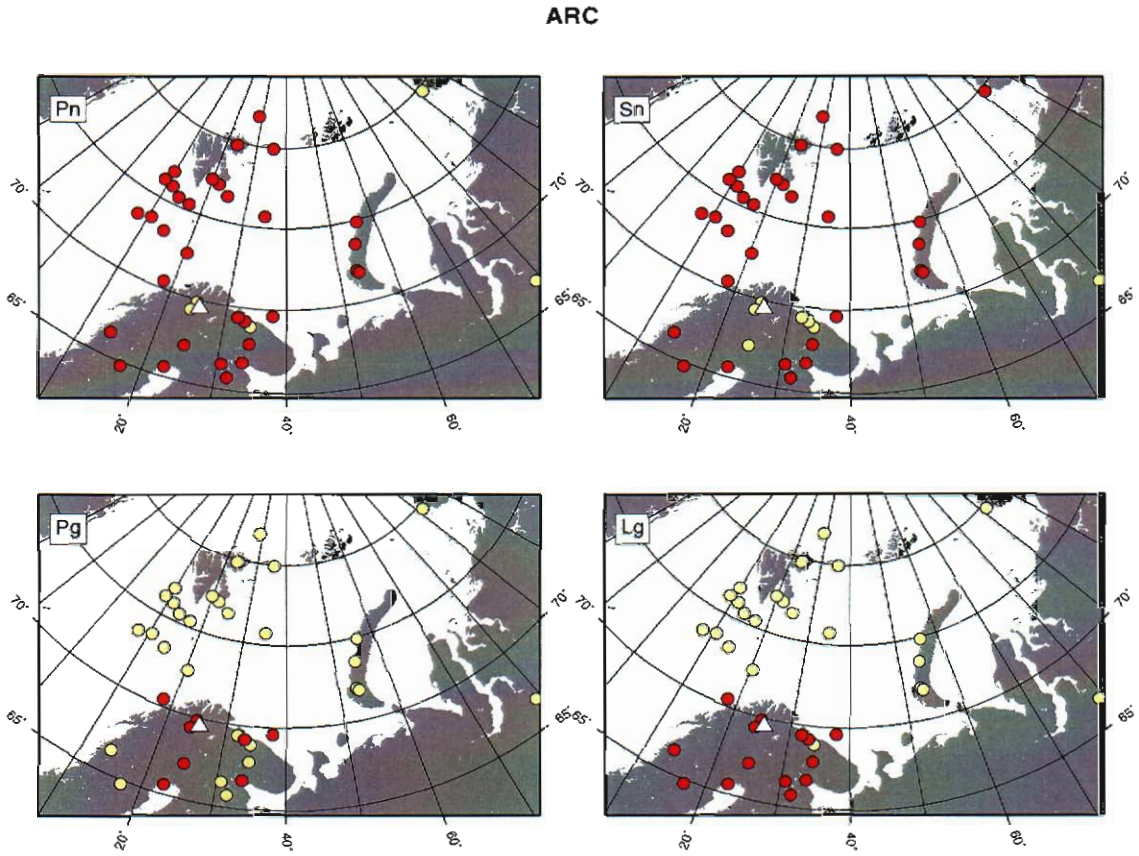

Figure 4.7. Phase observations shown as dark circles for Pn (upper left), Pg (lower left), Sn (upper right) and Lg (lower right) phases from the ARC station (white triangle). The light circles represent events with non-observable phases of the kind in question, but for which at least one other phase is visible.

4.3 Travel times and crustal model selection

An initial relocation of the 43 events in the database was performed during the re-analysis, using a crustal model for the Fennoscandia region, shown in **Table 4.2**. A fixed source depth of 10 km was used for all events. This model has a reasonably good, but not perfect fit to the observed arrival times, as shown by the travel-time curves in **Figure 4.8**. The Lg-phase arrivals have on the average a systematic and quite large negative residual, while the Sn phase arrivals tends to have positive residuals. The Pn arrivals in general have mostly negative residuals, most obvious around the 6 - 12 degree distance range. A relocation using the 'Barey' model for the Barents Sea (Schweitzer & Kennett, 2001) shown in **Table 4.2** gave much more consistent results between observed and theoretical travel times, as shown in **Figure 4.9**. The results are considered good enough that this model will

be used to calculate the theoretical travel times needed for the threshold monitoring of this region.

The RMS of residuals for individual events were also in general lower with the Barey model compared to the Fennoscandia model, as shown in **Figure 4.10**. Note that in this case free depth was allowed when locating the events with the Fennoscandian model. This provided somewhat smaller residuals than those shown in **Figure 4.8**, where a fixed depth of 10 km was used.

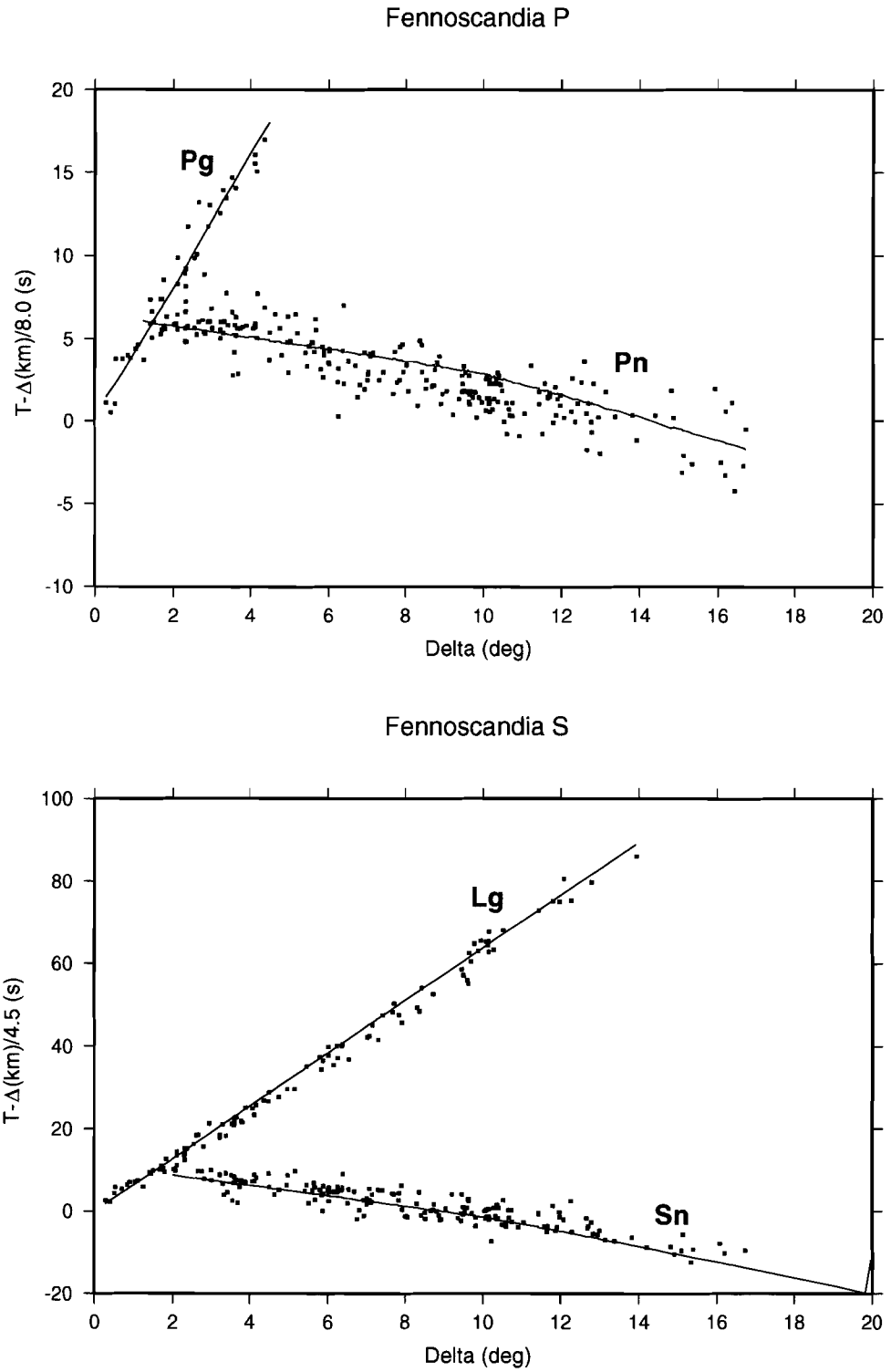

Figure 4.8. Calculated travel times (lines) and observed phase arrivals (squares) using the Fennoscandia model. The Pn and Lg arrivals have mostly negative residuals, while the Sn arrivals tend towards positive residuals. Note that the vertical scales are different for the P and S plots. Lg arrivals above ~8 degrees are from continental events recorded at the arrays in southern Fennoscandia (NRS, FIN).

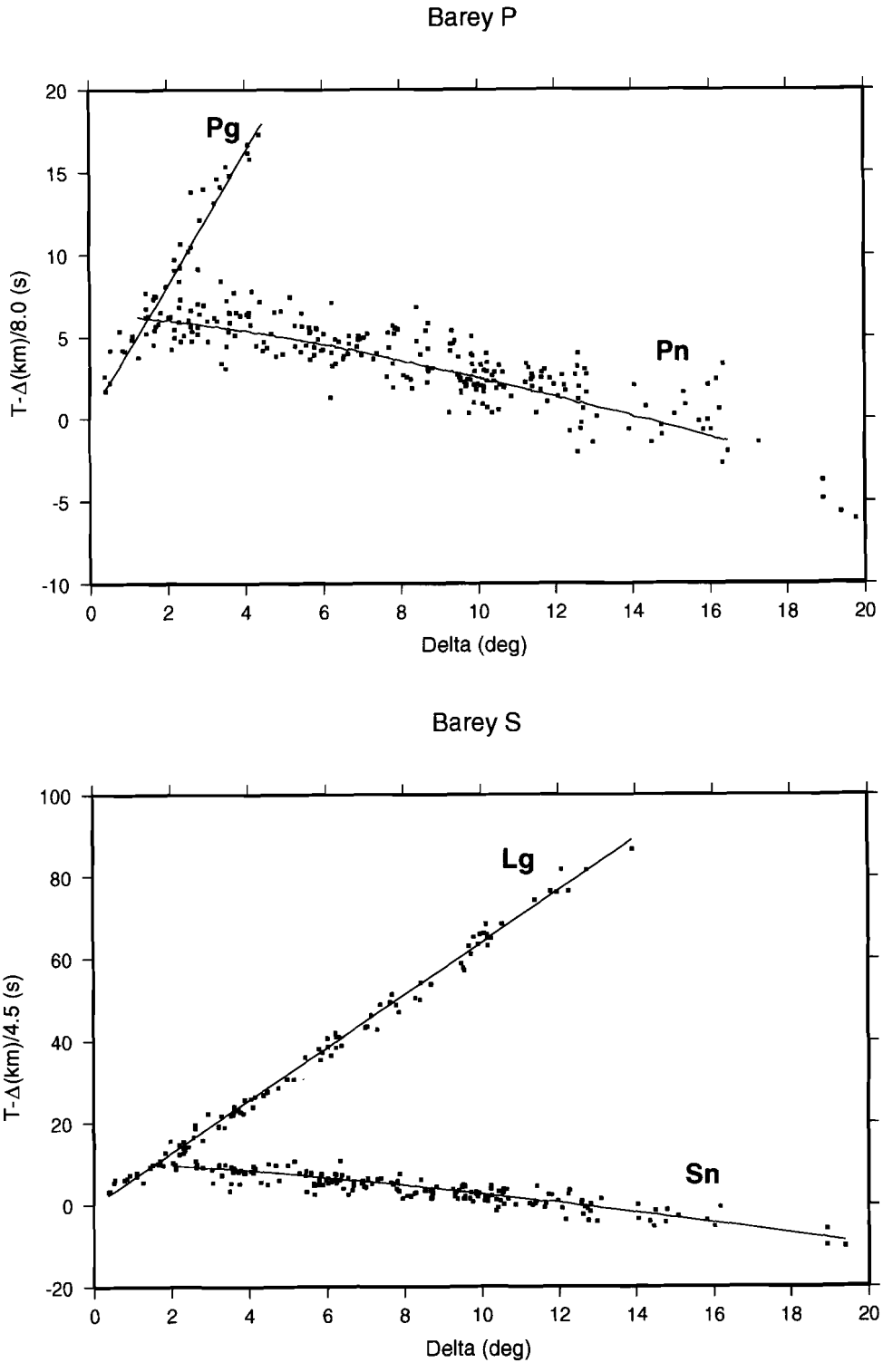

Figure 4.9. Theoretical travel times (lines) and observed phase arrivals (squares) using the Barey model from Schweitzer & Kennett (2001). The observed arrivals are distributed in a fairly symmetrical manner around the theoretical travel-time curves, implying that the model does not introduce systematic bias to the locations. Note that the vertical scales are different for the P and S plots.

Table 4.2: The Fennoscandia (left) and Barey (right) models used.

Fennoscandia			Barey		
Depth (km)	V_P	V_S	Depth (km)	V_P	V_S
0.0	6.20	3.58	0.0	6.20	3.58
16.0	6.20	3.58	16.0	6.20	3.58
16.0	6.70	3.87	16.0	6.70	3.87
40.0	6.70	3.87	41.0	6.70	3.87
40.0	8.15	4.705	41.0	8.10	4.58
95.0	8.15	4.705	70.0	8.23	4.65
95.0	8.25	4.763	210.0	8.26	4.67
210.0	8.30	4.792			

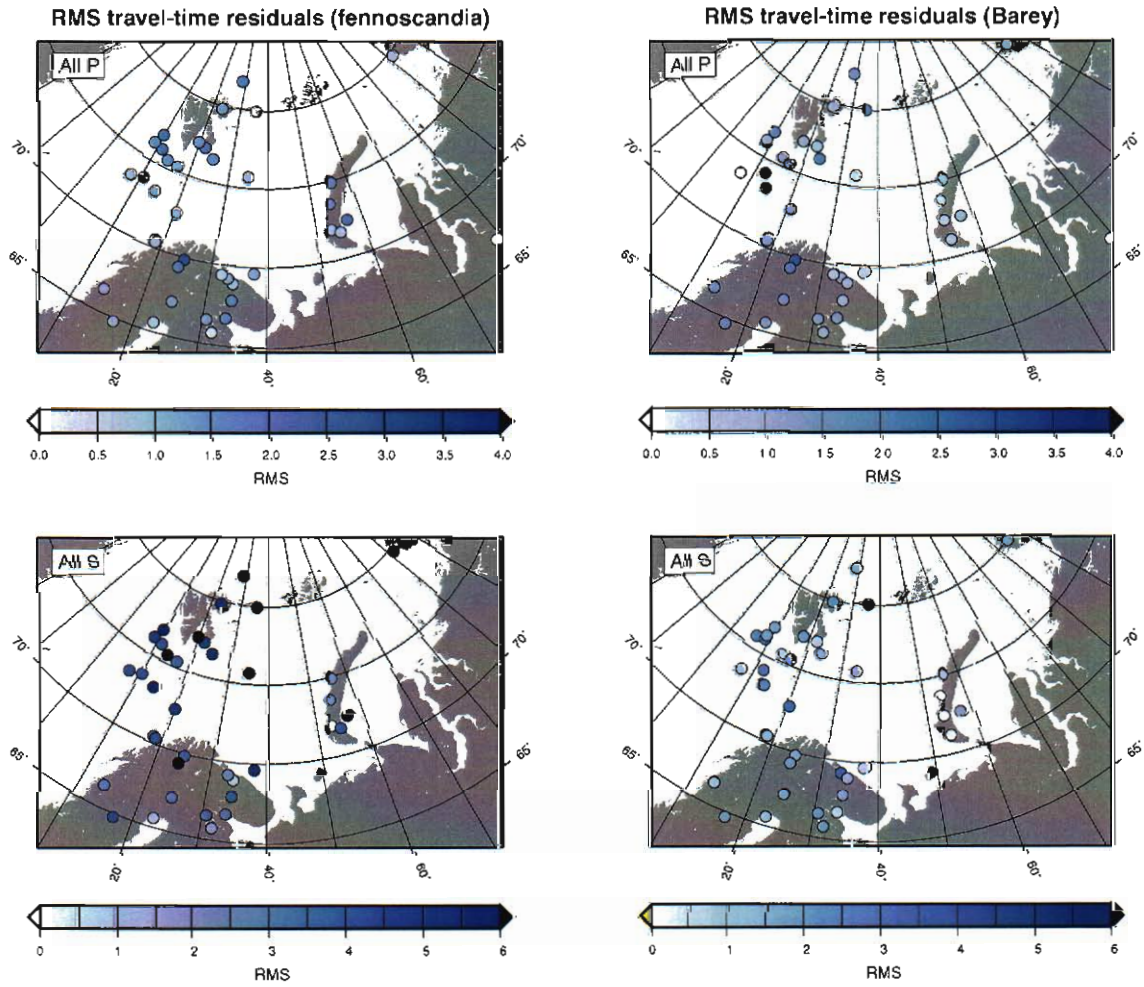

Figure 4.10. RMS of residuals of P (top) and S (bottom) phases for individual events located using the Fennoscandia (left) and Barey (right) models. The RMS values are generally lower for the Barey locations, in particular for the S phases.

5. Attenuation and Joint Inversion Studies

5.1 Inversion Procedure and Results

As detailed in Section 4, a database comprising a total of 43 events, selected to provide the best possible ray path coverage of the Barents Sea and adjacent areas was compiled and reanalyzed in a consistent manner. In this section, we apply this database (with a few minor extensions) to conduct a new joint inversion for obtaining attenuation relations for Pn, Pg, Sn and Lg phases.

The locations of the 45 events in the extended database and the stations used in the analysis are shown in **Figure 5.1**.

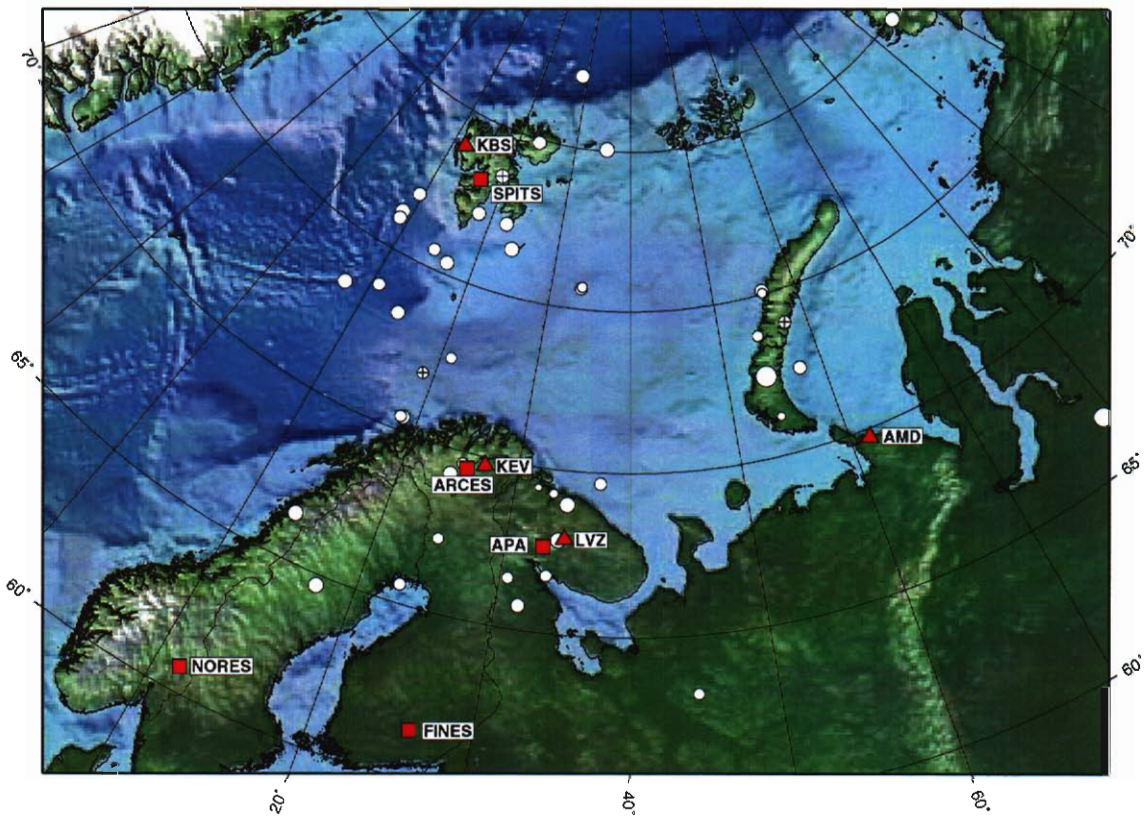

Figure 5.1. *Events (circles) and seismic stations used for deriving wave propagations characteristics of the Barents Sea and surrounding areas. Array stations are shown as squares, while 3C stations are shown as triangles. The symbol sizes for the events are proportional to the network magnitudes.*

Different from the previous approach described in Section 3, we have now jointly used all regional phases (Pn, Pg, Sn and Lg) in the inversion. An additional attenuation parameter

a_0 was introduced in the inversion, describing the total attenuation from source to the reference distance of 200 km. The resulting values of the attenuation parameters used in equation 1 are shown in **Table 5.1.**

$$M_L = \log A - \log e \cdot \alpha^0{}_i \cdot f + \log\left(\frac{\Delta}{200}\right)(a_i f + b) + S_i + 1.67 \qquad (1)$$

Table 5.1: ***The inversion results for the a, b and a0 coefficients (1s) for Pn, Sn, Pg and Lg phases used in the attenuation relation (equation 1).***

Phase	a	b	α
P_n	-0.002 ± 0.023	2.340 ± 0.099	0.584 ± 0.030
S_n	0.141 ± 0.028	2.021 ± 0.110	0.419 ± 0.037
P_g	0.091 ± 0.084	0.851 ± 0.366	-0.538 ± 0.035
L_g	0.534 ± 0.062	-0.186 ± 0.123	-0.609 ± 0.063

Figure 5.2 shows a comparison between the phase magnitude residuals calculated using the relations and parameters of Jenkins et al. (1998) and our inversion results. The results of Jenkins et al. (1998) revealed a high scatter between individual station and phase magnitudes, and also some systematic inconsistencies, most notably magnitudes calculated from different frequency bands at the same station. Magnitudes calculated from STA values in the 2-4 Hz passband are mostly higher than magnitudes calculated in the 3-6 Hz passband, which again are generally higher than magnitudes calculated from the 4-8 Hz passband. The coefficients used in this case were determined using data from eastern North America, central Asia and Australia. However, this relation is not primarily intended for local magnitude calculation, some of the scatter in the magnitudes from Pg and Lg arrivals in particular may be due to the small distance for some of these observations, below the lower distance limit of 1.8 used by Jenkins et al. (1998).

Phase magnitudes calculated using equation 1 and the parameters of **Table 5.1** are shown to the right of **Figure 5.2**. These results show that the scatter (expressed as standard deviation) was significantly reduced compared to the original calculations. There is also no apparent frequency dependency in the magnitude residuals.

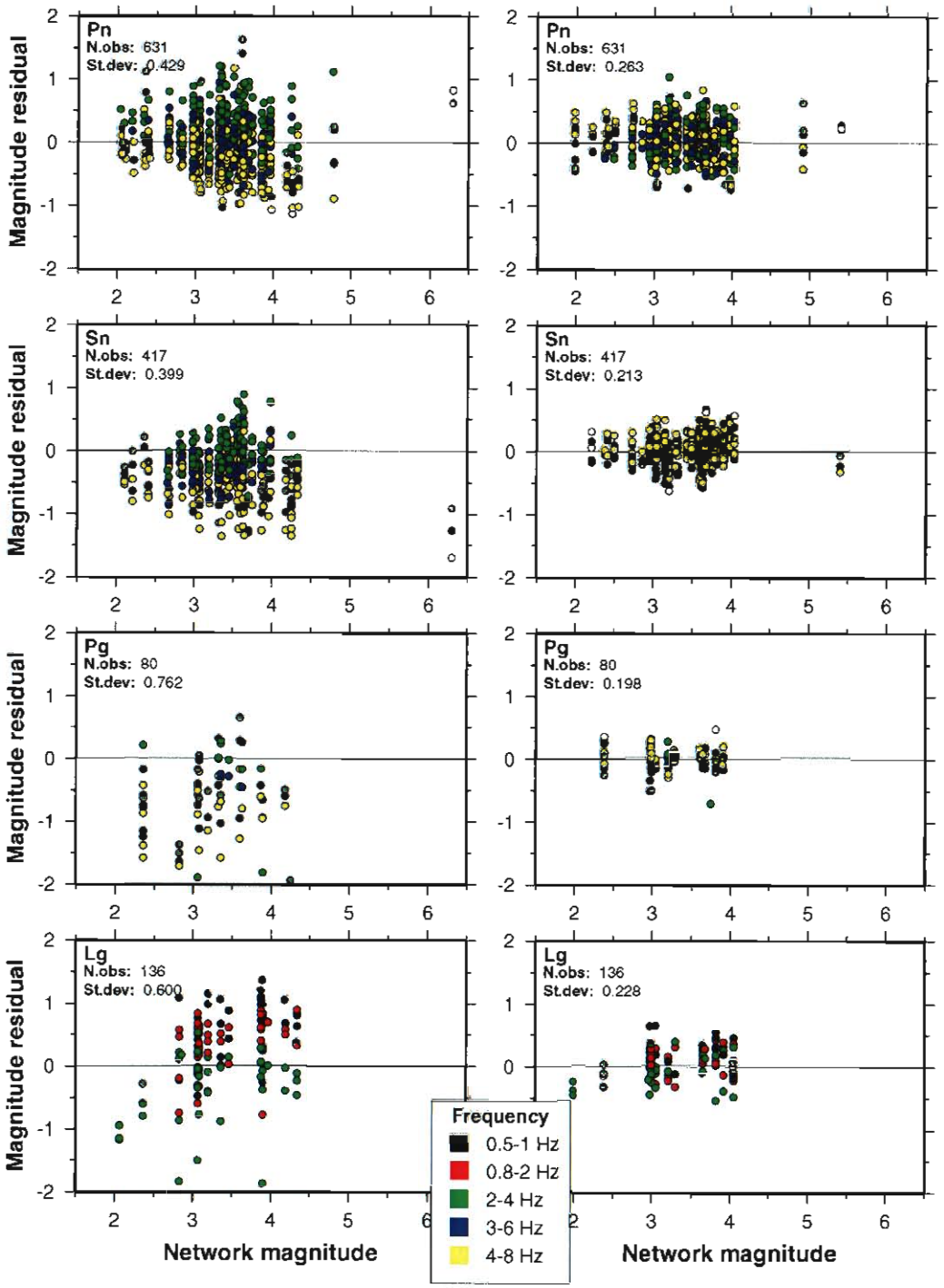

Figure 5.2. *Magnitudes calculated using the relation from Jenkins et al. (1998) (left) and this study (right) from individual amplitude readings, plotted vs. network magnitudes for the 45 events. Note the significant reduction in scatter (St. dev.) and also the absence of frequency-dependent effects when the relation from this study is used.*

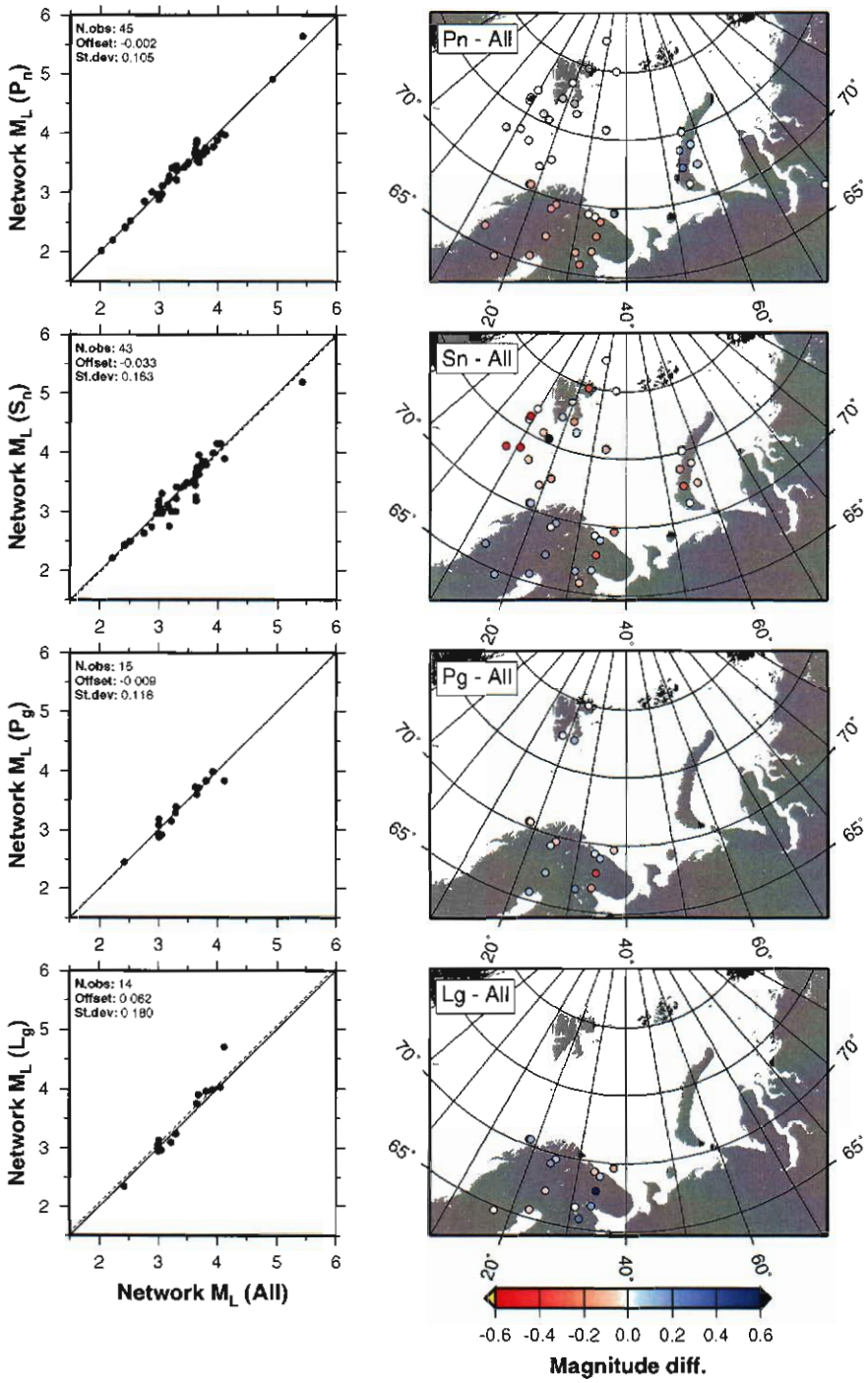

Figure 5.3. *Network event magnitude comparisons and maps of the geographical distribution of the magnitude differences for individual phase magnitudes compared to network magnitudes. Note that Sn magnitudes are overestimated for events that have paths predominantly within the Baltic shield, while events with paths that cross the Barents Sea have lower Sn magnitudes. Pg and Lg magnitudes appear to be quite stable within the limited distance range from which readings are available.*

Figure 5.3 shows comparisons of corrected network magnitudes compared to magnitudes calculated from individual phases. Although relative P and S magnitudes could be used as an aid in discriminating earthquakes and explosions, **Figure 5.3** shows that regional path effects in this area also give rise to substantial differences in magnitude. This is particularly visible for Pn and Sn magnitudes, as they are available for events covering the entire region. Events that predominantly have ray paths within Fennoscandia have larger Sn magnitudes, while the opposite is true for events that have ray paths crossing the sediment basins of the Barents Sea (Novaya Zemlya/Kara Sea and the western Barents Sea/ Mid-Atlantic ridge areas).

From this study, it is clear that Pn and Sn are the most useful phases for calculating magnitudes for events in the Barents Sea. In fact, **Figure 5.3** shows that Pg and Lg are mainly observed at close epicentral distances (< 300 km). This situation is quite different from what we have previously found for the Scandinavian Peninsula and the Baltic Shield, where Lg is the dominant phase on the seismogram out to at least 1000 km. Thus, event for a stable continental region, one may expect quite significant regional variations in the magnitude correction factors.

Table 5.2 shows mean magnitudes, number of observations and RMS of residuals for the Pn and Sn phases, in addition to network magnitudes and magnitudes calculated by the automatic GBF system for the 40 events in the initial database that have magnitude readings in the 3-6 Hz frequency band. The single-phase magnitudes in general have quite low residuals, and the Pn and Sn magnitudes are quite close for most events.

Table 5.2: Magnitudes, no. of observations and RMS of residuals for Pn-, Sn- and network magnitudes. Automatic magnitudes calculated by the GBF system (Ringdal & Kværna, 1989) and reference magnitudes (Ringdal & Kremenetskaya, 1999) are also shown.

Date/time	Lat.	Lon.	Pn			Sn			Network			GBF		Ref.
			Mag.	no	RMS	Mag.	no	RMS	Mag.	no	RMS	Mag.	no	
1990-167:12.43.26.91	68.95	34.62	3.76	2	0.31	3.99	2	0.26	3.87	4	0.31	-	-	
1990-297:14.58.06.49	72.50	54.08	5.66	1	-	5.16	1	-	5.41	2	0.25	-	-	5.6
1991-157:12.46.11.32	65.57	22.88	3.17	2	0.17	3.46	2	0.09	3.31	4	0.19	-	-	
1991-236:10.56.29.65	65.73	31.69	3.55	1	-	3.68	1	-	3.61	2	0.07	-	-	
1992-366:09.29.25.84	73.77	54.24	2.98	2	0.01	2.71	1	-	2.88	3	0.13	2.25	1	2.7
1993-005:10.19.34.40	64.68	17.29	3.99	4	0.27	4.16	3	0.13	4.06	7	0.26	3.61	7	
1995-013:04.34.08.58	75.95	8.90	3.50	8	0.28	3.46	4	0.07	3.48	12	0.24	-	-	
1995-021:01.58.07.21	70.43	18.39	2.99	6	0.05	3.35	4	0.14	3.13	10	0.20	2.99	10	
1995-054:21.50.00.15	71.19	54.53	2.36	1	-	2.36	1	-	2.36	2	0.00	-	-	
1995-063:18.29.04.36	82.25	28.71	3.69	6	0.21	3.67	5	0.18	3.68	11	0.20	3.10	1	
1995-101:20.07.23.02	80.05	35.67	3.71	5	0.18	3.83	4	0.23	3.76	9	0.21	3.25	2	
1995-102:08.18.52.49	69.26	33.38	2.36	4	0.25	2.50	1	0.00	2.39	5	0.23	2.04	5	
1995-133:22.38.51.04	76.89	9.54	3.60	9	0.14	3.48	4	0.07	3.56	13	0.14	3.13	3	
1995-161:18.45.34.11	75.70	33.88	2.57	3	0.09	2.61	3	0.13	2.59	6	0.12	2.01	2	
1995-164:19.22.38.41	75.10	56.02	3.50	5	0.22	3.56	5	0.18	3.53	10	0.20	2.74	2	3.5
1995-184:12.49.32.76	69.64	25.07	2.92	3	0.10	3.21	2	0.01	3.04	5	0.16	2.94	9	
1995-185:03.26.24.87	79.94	94.76	3.71	2	0.15	3.76	3	0.03	3.74	5	0.11	3.15	1	
1995-241:22.12.19.06	77.14	22.33	3.74	4	0.11	3.47	3	0.14	3.62	7	0.18	3.54	3	

Date/time	Lat.	Lon.	Pn			Sn			Network			GBF		Ref.
			Mag.	no	RMS	Mag.	no	RMS	Mag.	no	RMS	Mag.	no	
1995-261:03.26.06.18	66.51	30.64	2.87	6	0.18	3.13	3	0.06	2.95	9	0.19	2.96	11	
1995-313:01.10.23.59	66.73	33.51	2.91	6	0.06	3.10	3	0.05	2.98	9	0.11	3.12	11	
1995-329:19.41.26.68	77.17	18.14	3.66	6	0.31	3.70	6	0.11	3.68	12	0.23	3.50	5	
1996-013:17.17.23.57	75.02	56.02	2.50	2	0.17	2.46	2	0.22	2.48	4	0.19	1.90	2	2.4
1996-021:02.16.32.03	69.25	24.25	3.73	7	0.30	3.89	3	0.17	3.78	10	0.28	3.86	12	
1996-218:20.04.38.23	75.58	14.63	3.13	7	0.27	3.08	5	0.06	3.11	12	0.21	2.38	3	
1996-272:06.08.47.35	69.39	32.03	1.98	3	0.21	-	-	-	1.98	3	0.21	1.60	1	
1996-301:23.55.17.21	79.88	23.54	3.45	4	0.23	3.02	2	0.04	3.31	6	0.28	2.62	1	
1996-361:04.44.15.67	63.24	44.62	3.00	4	0.11	3.01	4	0.13	3.00	8	0.12	2.74	4	
1997-122:07.31.17.23	72.67	20.85	2.87	6	0.24	2.68	5	0.12	2.79	11	0.22	2.15	2	
1997-228:02.11.00.36	72.48	57.67	3.63	4	0.18	3.21	3	0.21	3.45	7	0.28	-	-	3.5
1997-279:12.33.27.04	76.44	24.01	3.78	4	0.10	3.85	3	0.15	3.81	7	0.13	3.27	5	
1997-279:21.17.31.53	73.84	10.78	3.27	6	0.17	2.93	1	-	3.22	7	0.20	2.96	2	
1997-279:21.29.18.26	73.38	7.42	3.85	4	0.10	3.36	2	0.18	3.68	6	0.26	2.95	5	
1999-229:04.44.37.19	67.85	34.15	4.02	6	0.20	4.02	4	0.06	4.02	10	0.16	3.90	13	
1999-290:12.07.16.70	70.43	18.64	3.59	7	0.19	3.84	3	0.07	3.67	10	0.20	3.79	13	
2000-225:07.30.41.31	69.66	37.38	3.40	8	0.34	3.14	3	0.02	3.33	11	0.31	2.80	8	
2000-316:02.01.06.65	75.35	16.76	3.57	6	0.32	3.97	4	0.22	3.73	10	0.35	3.46	4	
2000-341:00.34.40.15	76.17	8.77	3.92	4	0.09	3.52	3	0.22	3.74	7	0.25	2.94	4	
2000-360:03.50.28.47	73.32	14.01	3.72	8	0.20	3.69	6	0.19	3.70	14	0.20	3.39	9	
2001-090:11.30.55.35	66.41	13.67	3.93	8	0.24	4.17	6	0.13	4.03	14	0.24	4.00	13	
2001-122:15.59.43.93	67.23	24.70	2.95	5	0.07	3.22	2	0.07	3.03	7	0.14	3.07	10	

5.2 Example: The Novaya Zemlya seismic event 23 February 2002

As an example we show in **Table 5.3** the individual phase magnitude estimates of the 23 February 2002 event located on the northeastern coast of Novaya Zemlya. The consistency of these phase magnitudes are remarkably high.

Table 5.3: ***Phase magnitudes and network magnitudes for the 23 February 2002 event located on the northeastern coast of Novaya Zemlya, using the attenuation relations developed in this study.***

Station	Phase	Distance	Magnitude
AMD	Pn	509	3.19
AMD	Sn	509	3.15
LVZ	Pn	1055	3.22
LVZ	Sn	1055	3.01
SPITS	Pn	1095	3.44
SPITS	Sn	1095	3.11
ARCES	Pn	1144	2.97
ARCES	Sn	1144	3.08
KBS	Pn	1197	3.16
KBS	Sn	1197	3.19
FINES	Pn	1850	3.17

Magnitude type	Magnitude
Network Pn	3.19
Network Sn	3.11
Network All	3.15

6. Regional TM: Case Study 1 - Novaya Zemlya

6.1 Basic Grid Deployment

The attenuation parameters for the Barents Sea region using an attenuation relation modified after Jenkins et al. (1998) (Hicks et al., 2002) have been implemented in a regional threshold monitoring (TM) scheme for this area. **Figure 6.1** shows a map of the stations mentioned is this report, and also the location of a seismic event of magnitude about 3.2 that occurred on 23 February 2002, 01:21:12 near the eastern coast of Novaya Zemlya. This interesting event provides an excellent test of the monitoring procedures for Novaya Zemlya.

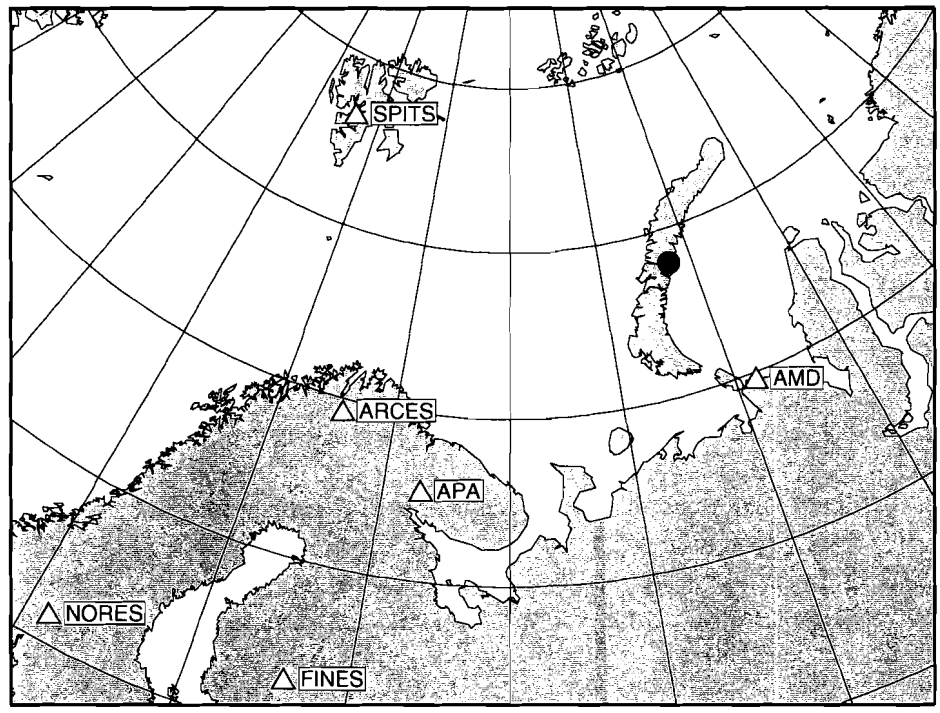

Figure 6.1. *Stations used for regional TM shown as white triangles. The location of the Novaya Zemlya seismic event of 2002-054:01.21.12 is shown by the black circle.*

The grid system used is shown in **Figure 6.2**, comprised of 961 grid points covering northern Fennoscandia, Kola Peninsula, Barents Sea, Novaya Zemlya, Kara Sea and northern Russia. Magnitudes based on the attenuation of Pg and Lg amplitudes were used for grid point to station distances within 1.5 degrees, while magnitudes for distances above 1.5 degrees and up to 20 degrees are based on Pn and Sn attenuation. This is in accordance with the distances at which these phases are observable in the actual region. Software to extract peak and mean threshold magnitudes for each grid point within a given time segment was used to analyze the TM results.

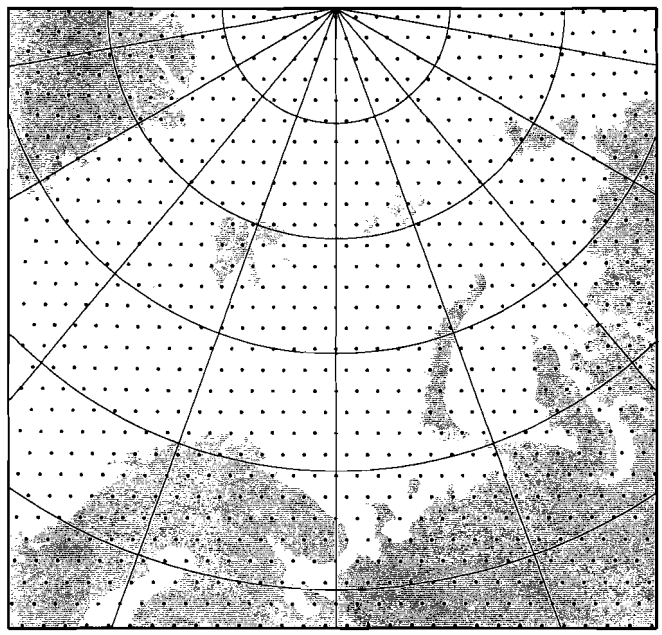

Figure 6.2. *Grid points used for regional threshold monitoring.*

6.2 Regional Threshold Monitoring Results

Figure 6.3 shows peak threshold magnitudes for each grid point for a 10-minute time segment surrounding the origin time of the 23 February 2002 seismic event, using the ARCES, SPITS, FINES and NORES array stations. The individual TM grid points have been resampled onto a continuous grid using a minimum curvature surface fitting algorithm. As seen from the figure, the resolution of the TM process for Novaya Zemlya is low, a large area (covering the entire island) is within 0.2 magnitude units. From**Figure 6.4** we find that the event on Novaya Zemlya creates a threshold peak of similar relative magnitude for targets within a large area. This implies that when monitoring a single target (such as the Novaya Zemlya test site) with this network, events located in a large part of the Barents Sea would be visible as peaks on the threshold trace. However, the absolute value of these peaks could be significantly different from the event magnitude, since these values depend upon the calculated "beam loss" when steering the threshold beam towards a target different from the actual event location

The large relative magnitude thresholds for areas close to the SPITS array (more than 0.8 magnitude units) visible in **Figure 6.4** for this time interval is caused by a small event located near the array.

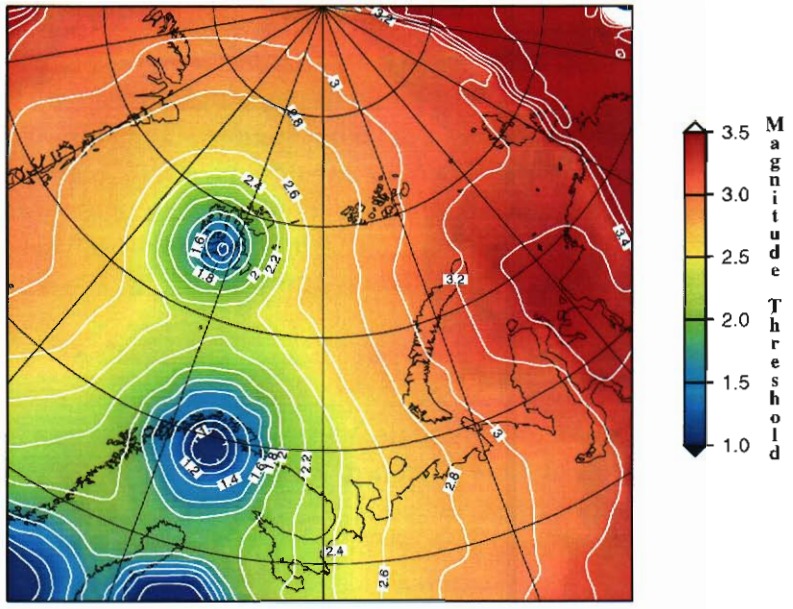

Figure 6.3. *Peak network magnitude thresholds for a 10 minute time interval starting 2002-054:01.16.00, using the ARCES, SPITS, FINES and NORES stations. Note the relatively good correspondence between the peak magnitude threshold at the event location and the estimated event magnitude of 3.15.*

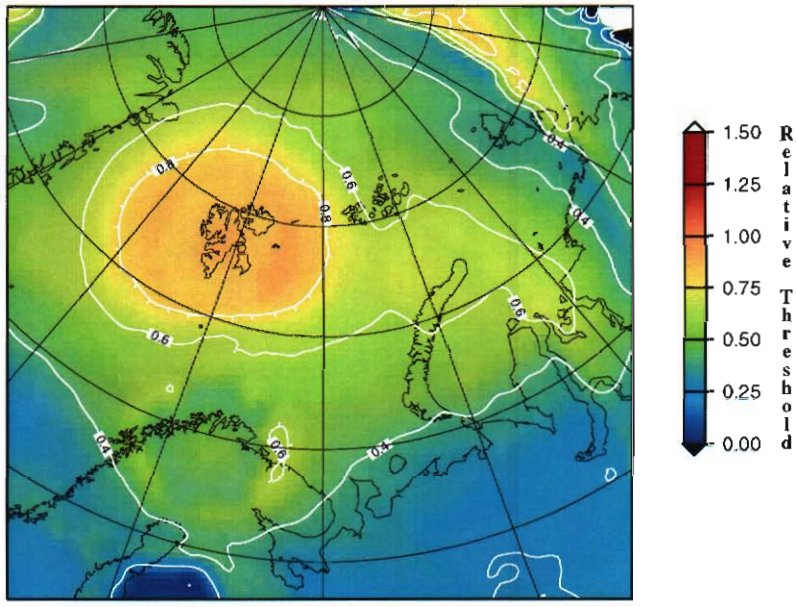

Figure 6.4. *Peak network magnitude thresholds with mean subtracted for the same time interval and stations as* ***Figure 6.3.*** *This essentially shows the height of the highest peak above the background level within the time interval for each grid point. Note the low sensitivity in the area of the event location in Novaya Zemlya.*

Figures 6.5 and **6.6** show TM results from the same time segment (2002-054:01.16.00 to 2002-054:01.26.00) as **Figures 6.3** and **6.4**, but with the APA array and AMD three-component station included in the processing. As one would expect, the AMD station in particular provides an improved resolution of magnitude thresholds for Novaya Zemlya due to its closer distance compared to the other stations. However, as a three-component station can not be "aimed" at different points through stacking of traces like the array stations, the AMD station does not provide significant azimuth resolution of the magnitude thresholds. This, combined with the closer proximity to the event explains for the large increase in the relative magnitude threshold (over 1 magnitude unit) surrounding the AMD station, as seen in **Figure 6.6**.

It is also of interest to compare the absolute magnitude thresholds that are obtained with and without the AMD and APA stations included in the processing. Comparing **Figures 6.3** and **6.5**, we note that there is (naturally) a significant improvement in areas near the AMD and APA stations when these stations are used. Of more interest is the improvement in monitoring Novaya Zemlya, to which the AMD station is the main contributor. The improvement ranges from 0.1 magnitude units in the north to 0.6 magnitude units in the south. Specifically, the thresholds range from 2.3 to 3.1 with AMD included, and from 2.9 to 3.3 without. The improvement in magnitude threshold for the southern Kara Sea is even larger, again due to the contribution from the AMD station.

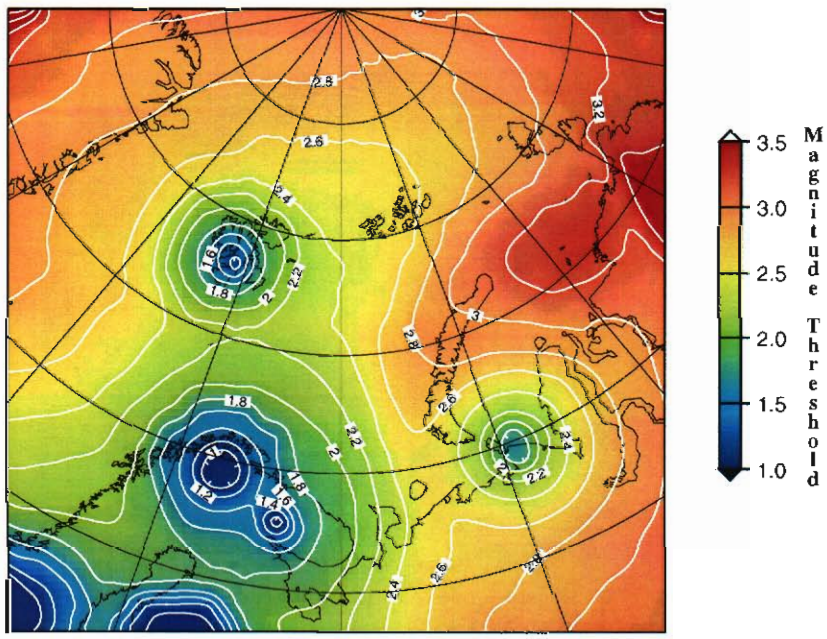

Figure 6.5. *Peak network threshold magnitudes as Figure 6.3, also including the APA and AMD stations. As expected, the AMD station south-east of Novaya Zemlya provides an improved resolution of the magnitude thresholds. Again, note the relatively good correspondence between the peak magnitude threshold at the event location and the estimated event magnitude.*

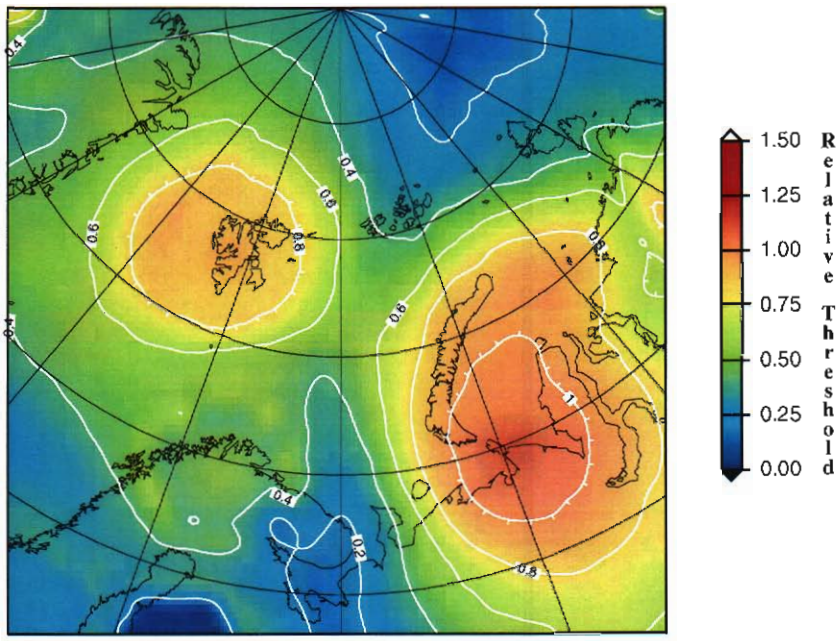

Figure 6.6. *Peak relative network threshold magnitudes for the data shown in* ***Figure 6.5****. Compared to* ***Figure 6.4*** *we find that this network shows a larger variation for the Barents Sea region.*

6.3 Threshold magnitudes during noise conditions

6.3.1 Regional Threshold Monitoring using Fennoscandian stations

The observations at the arrays, ARCES, SPITS, FINES and NORES were used for calculating threshold magnitudes for each of the grid points. **Figure 6.7** shows the threshold magnitudes during an interval without seismic signals, using the developed attenuation relations for Pn and Sn. We find large variations over the region, and in particular when approaching each of the arrays. However, for the region around the island of Novaya Zemlya the variations are modest, varying around a mean of magnitude 2.1-2.2.

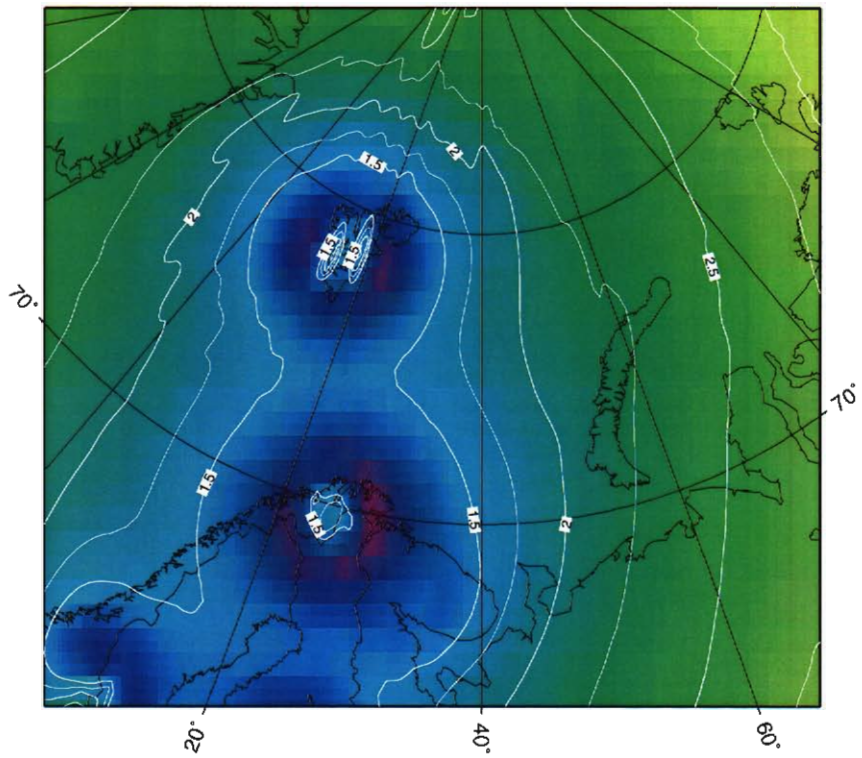

Figure 6.7. *Threshold magnitudes for the time instant 2002-054:01.11.19.0. Notice the improved monitoring capability in the vicinity of each of the arrays. Due to the absence of Pn and Sn for distances less than about 140 km, the threshold magnitudes show an increase at the ARCES and SPITS array locations.*

6.3.2 Regional Threshold Monitoring including the Amderma station

The KRSC group in Apatity, Russia has provided us with about 3 days of continuous data from the station in Amderma, located on mainland Russia, just south of the island of Novaya Zemlya. The data interval is centered around the origin time of the 23 February 2002 event located on the northeastern coast of Novaya Zemlya.

Figure 6.8 shows the threshold magnitudes during an instant without seismic signals, using the developed attenuation relations for Pn, Pg, Sn and Lg. In this plot, we have included both the Fennoscandian stations and the Amderma station. The time instant processed is the same as that of **Figure 6.7**. We find large variations over the region, and in particular when approaching each of the arrays. Comparing **Figure 6.8** to **Figure 6.7**, we note that the inclusion of the Amderma station causes significant variations in threshold magnitudes even within the island of Novaya Zemlya, ranging from 1.4 at the southern tip to 2.2 at the northern tip. This implies that a regional threshold monitoring scheme for Novaya Zemlya when using this particular network has to be divided into geographical sub-regions having similar threshold magnitudes during background noise conditions.

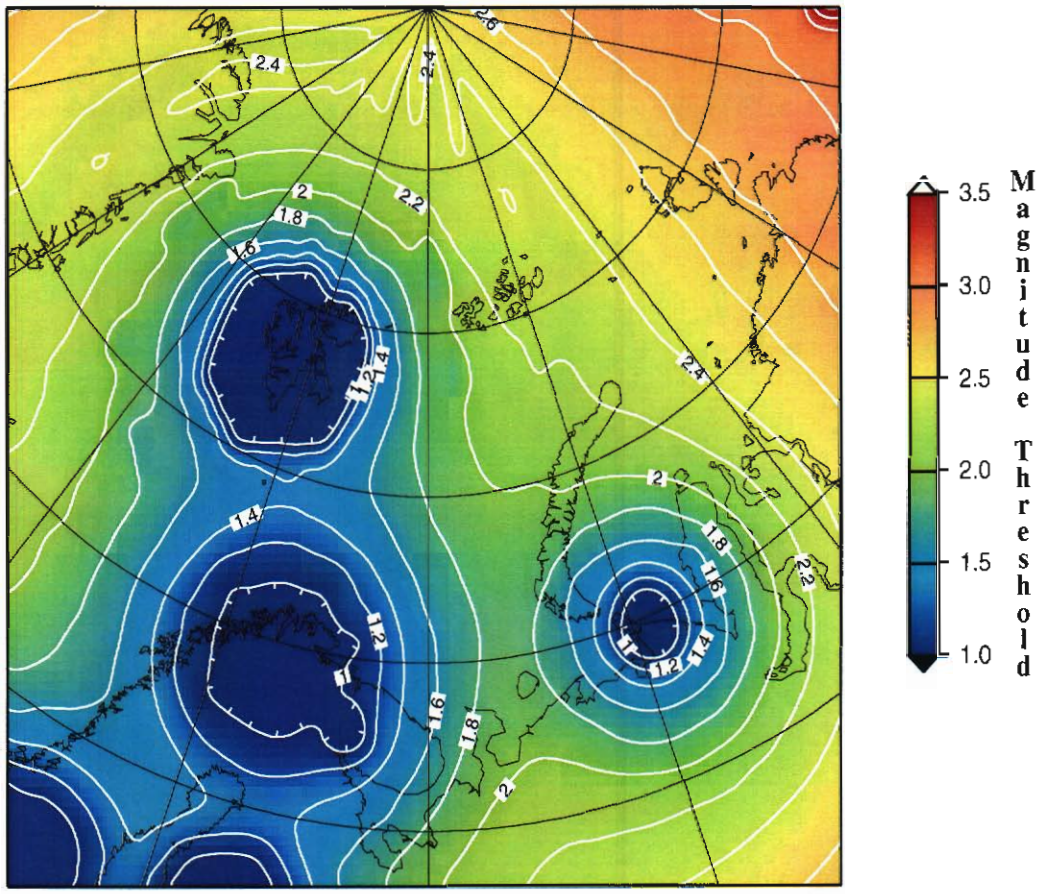

Figure 6.8. *Threshold magnitudes for the time instant 2002-054:01.11.20.0, including data from the AMD station. Notice the improved monitoring capability in the vicinity of each station. For distances above 1.5 degrees of each station we have considered the Pn and Sn phases, whereas Pg and Lg have been used for distances less than 1.5 degrees.*

6.4 Tradeoff Study - Beam coverage versus resolution

We have investigated in more detail the variations in threshold magnitudes for the Novaya Zemlya region, with the view to assess the tradeoff between beam radius (i.e. the desire to cover a large target area with a single threshold beam) and beam focusing sharpness. Toward this end, we deployed a dense grid with an areal extent of about 500 x 500 km as shown in **Figure 6.9**. For each of the grid nodes we calculated magnitude thresholds for the 2 hour time interval 00:00 - 02:00 on 23. February 2002. 01:21:12.1 was the origin time of the magnitude 3.15 event located about 100 km north-east of the former nuclear test site.

Regions of different sizes were constructed by selecting grid points within different radii from the former nuclear test site. **Figure 6.10** shows the variations in threshold magnitudes for a circular region with a radius of 20 km around the test site. The blue line shows the average threshold, whereas the red lines represent the minimum and maximum values. **Figures 6.11-6.13** show similar curves for regions with radii of 50, 100 and 200 km, respectively.

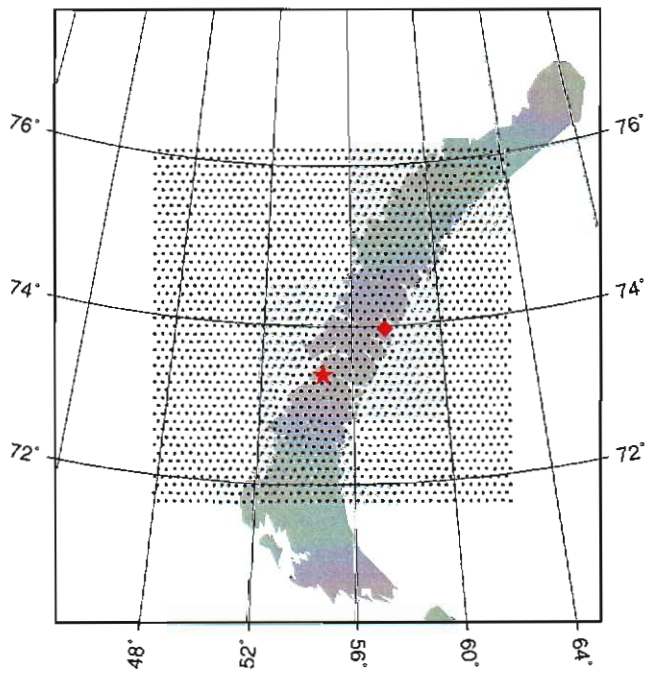

Figure 6.9. *Dense grid deployment around Novaya Zemlya (grid spacing 11 km). The red star shows the location of the former nuclear test site, whereas the red diamond shows the location of the event on 23 February 2002 with origin time 01:21:12.1.*

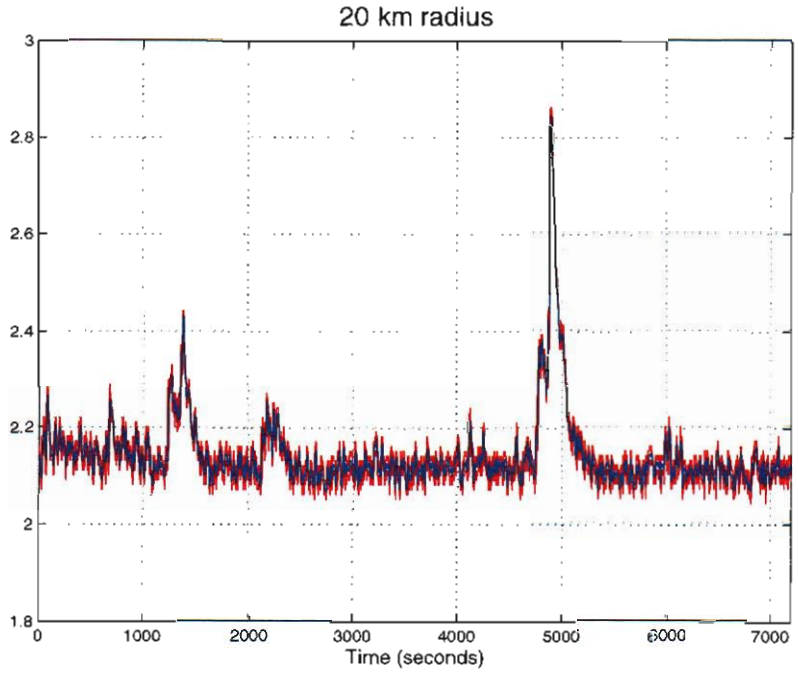

Figure 6.10. *Threshold magnitudes for the time interval 00:00 - 02:00 on 23. February 2002 for a 20 km radius target region centered around the former nuclear test site. The peak at about 5000 seconds corresponds to signals for the 3.15 event located about 100 km north-east of the test site.The blue line shows the average threshold, whereas the red lines represent the minimum and maximum values.*

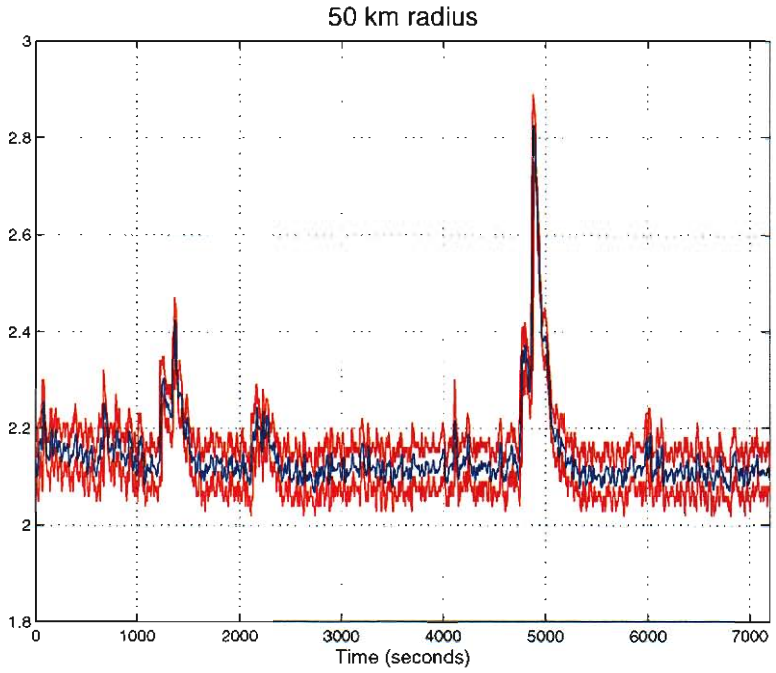

Figure 6.11. *Same type of plot as in* ***Figure 6.10****, but with a 50 km radius target region centered around the former nuclear test site.*

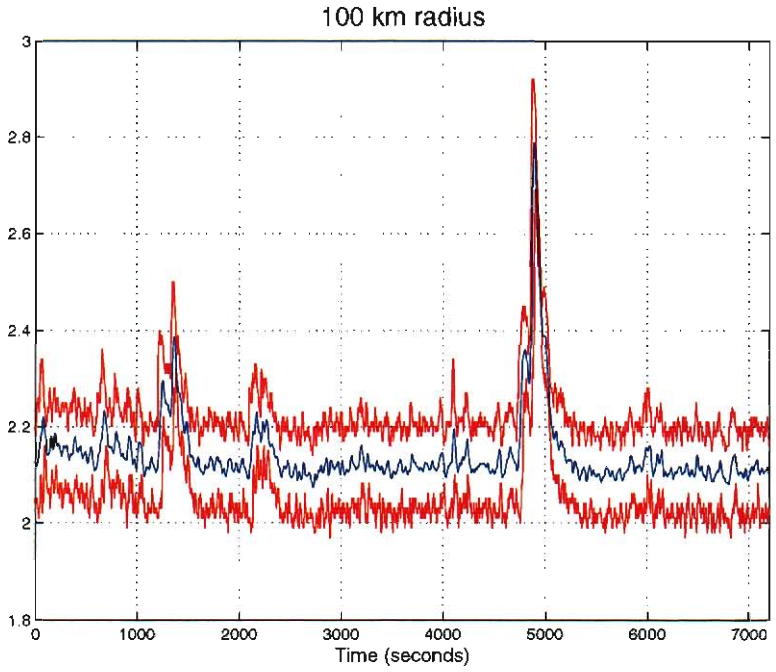

Figure 6.12. *Same type of plot as in* ***Figure 6.10****, but with a 100 km radius target region centered around the former nuclear test site.*

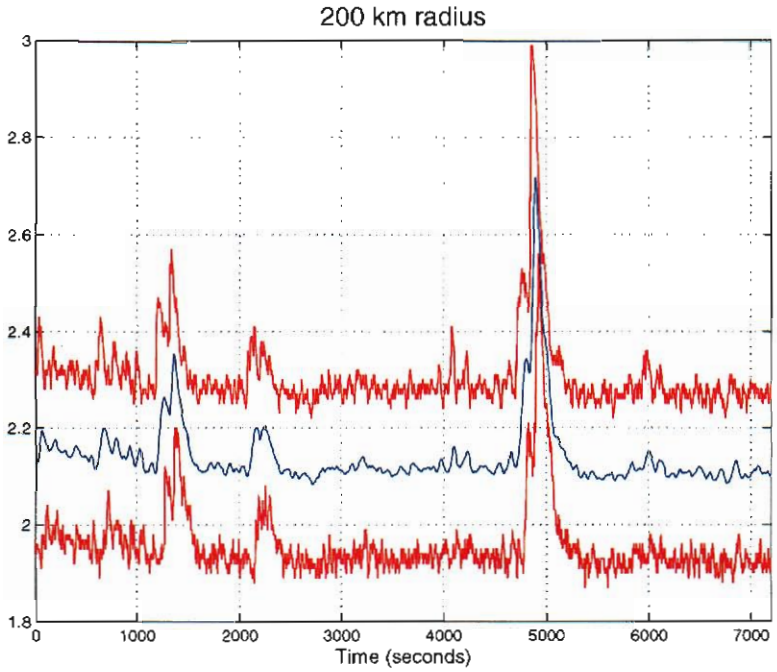

Figure 6.13. *Same type of plot as in **Figure 6.10**, but with a 200 km radius target region centered around the former nuclear test site.*

It is interesting to notice that even for a region with 100 km radius, the variations in threshold magnitudes are all within 0.2 magnitude units. It will therefore be meaningful to represent the monitoring threshold of the entire region with the values of a single target point, together with uncertainty bounds as shown in **Figures 6.10-6.13**. For areas with larger variations in threshold magnitudes, like in the vicinity of the arrays, a 100 km radius target region will obviously show larger differences between the maximum and minimum values.

We would like to comment on the threshold magnitude of the peak corresponding to the event located north-east of the test site. In cases where an event actually occur in the target region, the magnitude thresholds will often be biased low. In **Figure 6.13** we find a maximum value of about 3.0, whereas the event magnitude is estimated to 3.15. In such cases a maximum-likelihood magnitude estimation algorithm should be activated. However, for small events with a size close to the threshold magnitudes, this bias will not be significant.

In conclusion, these results show that for areas that are at large distances from the nearest station, a site-specific threshold monitoring will give threshold magnitudes that are representative (within a few tenths of a magnitude) over fairly large areas (up to several hundred km). However, in cases when a more dense network located close to the monitored region is used, the resolution of the TM method is improved. In such cases, a larger number of target points are required for successful monitoring of a given target region.

7. Regional TM: Case Study 2 - Kola Peninsula

7.1 Introduction

As a second case study of the performance of the regional threshold monitoring system, we have selected the mining areas in the Kola Peninsula, Russia. **Figure 7.1** shows the location of the major mines in this area, together with the location of the two seismic arrays ARC and APA. Both the primary IMS array ARC and the non-IMS station APA record high-SNR observations of all important regional phases at a range up to at least 500 km, which is the maximum distance range being considered in this case study. Furthermore, for the more distant recordings, these phases are well-separated in time.

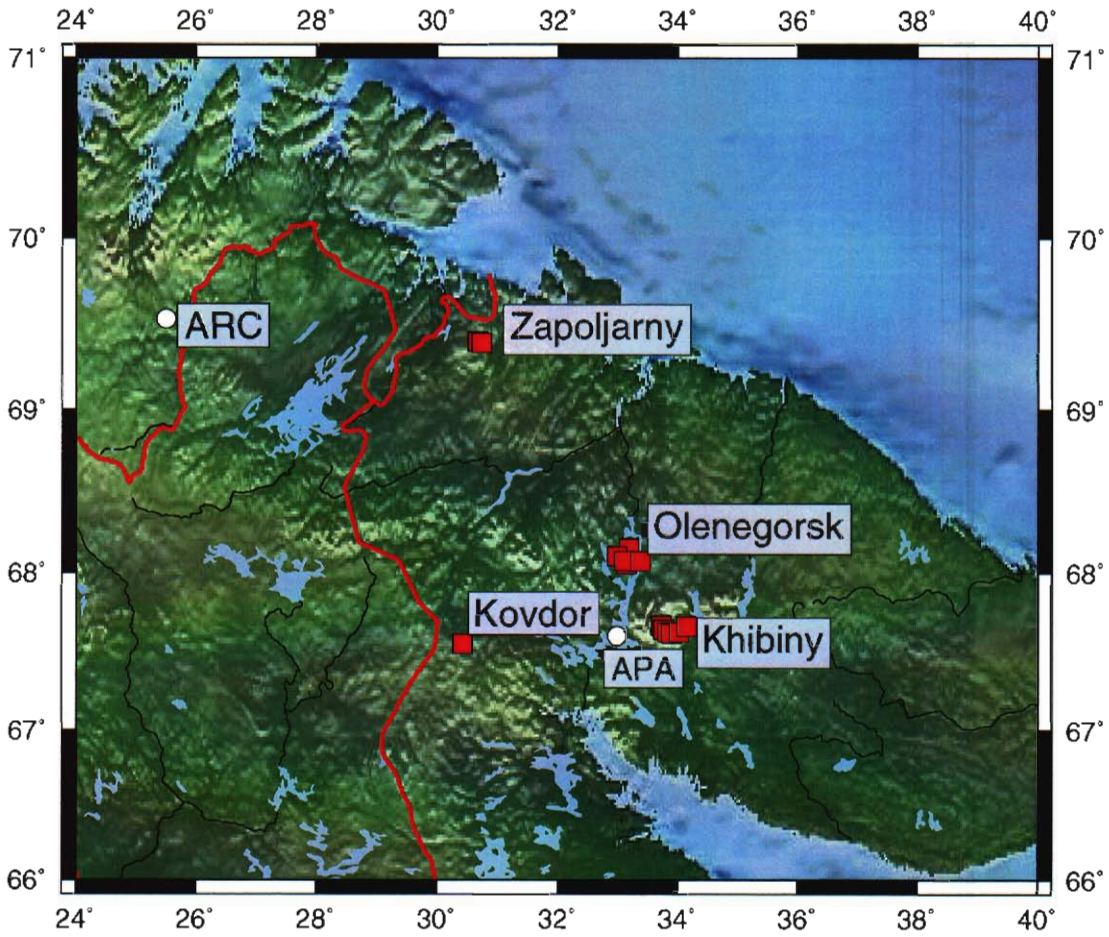

Figure 7.1. *Map of the Kola Peninsula with the main mining areas. Also shown are the locations of the ARCES and Apatity arrays.*

Under a separate project funded by DoE, an effort is being undertaken to collect ground truth information, and explosion and rockburst observations for mines of the Kola peninsula. Such information is regularly collected from the mine operators by KRSC, and will serve as a reference set for our studies. The mining areas comprise Khibiny, Olenegorsk, Kovdor and Zapolyarnyi.

In particular, the mines of the Khibiny Massif provide a natural laboratory for examining and contrasting the signals generated by different types of mining explosions and rockbursts. Of the five mines in the Massif, three have both underground operations and surface pits. Shots underground range in size from very small (~2 tons) with only a few delays and durations on the order of a few hundred milliseconds, to very large (400 tons) with many delays and durations approaching a half second (Ringdal et al., 1996). Shots above ground range from 0.5 tons to 400 tons with a wide range of delays and durations. Induced seismicity is frequent and triggered rockbursts accompany a significant fraction of the underground explosions (Kremenetskaya and Trjapitsin, 1995).

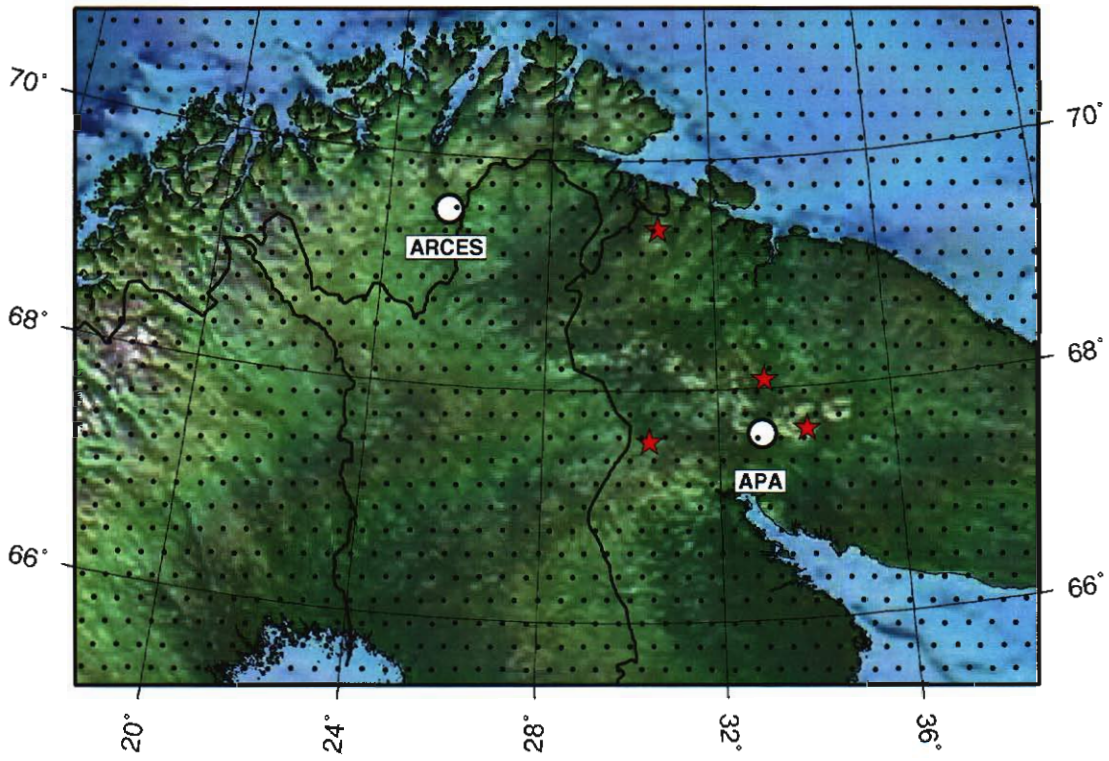

Figure 7.2. *Grid points used for regional threshold monitoring of the Kola Peninsula. The grid spacing is 0.2 degrees.*

The grid system used for this study is shown in **Figure 7.2**, and is based on a dense grid spacing of 0.2 degrees. In computing the threshold traces, magnitudes based on the attenu-

ation of Pg and Lg amplitudes were used for grid point to station distances within 2 degrees, while magnitudes for distances above 2 degrees are based on Pn and Sn attenuation (see **Table 7.1**). This is in accordance with the distances at which these phases are observable in the actual region. The frequency band used in the study was 3-6 Hz for all phases, except for Lg for which we used 2-4 Hz. Software to extract peak and mean threshold magnitudes for each grid point within a given time segment was used to analyze the TM results.

Table 7.1: Parameters used for Regional Threshold Monitoring of the Kola mining areas

Travel time model	'barey' - Schweitzer and Kennett, 2002
Attenuation model	Hicks et al., 2002
Grid Spacing	0.2 degrees
Pg distance range	0 - 2 degrees
Pn distance range	2 - 20 degrees
Lg distance range	0 - 2 degrees
Sn distance range	2 - 20 degrees
Pg frequency band	3 - 6 Hz
Pn frequency band	3 - 6 Hz
Lg frequency band	2 - 4 Hz
Sn frequency band	3 - 6 Hz

7.2 Processing example 1

Figure 7.3 shows mean threshold magnitudes for each grid point for a 1-hour time segment starting at 2002-102:06.30. Even if this time interval is not without seismic events, this figure is representative of the combined TM capabilities of ARC and APA during typical noise conditions. In this and other similar plots, the individual TM grid points have been resampled onto a continuous grid using a minimum curvature surface fitting algorithm. As seen from the figure, the monitoring capability is between 0.5 and 1.0 m_b units for the mining sites (marked as black squares).

Figure 7.4 shows the threshold time traces for a two hour interval surrounding the interval described previously. We have plotted the threshold trace of the grid point closest to the actual mine for each of the four major mining sites. There is one large mining explosion (mine 5 of the Khibiny group) during this time interval, and this explosion causes a peak for each beam. Otherwise, the typical background threshold is between 0.5 and 1.0 m_b units, consistent with **Figure 7.3**.

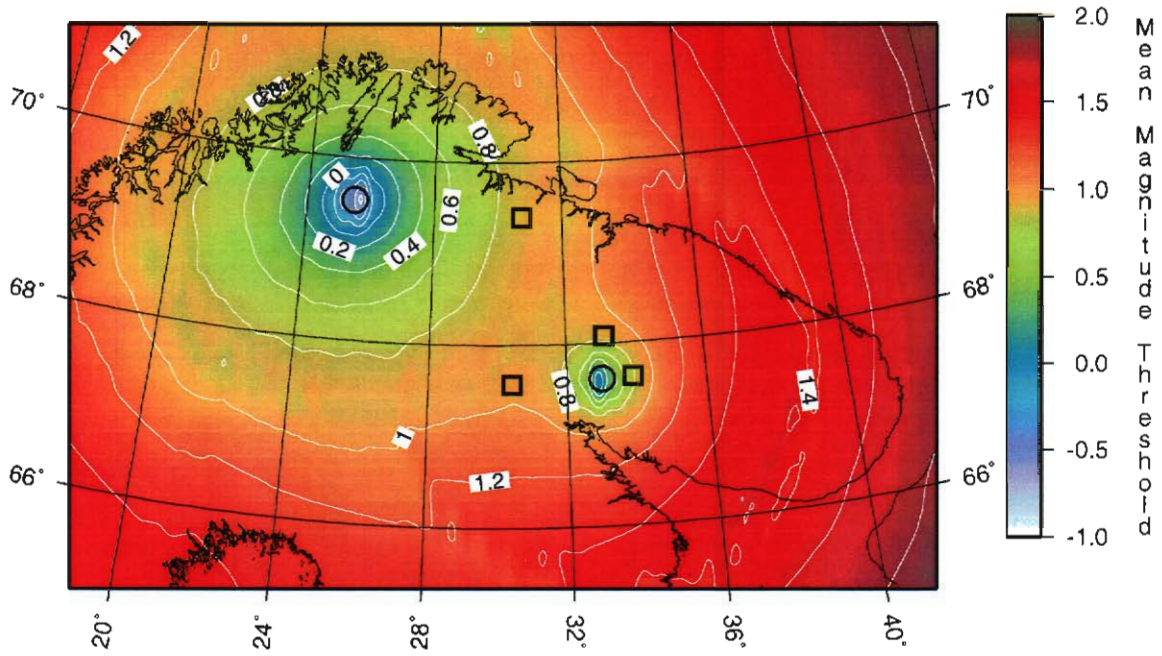

Figure 7.3. *Mean network magnitude thresholds for a 1-hour time interval starting 2002-102:06.30, using the ARCES and Apatity arrays (black circles). The locations of the mining areas Khibiny, Olenegorsk, Kovdor and Zapoljarny (see* ***Figure 7.1****) are shown by black squares.*

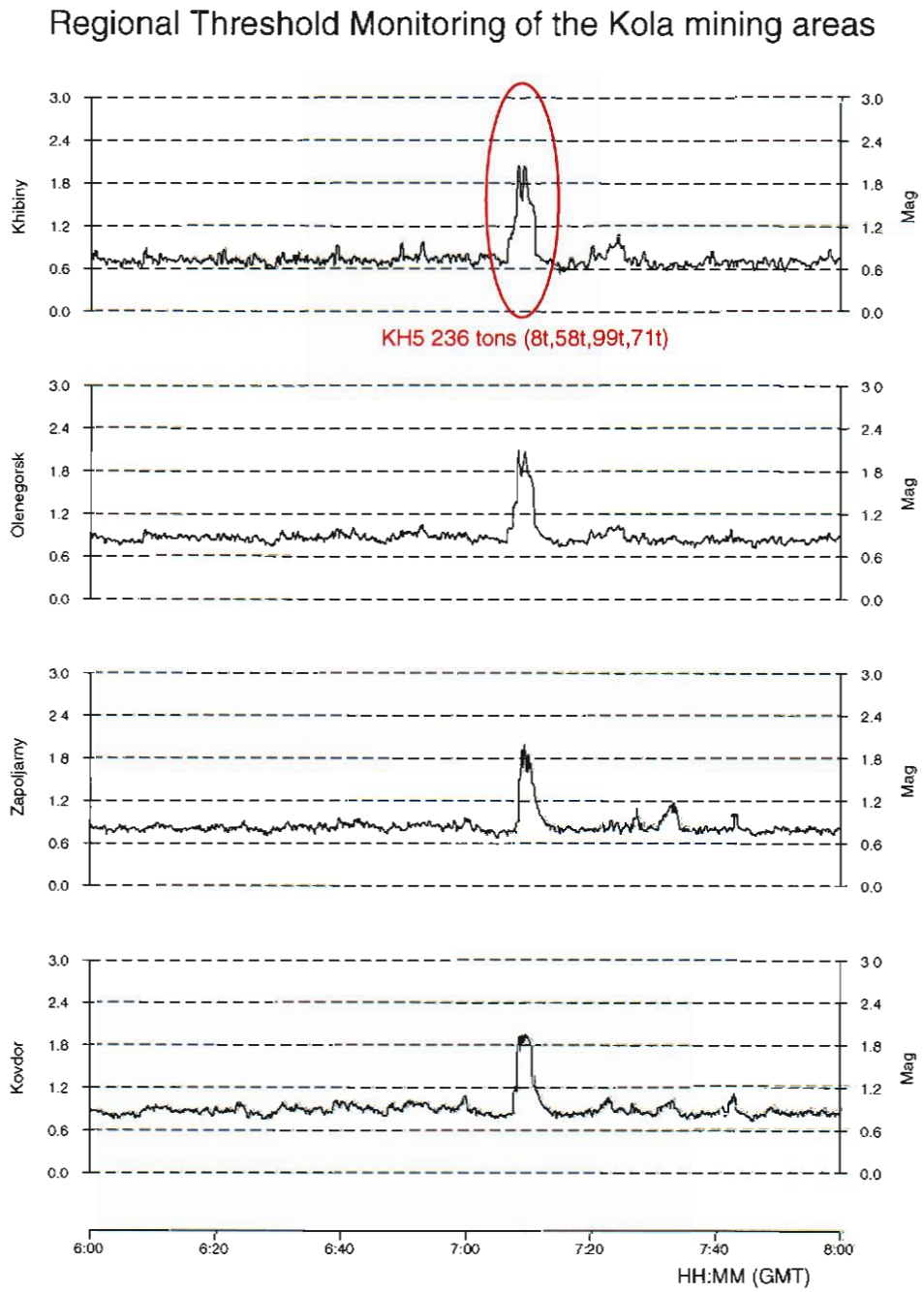

Figure 7.4. *Network magnitude thresholds for the grid points closest to the four mining areas shown in* ***Figure 7.1****, for the 2-hour time interval starting 2002-102:06.00. The threshold peak corresponds to an explosion in the open mine Koashva (KH5) located in the Khibiny area. The total yield of the ripple-fired explosion was reported to 236 tons, and consisted of 4 smaller explosions with yields of 8, 58, 99 and 71 tons, respectively.*

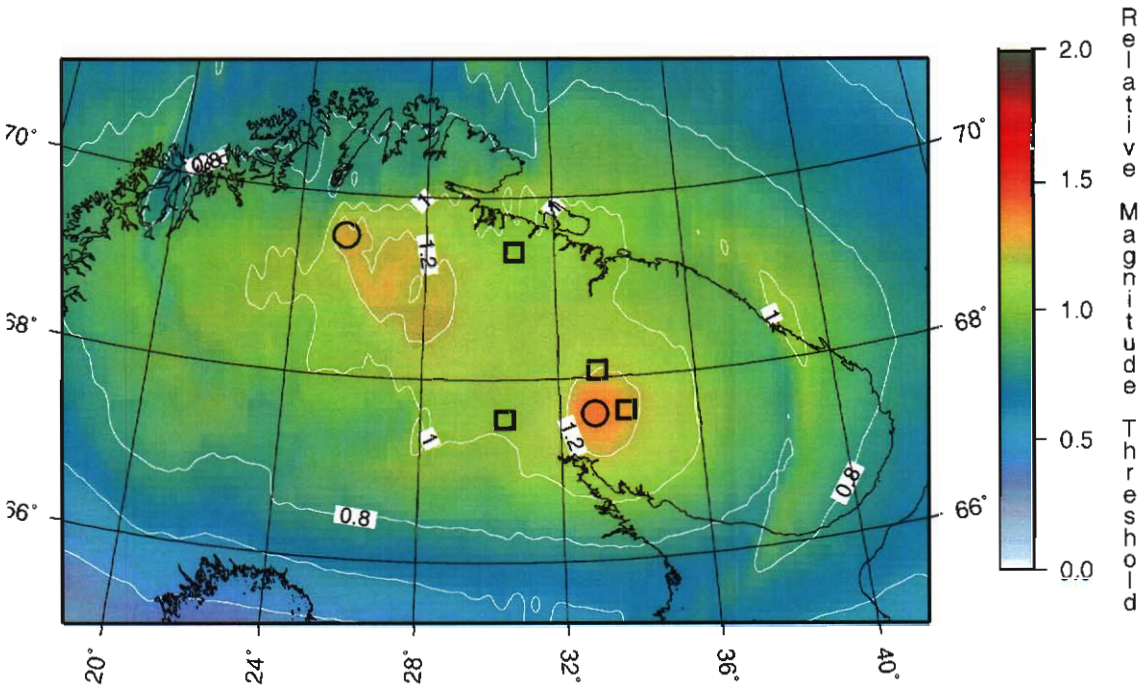

Figure 7.5. *Peak network magnitude thresholds with mean subtracted for the same 1-hour time interval as shown in* ***Figure 7.3****.*

Figure 7.5 shows the peak network magnitude thresholds with mean subtracted for the same 1-hour time interval as shown in **Figure 7.3**. This essentially shows the height of the highest peak above the background level within the time interval for each grid point. Note that the event in the Khibiny mine KH5 (see **Figure 7.4**) creates a significant threshold peak in almost the entire region.

7.3 Processing example 2

Figures 7.6- 7.8 show a second example of threshold plots, similar to the plots shown in **Figures 7.3-7.5**. In this second case, the time interval processed is a two-hour interval starting at 2002-102:10.00, i.e. some hours later during the same day. The mean magnitude thresholds (**Figure 7.6**) are almost identical to the mean thresholds for the first interval (**Figure 7.3**), which shows that the background noise level is stable. The individual time traces for each of the four mining sites (**Figure 7.7**) show a quite significant activity during these two hours, with confirmed mining explosions both at Khibiny, Olenegorsk and Zapolyarnyi. As expected, there is a corresponding threshold increase on all the traces for each mine explosion, but in each case the increase in threshold level is greatest for the actual site of the explosion. There is also an unknown event (perhaps a small earthquake) that is located outside of the mining areas. The peak network threshold magnitudes with mean subtracted (**Figure 7.8**) are quite similar to those in **Figure 7.5**.

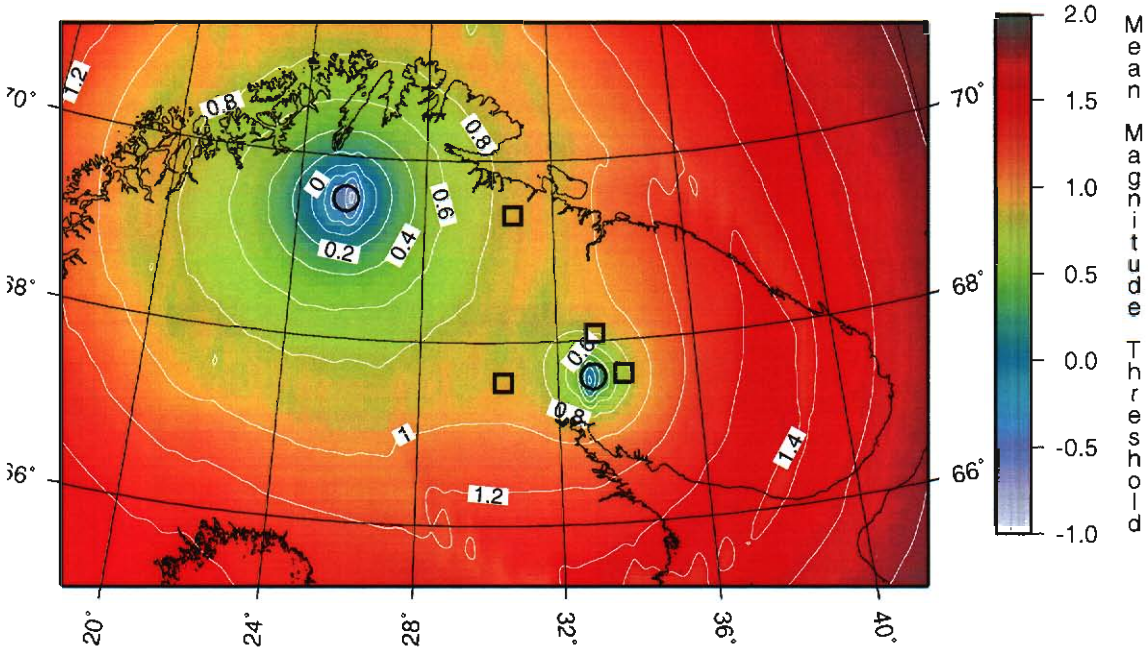

Figure 7.6. *Mean network magnitude thresholds for a 2-hour time interval starting 2002-102:10:00.*

7.4 Processing a 24 hour interval

Figure 7.9 shows network magnitude thresholds for the grid points closest to the four mining areas Khibiny, Olenegorsk, Zapoljarny and Kovdor for the entire day 12 April 2002. This is the same day from which the two previous time segments were extracted. During this day 10 events are found which are located in three of these mining areas, of which 6 are confirmed by KRSC. The corresponding mines and threshold peaks are indicated by red arrows.

7.5 Summary

Using data from the ARCES and Apatity arrays, we have implemented a regional threshold monitoring scheme for northern Fennoscandia, including the Kola Peninsula. For the most active mining areas in this region (Khibiny, Olenegorsk, Zapoljarny and Kovdor), the magnitude thresholds during "normal" noise conditions vary between 0.7 and 1.0 magnitude units. During the studied time interval (12 April 2002), 10 out of 18 peaks exceeding threshold magnitude 1.2 at any of the mining areas were caused by events in the actual mining areas. However, the spatial resolution of the threshold magnitudes when using the ARCES and Apatity arrays is quite low, such that the mining events also created significant threshold peaks for the other mining areas.

This implies that for a regional threshold monitoring scheme for the Kola Peninsula it will be sufficient to deploy a set of targets for the most active mining areas. When a threshold

peak is found at any of these targets, the peaks have to be associated to seismic events as outlined for the Kursk study of Section 2.

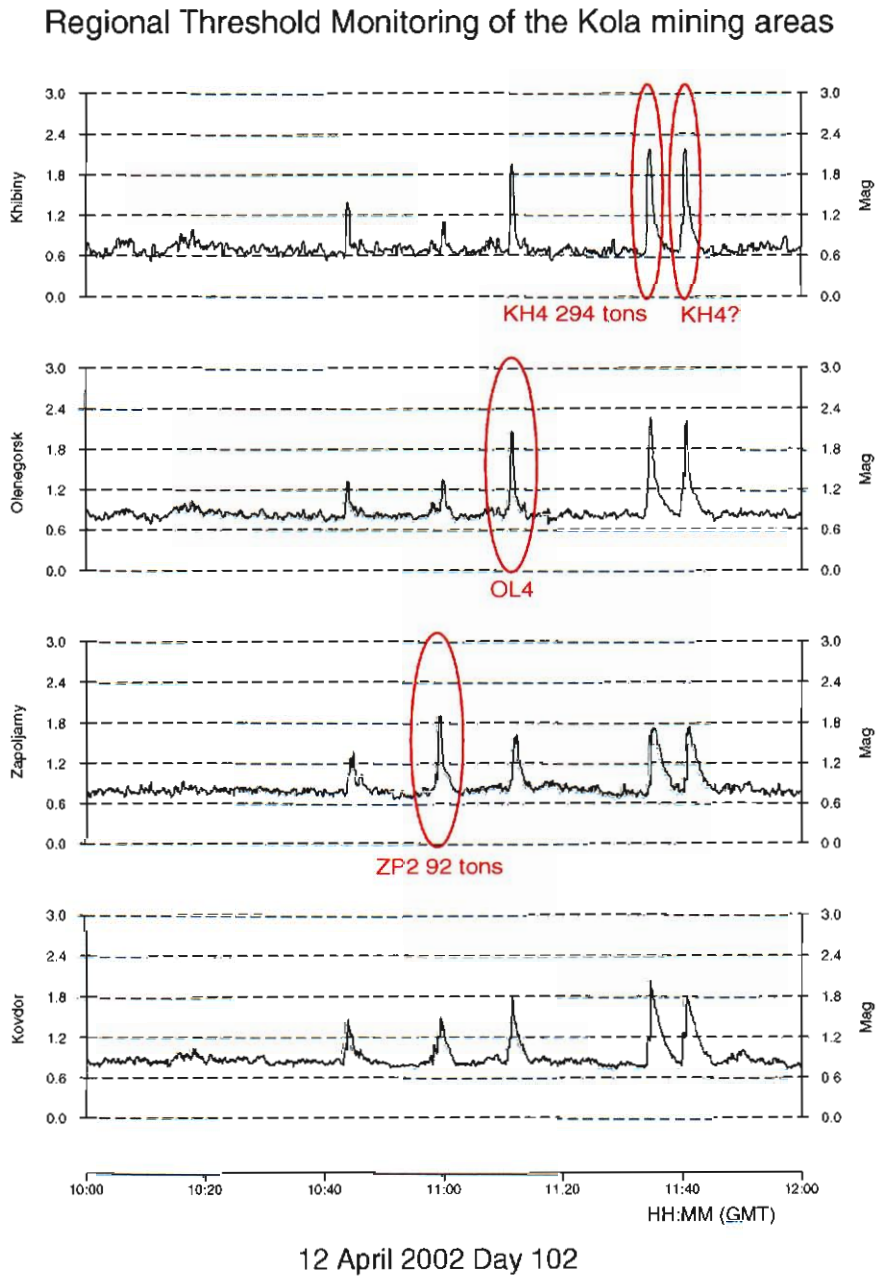

Figure 7.7. *Network magnitude thresholds for the grid points closest to the four mining areas shown in* ***Figure 7.1****, for the 2-hour time interval starting 2002-102:10.00. Five significant threshold peaks are seen during this time interval, of which three are mining explosions reported by the KRSC. The last peak at 11:40 is believed to be an additional explosion at the Central Khibiny mine KH4. The first peak at 10:44 is caused by an event located approximately 70 km south-west of the Apatity array.*

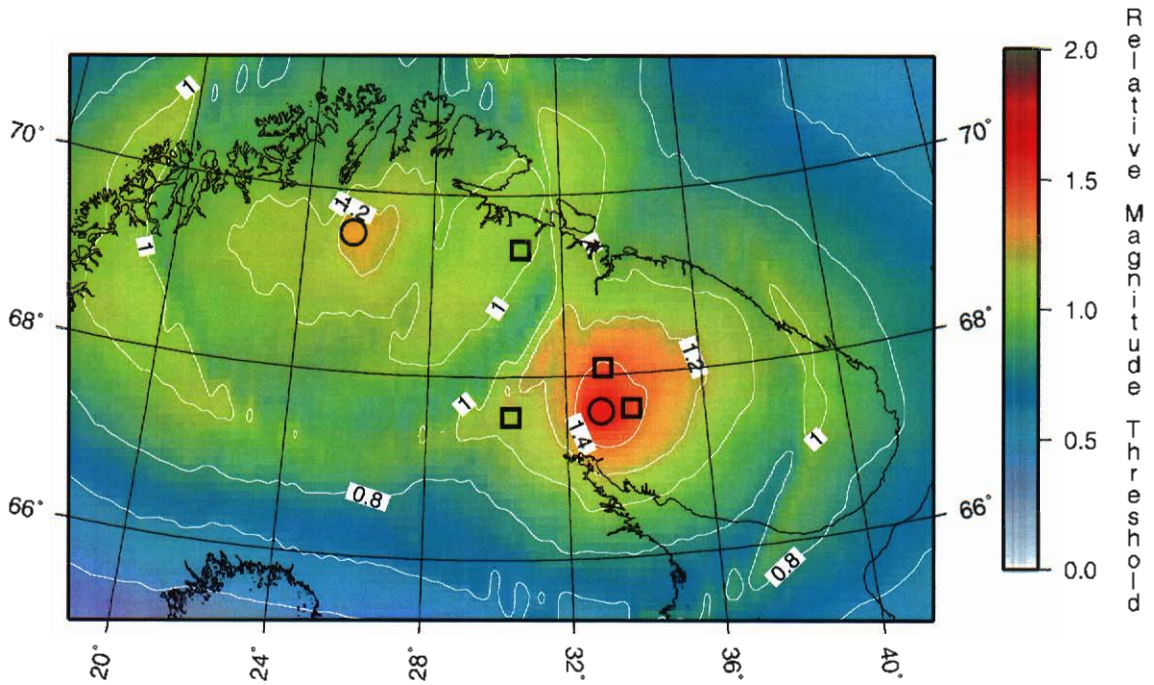

Figure 7.8. *Peak network magnitude thresholds with mean subtracted for the same 2-hour time interval as shown in* ***Figure 7.6****. This essentially shows the height of the highest peak above the background level within the time interval for each grid point. The five events occurring in the region during this time interval create significant threshold peaks in the entire region.*

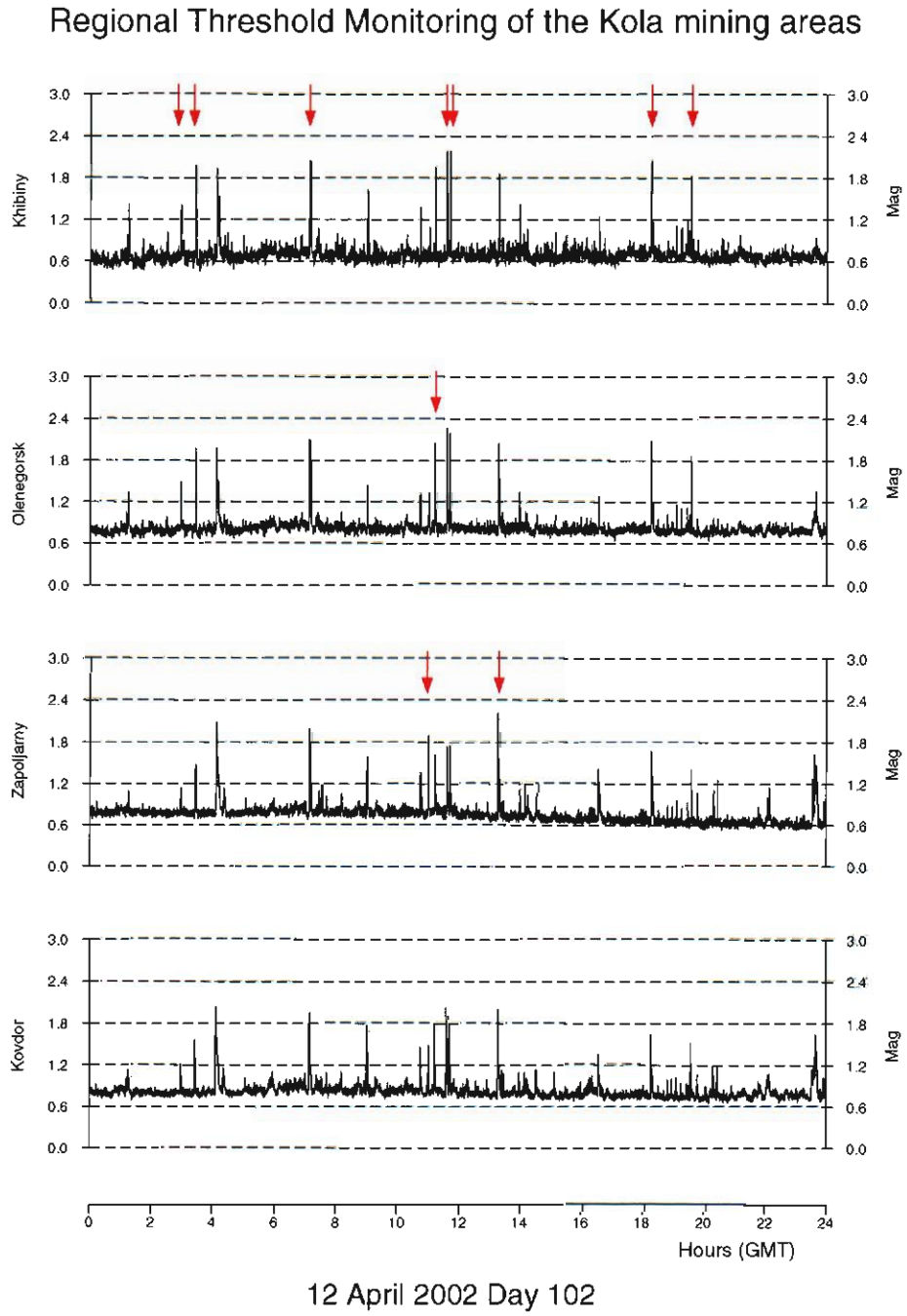

Figure 7.9. *Network magnitude thresholds for the grid points closest to the four mining areas Khibiny, Olenegorsk, Zapoljarny and Kovdor for 12 April 2002. During this day 10 events are found which are located in three of these mining areas, of which 6 are confirmed by KRSC. The corresponding mines and threshold peaks are indicated by red arrows.*

8 Program description

This section describes the organization of the processing software and provides a description of the programs used for Regional Threshold Monitoring.

8.1 Software Directory Organization

The Regional TM software and static data are organized under one top-directory with the following sub-directories, see **Figure 8.1**.

- sw<version> - Software.
  bin - Binaries used for Regional TM.
  src - Source code for Regional TM executables.
  lib - Libraries used by the Regional TM executables.
  libsrc - Source code for libraries.

- config<version> - Definition of static data.
  Beamset - Beam parameters for each station
  libdata - Attenuation relations, velocity models and station corrections.

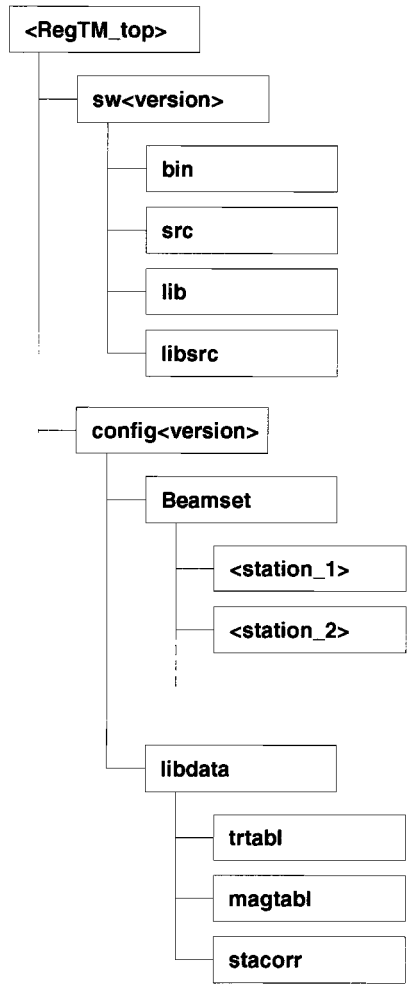

Figure 8.1. *Regional TM source directory organization.*

8.2 Data Directory Organization

The Regional TM system uses a flat file system to store input and output data, see **Figure 8.2**. The data files for a Regional TM processing session are stored in a directory tree which contain the result files and intermediate files.

- STA - Processed short term average (STA) data for each station/beam.
- TM - TM processing information and results
- Tm_types - A directory tree representing the various TM type/station/phase combinations
- scratch - temporary data storage used by the Regional TM system

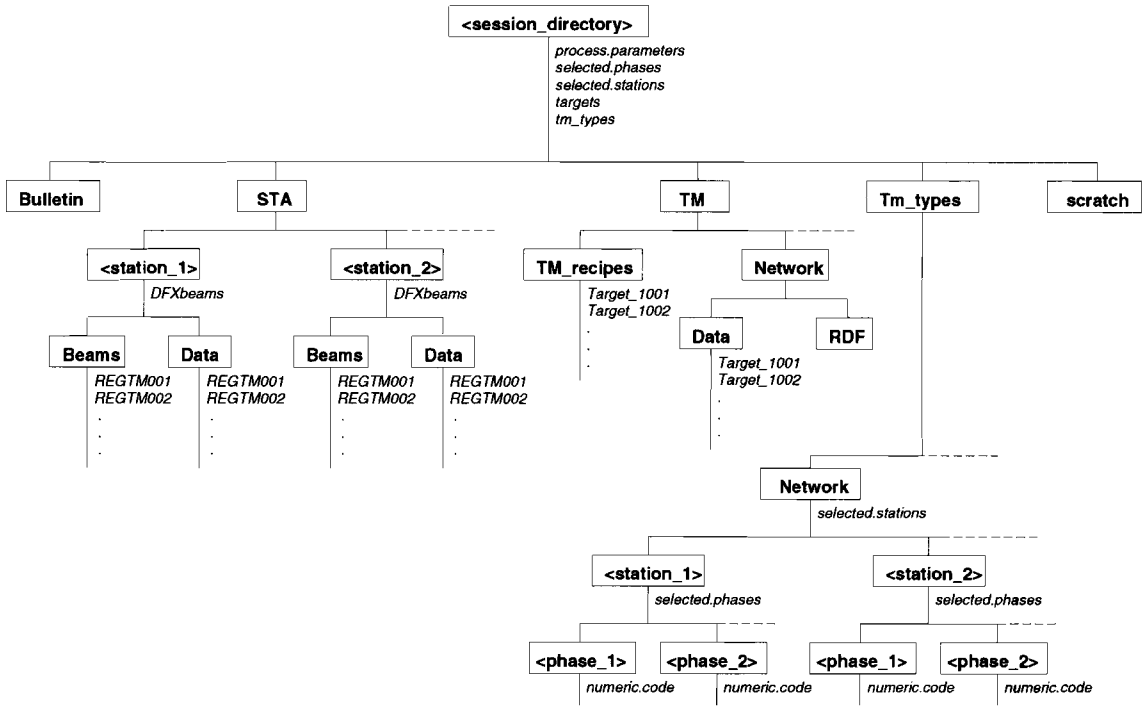

Figure 8.2. *Processing session data directory organization.*

8.3 Program description

The Regional TM system consists of the following main processing units:

- **MakeGrid**
- **CreateRegTMSession**
- **tm_regrec**
- **RegTMthreshold**
- **TMplot**

The following paragraphs describe the design of these units, including any constraints or unusual features in the design. The logic of the software and any applicable procedural commands are also provided.

8.3.1 MakeGrid

This unit generates the geographic grid coordinates used to calculate the detectability map, and writes the coordinates to a file.

Input

MakeGrid has a number of arguments either read from the command line or from a parameter file. The par file may contain the parameters shown in **Table 8.1**. Parameters in parameter files may be overridden by placing them after the par=<*parfile*> specification on the command line. The same format is used for the par file and the command line. The search order is from left to right on the command line, with precedence given to parameters found later if there are multiple specifications.

Table 8.1: MakeGrid Parameters

Parameter	Default	Description
lat	none (required)	Latitude grid center in degrees
lon	none (required)	Longitude grid center in degrees
latstep	0.3	Latitude grid step in degrees
lonstep	0.3	Longitude grid step in degrees
nlat	32	Number of grid steps in latitude

Table 8.1: MakeGrid Parameters (Continued)

Parameter	Default	Description
nlon	32	Number of grid steps in longitude
outdir	./	Path where to put the output file
outfile	none (required)	Name of output file

Output

MakeGrid generates the grid coordinates to be used by the CreateRegTMSession program. The result is written to a user-defined file.

8.3.2 CreateRegTMSession

CreateRegTMSession initializes a Regional TM processing session for a grid system created using *MakeGrid,* including creating directories, calculating beam recipes am initializing circular files.

Input

Although it is possible to enter every argument on the command line, it is most convenient to use a parameter file. The par file may contain the parameters shown in **Table 8.2**. Parameters in parameter files may be overridden by placing them after the par=<*parfile*> specification on the command line. The same format is used for the par file and the command line. The search order is from left to right on the command line, with precedence given to parameters found later if there are multiple specifications.

Table 8.2: CreateRegTMSession Parameters

Parameter	Default	Description
staticdir	none (required)	Location of constant values used in TM processing
session_directory	none (required)	Location of the top level data directory tree
stlist	none (required)	Comma-delimited station list
phases	none (required)	Phase names to use
targfile	none (required)	File containing beam point grid (from MakeGrid)
tmtypes	none (required)	TM type(s) to use

Table 8.2: CreateRegTMSession Parameters (Continued)

Parameter	Default	Description
ttmodel	barey	Velocity model to use for travel-time estimation
attrelfile	attrel.dat	File containing attenuation parameters
stacorfile	stacorr.dat	File containing station corrections
staloop	none (required)	Number of samples to create in STA circular files
stasamp	0.25 sec	STA sample rate
stanullval	-2.0	STA data gap value
tmloop	none (required)	Number of samples to create in TM circular files
tmsamp	1.0 sec	TM sample rate
tmsamp	1.0 sec	TM sample rate
tmnullval	-2.0	Value to use for missing data
tmplen	1.0 sec	Time window for P-phases
tmslen	5.0 sec	Time window for S-phases
tmconf	0.9	Confidence level
pstdev	0.4	Uncertainty (st.dev.) for P-type phase magnitudes
pampsrc	5.0	Search window length for maximum P amplitudes
paddsrc	2.0	Additional search window length to accommodate uncertainties in the P-phase travel time model
sstdev	0.4	Uncertainty (st.dev.) for S-type phase magnitudes
sampsrc	5.0	Search window length for maximum S amplitudes
saddsrc	2.0	Additional search window length to accommodate uncertainties in the S-phase travel time model

Output

CreateRegTMSession creates the directory structure needed for the TM processing (shown in **Figure 8.2**) initializes circular diskloops for STA and TM data, and calls *tm_regrec* (see below) that sets up processing parameters required for each grid point.

8.3.3 tm_regrec

tm_regrec creates processing recipes for individual grid points based on the global processing parameters. It is initially called by *CreateRegTMSession*, but can be run alone to recalculate recipes if required without initializing diskloops.

Input

tm_regrec reads the required input parameters from files within the session directory tree, and thus only requires the path to the top level of this directory tree, given on the command line.

Output

The processing recipes are placed in the <session_directory>/TM/TM_recipes/ directory as files with names corresponding to the target names given in the <session_directory>/ targets file.

8.3.4 RegTMthreshold

RegTMthreshold calculates TM values for each grid point based on the STA data. The STA data must be calculated beforehand using *EP* or alternatively *DFX*.

Input

RegTMthreshold requires four parameters that are read from the command line or parameter file, given in **Table 8.3**. Parameters in parameter files may be overridden by placing them after the par=<*parfile*> specification on the command line. The same format is used for the par file and the command line. The search order is from left to right on the command line, with precedence given to parameters found later if there are multiple specifications.

The two methods available are upplim (90% upper magnitude limit for non-detected events) and detection (90% detection threshold calculation). The latter has two additional parameters.

Table 8.3: RegTMthreshold Parameters

Parameter	Default	Description
session_directory	none (required)	Path to TM session directory
t1	none (required)	Processing start time
t2	none (required)	Processing end time
method	none (required)	`upplim` or `detection`
ndetsta	3	Number of stations required for detection when using `method=detection`
detsnr	4.0	SNR required for phase detection when using `method=detection`

Output

RegTMthreshold writes to existing circular diskloop files in the <session_directory>/TM/<tmtype>/Data/ directory or directories (depending on *tm_types* specified.

8.3.5 TMplot

TMplot extracts peak and mean TM magnitudes for each grid point from the diskloops for plotting.

Input

TMplot has a number of arguments either read from the command line or from a parameter file. The par file may contain the parameters shown in **Table 8.4**. Parameters in parameter files may be overridden by placing them after the par=<*parfile*> specification on the command line. The same format is used for the par file and the command line. The search order is from left to right on the command line, with precedence given to parameters found later if there are multiple specifications.

Table 8.4: TMplot Parameters

Parameter	Default	Description
session_directory	none (required)	path to top level of TM directory tree
t1	none (required)	start time of the segment to extract
t2	none (required)	end time of the segment to extract
outgrid	none (required)	path and filename of output file
tmsamp	none (required)	sample rate of TM circular files
hrgrid	0	If >0, output files will also be created for 1-hour segments

Output

TMplot generates files containing target locations and TM values in the specified location. The filename given in the parameter <outgrid> consists of three columns containing latitude, longitude (geographic coordinates) and peak TM values within the specified time interval for each grid point. A file named <outgrid>.mean consists of four columns containing latitude, longitude, (peak minus mean) and mean TM values. The data in these files should be simple to import and plot with any freeware or commercial mapping software like GMT and MatLab.

If the hrgrid parameter is set, additional files (peak and mean) are created with suffixes .00, .01, etc. for each hour throughout the specified time interval.

9 Conclusions and Recommendations

9.1 Conclusions

9.1.1 Regional Database and Attenuation Relations

A database comprising 45 seismic events, selected to provide the best possible ray path coverage of the Barents Sea and adjacent areas, has been compiled and reanalyzed in a consistent manner. This has resulted in new regional attenuation relations for Pn, Sn, Pg and Lg, together with a preferred average velocity model to be used for predicting the travel times of regional phases. We have applied these attenuation relations to develop and assess a regional threshold monitoring scheme for selected subregions of the European Arctic.

Amplitude inversion has been used in this study to resolve new attenuation coefficients and station corrections for estimating magnitudes from STA amplitude observations for Pn, Pg, Sn and Lg phases in the Barents Sea region. The distance range of observations on which the Pg and Lg relations are based is limited; a future study using a greater number of continental events could most likely provide a relation for STA based Lg magnitudes that is applicable at larger distances, albeit limited to paths within Fennoscandia.

The pattern of Lg arrivals and associated amplitudes supports the previously published indications that the deep sediment basins and Moho topography under the Barents Sea efficiently block Lg wave energy from crossing. From this, it is clear that Pn and Sn are the most useful phases for calculating stable and consistent magnitudes for events in the Barents Sea.

The 'BAREY' model from Schweitzer and Kennett (2002), based on a model for the Barents Sea area from Kremenetskaya et al. (2001), provides the smallest overall travel-time residuals when locating events within the vicinity of the Barents- and Kara Seas.

The seismic station in Amderma can be tied in to the regional network in Fennoscandia and on the Svalbard archipelago using an appropriate crustal model, and is able to provide important information regarding the location of events in the eastern parts of the Barents Sea and the Kara Sea (Schweitzer and Kennett, 2002). Magnitudes calculated at this station are on the whole consistent with the other observations.

The attenuation in the Barents Sea region differs somewhat from that observed in other stable tectonic regions, as evidenced by the fact that the coefficients given by Jenkins et al. (1998) for such regions do not give consistent magnitudes across frequencies, phases and stations for our amplitude observations from the events in the Barents Sea region.

9.1.2 Regional Threshold Monitoring

We have successfully developed a methodology and associated software for regional seismic threshold monitoring, and applied it to distinct regions of different sizes in the Barents Sea, Novaya Zemlya and the Kola Peninsula.

The Kursk accident on 12 August 2000 and subsequent underwater explosions occurring during the fall and winter of 2000 provided an excellent opportunity to test and evaluate the usefulness of the threshold monitoring method By tuning the processing parameters using the recordings of the Kursk accident, we were able to consistently monitor the numerous underwater explosions in the area around the accident site down to magnitude 1.5. The study demonstrated that the threshold traces steered to the accident site also provided excellent results for the underwater explosions that occurred in a relatively small geographical area (some tens of kilometers across) surrounding the accident site.

An initial grid system with an approximately 100-km grid spacing has been deployed to cover the entire Barents Sea region, and the observations at the arrays, ARCES, SPITS, FINES and NORES have been used for calculating threshold magnitudes for each of the grid points. During an interval without seismic signals, the threshold magnitudes showed large variations over the region, and, in particular, in the vicinity of each array. However, for the region around the island of Novaya Zemlya the variations are modest, varying around a mean of magnitude 2.1-2.2, when using this array network.

In order to investigate in more detail the variations in threshold magnitudes for the Novaya Zemlya region, we have deployed a dense grid with an areal extent of about 500 x 500 km around the former Novaya Zemlya nuclear test site. For each of the grid nodes, we calculated magnitude thresholds for the two-hour time interval 00:00 - 02:00 on 23. February 2002. At 01:21:12.1 there was an event with a magnitude of about 3, located about 100 km northeast of the former nuclear test site.

Regions of different sizes have been constructed by selecting grid points within different radii from the former nuclear test site. Average, minimum and maximum threshold magnitudes have been compared for circular regions with radii of 20, 50, 100 and 200 km, respectively. The most important result is that even for a target region with radius as large as 100 km, the variations in threshold magnitudes are all within 0.2 magnitude units. This applies both for the time interval with the event and for background noise conditions. For the investigated station geometry, it will therefore be meaningful to represent the monitoring threshold of the entire Novaya Zemlya region with the values of a single target point, together with the á priori determined uncertainty bounds.

For areas with larger variations in threshold magnitudes, like in the vicinity of the arrays, a 100-km radius target region will obviously show larger differences between the maximum and minimum values. Examples illustrating this point have been shown.

In cases when data from the Amderma station can be retrieved we find significant variations in threshold magnitudes over the island of Novaya Zemlya, ranging from 1.4 at the southern tip to 2.2 at the northern tip during noise conditions. This applies to the time interval immediately preceding the event on 23 February 2002. During this time interval, the monitoring capability for the former nuclear test site is lowered by about 0.3 magnitude units to about 1.9. This implies that a regional threshold monitoring scheme for the NZ region has to be divided into geographical sub-regions having similar threshold magnitudes during background noise conditions.

Using data from the ARCES and Apatity arrays, we have implemented a regional threshold monitoring scheme focusing on the Kola Peninsula. For the most active mining areas in this region (Khibiny, Olenegorsk, Zapoljarny and Kovdor), the magnitude thresholds during "normal" noise conditions vary between 0.7 and 1.0 magnitude units. During the studied time interval (12 April 2002), 10 out of 18 peaks exceeding threshold magnitude 1.2 at any of the mining areas were caused by events in the actual mining areas. However, the spatial resolution of the threshold magnitudes when using the ARCES and Apatity arrays is quite low, such that the mining events also created significant threshold peaks for the other mining areas.
This implies that for a regional threshold monitoring scheme for the Kola Peninsula it will be sufficient to deploy a set of targets for the most active mining areas. When a threshold peak is found at any of these targets, the peaks have to be associated to seismic events as outlined for the Kursk study.

9.2 Recommendations

We recommend that the work with amplitude attenuation relations for regional phases in Fennoscandia and adjacent areas be continued and extended to broader regions. The development of consistent regional magnitude scales is an important problem which still is far from a solution, but the results obtained in this study are encouraging.

The software which has been developed for this project should be considered for operational implementation. The necessary procedures and parameters for such implementation are provided in this report.

The automatic explanation facility for peaks on the threshold traces provided in this report assumes that a reasonably accurate on-line seismic detection bulletin is available. The joint development of combined threshold monitoring and reliable automatic detection bulletins is a future priority area.

The application of the regional threshold monitoring technique to other regions of monitoring interest should be considered. It would be particularly useful to investigate the benefits of adding local (non-IMS) stations to the IMS Primary and Auxiliary networks in such applications.

10. References

Hicks, E.C., Kværna, T., Mykkeltveit, S., Schweitzer, J. and Ringdal, F. (in press), *Travel-times and attenuation relations for regional phases in the Barents Sea region*, Pure and Applied Geophysics, in press.

Jenkins, R.D., T.J. Sereno and D.A. Brumbaugh (1998). Regional attenuation at PIDC stations and the transportability of the S/P discriminant. AFRL-VS-HA-TR-98-0046, Science Applications International Corporation, San Diego, CA, USA

Kremenetskaya, E.O. and V.M.Trjapitsin (1995): Induced seismicity in the Khibiny Massif (Kola Peninsula), Pure and Applied Geophysics, 145(1), 29-37.

Kremenetskaya, E., Asming, V., and Ringdal, F. (2001). Seismic location calibration of the European Arctic, Pure Appl. Geophys. 158, 117-128.

Kværna, T., J. Schweitzer, L. Taylor and F. Ringdal (1999). Monitoring of the European Arctic using Regional Generalized Beamforming, Semiannual Technical Summary 1 October 1998 - 31 March 1999, NORSAR Sci. Rep. 2-98/99, Kjeller, Norway

Ringdal F., E.Kremenetskaya, V.Asming, I.Kuzmin, S.Evtuhin, V.Kovalenko (1996): Study of the calibration explosion on 29 September 1996 in the Khibiny Massif, Kola Peninsula. Semiannual Technical Summary 1 April - 30 September 1996, NORSAR Sci. Rep. 1-96/97, Kjeller, Norway.

Ringdal F., T. Kværna and B. Paulsen (2000): Seismic events in the Barents Sea at and near the site of the Kursk submarine accident on 12 August 2000. Semiannual Technical Summary 1 April - 30 September 2000, NORSAR Sci. Rep. 1-2000/2001, Kjeller, Norway, 77-88

Schweitzer, J., and Kennett, B.L.N. (2002), Comparison of location procedures - the Kara Sea event 16 August 1997, Semiannual Technical Summary, 1 July - 31 December 2001, NORSAR Sci. Rep. 2-2001/2002, Kjeller, Norway, 97-114.